THE
PHYSICAL REVIEW
A journal of experimental and theoretical physics established by E. L. Nichols in 1893

SECOND SERIES, VOL. 63, NOS. 9 AND 10 MAY 1 AND 15, 1943

Intensity of Cosmic Rays at Low Altitude and the Origin of the Soft Component

KENNETH GREISEN
Cornell University, Ithaca, New York
(Received March 15, 1943)

Absorption curves have been obtained for cosmic rays at low altitude, with absorbers of carbon, iron, and lead. The separate intensities of fast mesotrons, slow mesotrons, and electrons have been deduced from the differences between the absorption curves. The number of slow mesotrons found is much greater than the number which may have descended from the mesotrons observed at a higher altitude, thus indicating considerable production of low energy mesotrons at low altitudes. The number of electrons is much too small to allow the conclusion that all of the energy of decaying mesotrons goes into shower production. Unless the lifetime-to-mass ratio for mesotrons is larger than presently accepted values, the results favor the conclusion that *less than half* of the energy of the mesotrons goes to the electron component.

INTRODUCTION

NEAR the base of the atmosphere or under any very heavy absorber, almost the entire electron component of cosmic rays must have its origin from decay and collision processes of mesotrons, chiefly from the decay. Thus the relative intensity of mesotrons and electrons at low altitude (or under a heavy absorber) may be used to furnish information regarding mesotron decay. This has been pointed out by Euler and Heisenberg,[1] who found the existing data in accord with a rough calculation based on the assumption that the mesotron decays into an electron and a neutrino with a lifetime of 2 microseconds. More recently, Nelson[2] was able to conclude, on the basis of data taken by Neher and Stever,[3] that the relative intensities were consistent with a lifetime of 2.8 microseconds, again providing that only half of the mesotron energy goes to the electron component. The relative intensities reported by Nielsen, Ryerson, Nordheim, and Morgan[4] have led Nordheim[5] to conclude that probably *less* than half of the mesotron energy goes into shower production. But this conclusion was based on a very small value of the mesotron lifetime (1.25 microseconds), and would have been different if a lifetime of 2 microseconds or more had been assumed.

The definiteness of the above conclusions has been limited both by experimental difficulties in determining the ratio of electron and mesotron intensities, and by inaccuracies in the theories used to predict the number of electrons which should be observed as a result of mesotron decay and collision processes. Recent additions to these theories, made by Rossi and Greisen,[6] Rossi and

[1] H. Euler and W. Heisenberg, Ergeb. d. exakt. Naturwiss. **17**, 1 (1938).
[2] E. Nelson, Phys. Rev. **58**, 771 (1940).
[3] H. V. Neher and H. G. Stever, Phys. Rev. **58**, 766 (1940).
[4] W. M. Nielsen, C. M. Ryerson, L. W. Nordheim, and K. Z. Morgan, Phys. Rev. **59**, 547 (1941).
[5] L. W. Nordheim, Phys. Rev. **59**, 554 (1941).
[6] B. Rossi and K. Greisen, Phys. Rev. **61**, 121 (1942).

Klapman,[7] and Richards and Nordheim,[8] have made it possible to calculate more accurately the number of electrons which should be observed above certain energy limits. The present experiments were designed so as to eliminate some of the experimental uncertainty in the ratio of the two intensities.

Most of the experimental difficulties in determining the relative intensity of mesotrons and electrons (from counting rates in Geiger-Müller counters below different amounts of absorber) arise from the comparatively small value of the electron intensity. Since one must rely on small differences between large counting rates, the statistical errors as well as all small systematic errors become important. The effect of meteorological changes (pressure, temperature, distribution of air mass) is great, and the number of low energy mesotrons stopped by the absorbers must be determined. The effect of side showers incident upon a counter telescope creates a significant error, and the transition effects observed as the absorber is changed become important. Moreover, the fraction of the electrons recorded depends strongly on the energy limit set by the apparatus, which must therefore be known.

EXPERIMENTAL ARRANGEMENT

The arrangement of counters used for the principal measurements is shown in Fig. 1. The fourteen counters arranged in a semicylinder were

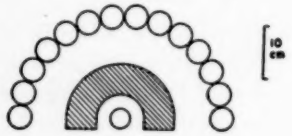

FIG. 1. Counter arrangement used in principal measurements.

60 cm long and were all connected in parallel. The central counter was 20 cm long. The principal measurements were of the coincidence rate between the central counter and the outer ones, as different absorbers were placed between the counters. Since the outer counters cover almost the entire solid angle above the central counter, the rates obtained give an intensity integrated over all angles. This serves a twofold purpose: (1) The error due to side showers is eliminated, since we wish to record the rays traversing the central counter in all directions, and (2) the counting rate is high, so that a high statistical accuracy may be obtained in a comparatively short time.

The absorbers used were cylindrical in shape. The energy limits set for electrons by the smallest absorbers were determined with fair precision by constructing these absorbers of a material of low atomic number, carbon (for which the "straggling" in the energy loss is small). Throughout the measurements with other absorbers (iron and lead), a central absorber of carbon was kept in place, so that only those electrons were recorded which emerged from the iron or lead with an energy of about 10^7 ev.

The errors in the counting rates, due to chance coincidences and inefficiency of the counters, were very small (a few tenths of a percent) and were determined by auxiliary measurements of the resolving time of the apparatus and the inefficiency of the counters. Other more serious sources of error are discussed in detail below.

DEVIATIONS DUE TO METEOROLOGICAL CHANGES

A simple correction for pressure and temperature changes cannot be made, since the cosmic-ray intensity depends on the distribution of air mass and temperature above the apparatus, more than on the values of pressure and temperature at any one point. Therefore an attempt was made to obtain an empirical correction simultaneously for all meteorological fluctuations, by using the deviations from the average of two "standard" rates, which were taken repeatedly during the running of the experiment, on alternate nights, for periods of more than 12 hours. These were the rate with the maximum lead absorber and the rate with only a small thickness of carbon as absorber. The statistical errors in the individual runs were less than 0.5 percent.

The "standard" rates were utilized as follows. Since the rates had been taken so often, it could be assumed that the simple averages were the

[7] B. Rossi and S. J. Klapman, Phys. Rev. **61**, 414 (1942).
[8] J. A. Richards, Jr., and L. W. Nordheim, Phys. Rev. **61**, 735 (1942). We are indebted to the authors for communicating their numerical results to us.

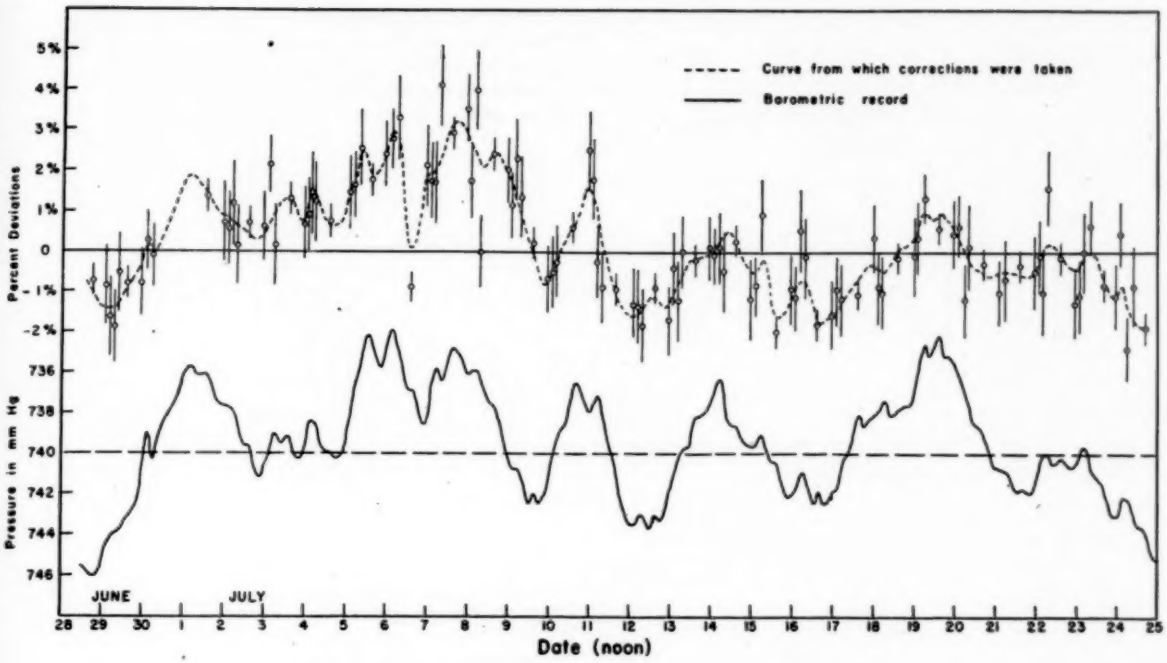

FIG. 2. Percent deviations due to meteorological changes.

correct rates for the average environmental conditions. The percent deviations of the individual runs from the average rates were plotted against the mean time at which the individual rates were obtained. In spite of the fact that the rates with the maximum lead absorber included only mesotrons, while the rates with the small carbon absorber included also the electron component, there was nothing to indicate that the two graphs of percent deviations against time should not be superposed; therefore, the points taken with both absorbers were plotted together, giving a graph of percent deviation from the mean which should be valid for all the intermediate absorbers as well. The corrections for the rates taken with the other absorbers were read from this graph, according to the mean time at which the rates were obtained. From these corrected rates, the average rate was computed for each absorber used.

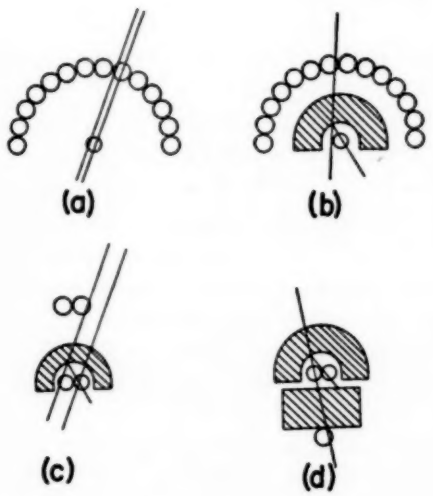

FIG. 3. Illustrating errors due to showers and secondary particles, and methods of correction.

In Fig. 2 we have plotted the percent deviations from the average, including the individual runs not only with the "standard" absorbers but with the intermediate absorbers as well. For comparison, we have also drawn the barometric record for the same period of time. It is obvious from this graph that changes in cosmic-ray intensity are not always exactly "in phase" with corresponding changes in barometric pressure, and that the same change in barometric pressure does not always accompany the same change in cosmic-ray intensity.

EFFECT OF INCIDENT SHOWERS AND SECONDARIES GENERATED IN THE ABSORBER

Figure 3a illustrates the error associated with showers incident upon the apparatus, which leads

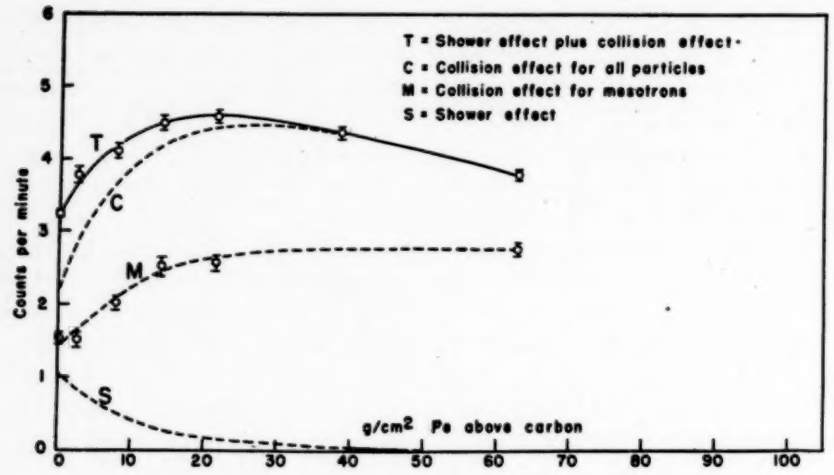
T = Shower effect plus collision effect
C = Collision effect for all particles
M = Collision effect for mesotrons
S = Shower effect
Counts per minute
g/cm² Pb above carbon

FIG. 4a. "Shower" and "collision" effects in iron.

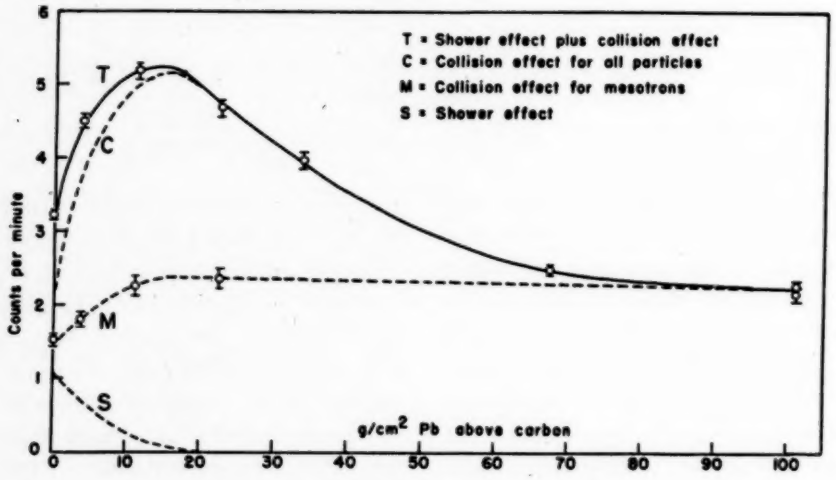
T = Shower effect plus collision effect
C = Collision effect for all particles
M = Collision effect for mesotrons
S = Shower effect
Counts per minute
g/cm² Pb above carbon

FIG. 4b. "Shower" and "collision" effects in lead.

to an underestimate of the number of electrons striking the apparatus. Except for very small absorbers, this effect is unimportant, because there is no error unless both particles have enough energy to penetrate the absorber. Even for small absorber thicknesses the effect is not very large, because of the great spread of air showers. For brevity we shall refer to this effect as the "shower effect."

Figure 3b illustrates an error in the opposite direction, due to secondary particles generated in the absorber. This is a sort of "transition effect" which may be described as an increase in effective size of the central counter due to the presence of the absorber. We shall refer briefly to this effect as the "collision effect," because it is largely caused by collision electrons knocked out of the absorber by mesotrons.[9]

In order to determine the error due to the shower and collision effects, an auxiliary experiment was performed with counters arranged as in Fig. 3c. The two upper counters were connected in parallel, and threefold coincidences between these and the lower counters were recorded as a function of absorber thickness, with the same absorbers as were used in the principal measurements. For comparison, we also recorded the

[9] Admittedly the term "collision effect" is not entirely appropriate, since a large part of this effect is caused by showers generated in the absorber. The only real distinction between the "shower" and "collision" effects, as we have called them, lies in whether the multiplicity existed above the absorber or was caused by the absorber.

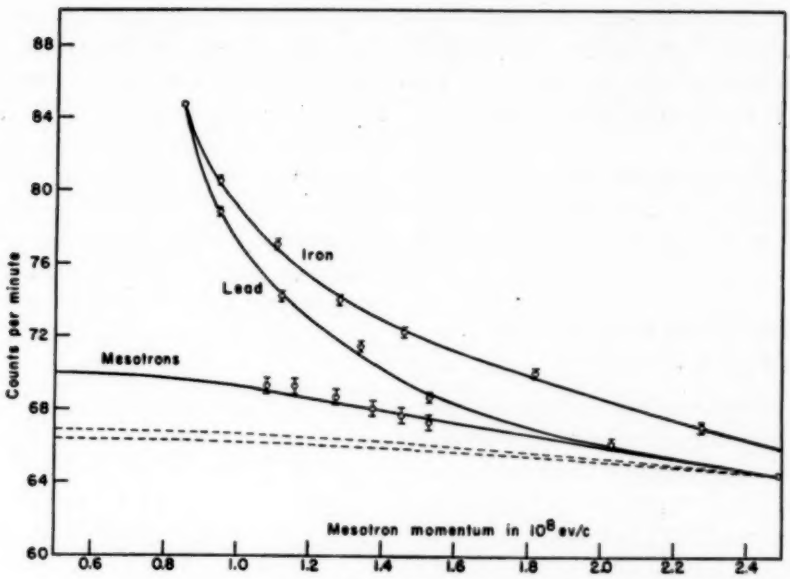

FIG. 5. Absorption curves in iron and lead.

twofold coincidence rate between the upper counters and *one* of the lower counters. It can easily be shown that the threefold coincidence rate obtained in this experiment is proportional to the *sum* of the errors due to the shower effect and the collision effect.[10] The proportionality constant is the ratio of the coincidence rate in the principal experiment to the twofold coincidence rate in this auxiliary experiment, which ratio had the same value (3.42), within statistical errors, for all of the absorbers used.

TABLE I. Corrections to counting rates, and final corrected rates.

Absorber	Average rate corrected for meteorological changes only	Net correction for "collisions" and "showers"	Net corrections for inefficiency and chance coincidences	Corrected rate
None	90.3 min.$^{-1}$	+0.3 min.$^{-1}$	+0.1 min.$^{-1}$	90.7 min.$^{-1}$
1.36 g/cm^{2}C	87.8	−0.5	+0.1	87.4
2.84 g/cm^{2}C	85.7	−1.1	+0.1	84.7
4.2 g/cm^{2}C	83.7	−1.5	+0.1	82.3
6.1 g/cm^{2}C	81.6	−1.8	+0.1	79.9
2.84 g/cm^{2}C				
+2.5 g/cm^{2}Fe	82.4	−2.0	+0.1	80.5
+7.8 g/cm^{2}Fe	80.1	−3.1	+0.1	77.1
+14.0 g/cm^{2}Fe	77.8	−3.9	+0.1	74.0
+21.4 g/cm^{2}Fe	76.3	−4.2	+0.1	72.2
+38.2 g/cm^{2}Fe	74.2	−4.3	+0.1	70.0
+62.8 g/cm^{2}Fe	70.8	−3.8	+0.1	67.1
2.84 g/cm^{2}C				
+3.8 g/cm^{2}Pb	81.8	−3.1	+0.1	78.8
+11.3 g/cm^{2}Pb	78.9	−4.8	+0.1	74.2
+22.5 g/cm^{2}Pb	76.0	−4.6	+0.1	71.5
+33.8 g/cm^{2}Pb	72.6	−4.0	+0.1	68.7
+67.5 g/cm^{2}Pb	68.6	−2.5	+0.1	66.2
+101 g/cm^{2}Pb	66.7	−2.3	+0.1	64.5

In Figs. 4a and 4b we have plotted the results of this auxiliary experiment. The uppermost curve (T) represents the sum of the errors due to shower and collision effects, determined as explained in the above paragraph. The correction to be applied to the counting rates in the principal experiment, however, is the difference between these two errors, rather than the sum. Fortunately the shower effect is small and decreases rapidly as the absorber thickness is increased. From the results obtained with very small absorbers in the experiment described above, it was possible to estimate the magnitude of this effect for zero absorber, while the variation of the effect with absorber thickness could be roughly calculated; such estimates (admittedly not exact) have led to the curves S, the lowest dashed curves in Figs. 4a and 4b. Curve C represents the difference between the ordinates of T and S; i.e., the collision effect alone. The corrections applied to the

[10] This conclusion rests on two assumptions: (1) That for two particles striking the apparatus simultaneously in such a direction that one of them penetrates one of the lower counters, it is equally likely that the second particle should penetrate the same counter or an identical counter adjacent to the first; and (2) that particles which pass by the central counter at distances greater than a counter diameter (4 cm) do not produce secondaries which discharge the counter. The first assumption is justified by the large spread of air showers; the second by the small average spread of showers in iron or lead.

counting rates are given by the differences between the ordinates of C and S. The curves M in Figs. 4a and 4b represent the collision effect for mesotrons alone, as determined with the arrangement shown in Fig. 3d.

In Table I we list the absorber thicknesses used in this experiment, and the corresponding counting rates, together with the corrections applied to the rates.

SEPARATION OF MESOTRON AND ELECTRON INTENSITIES

The method of obtaining the separate intensities of mesotrons and electrons from the counting rates resembles a method recently used by Auger[11] in analyzing measurements taken at a higher altitude. The momentum limits for mesotrons were calculated, corresponding to all of the absorbers used in the experiment, from the range-momentum relations given by Rossi and Greisen.[12] (In determining the ranges, the average absorber thicknesses were used, taking into account the differences in absorber thickness for mesotrons arriving in different directions.) The counting rates obtained with the iron and lead absorbers were plotted as a function of these momentum limits, yielding the two upper curves in Fig. 5. At each abscissa on this graph, the ordinate representing the mesotron intensity must have been the same for both the iron and the lead absorber. The difference between the curves arises from the fact that more electrons penetrate the iron; i.e., thicknesses of iron and lead which are equivalent for mesotrons are not equivalent for electrons. In fact, for electrons of energy large compared with the critical energies (25 Mev in iron, 7 Mev in lead), the iron and lead are equivalent for electrons in *radiation lengths* (14.4 g/cm² in iron, 5.9 g/cm² in lead). Thus in order to penetrate the maximum thickness of iron, the electrons must traverse, on the average, in addition to the carbon, only 4.75 radiation lengths of iron, while the corresponding thickness of lead is 15.8 radiation lengths.

It was assumed that no electrons penetrate the thickness of lead equivalent (for mesotrons) to the maximum thickness of iron.[13] The difference between the two absorption curves at this abscissa represents the number of electrons which can penetrate a smaller thickness of lead (the thickness which is equivalent for electrons to the maximum thickness of iron). By subtracting this difference from the lead absorption curve at the appropriate abscissa, one point is obtained on an extrapolated curve representing the total mesotron intensity (see Fig. 5). The difference between this extrapolated curve and the iron absorption curve at another thickness of iron may be subtracted from the lead absorption curve at a still smaller abscissa. By proceeding in this way, the six points on the "Mesotron" curve in Fig. 5 have been obtained. We are assisted in drawing the curve by the fact that it must be tangent to the lead absorption curve at the greatest thicknesses, and must become horizontal as the momentum approaches zero (not only because of the increase in the decay probability per cm as the velocity decreases, but also because of the increase in the energy loss).

TABLE II.

Absorber	Average energy limit for electrons (Mev)	Total number of electrons per min.	Electrons from collision processes	Electrons from remaining sources
None	3.4	20.8	7.6	13.2
1.36 g/cm²C	6.4	17.6	5.6	12.0
2.84 g/cm²C	10.0	15.1	4.2	10.9
4.2 g/cm²C	13.6	12.8	3.4	9.4
6.1 g/cm²C	18.9	10.8	2.7	8.1
2.84 g/cm²C +62.8 g/cm²Fe	350	2.0	0.0	2.0

The only questionable part of the above procedure is the determination of thicknesses of iron and lead which are exactly equivalent for electrons. Actually, different absorbers can never be equivalent for all electrons, because of the difference in critical energies. However, the carbon absorber kept permanently under the iron and lead removes from consideration the many electrons of energy below 10^7 ev which emerge from the lead. If the energy limit set by the carbon absorber had been somewhat higher (several times the critical energy in iron, 25 Mev), we should have been able to say the iron and lead

[11] P. Auger, Phys. Rev. **61**, 684 (1942).
[12] B. Rossi and K. Greisen, Rev. Mod. Phys. **13**, 240 (1941).
[13] This assumption is justified by the graphs in Fig. 4b, which show that at this thickness the transition effect for all particles traversing the lead agrees with the transition effect for mesotrons alone.

absorbers were exactly equivalent in radiation lengths; as it is, this is still true after such thicknesses of iron and lead that the energy limit has been so increased. Thus, the average energy loss of the electrons barely capable of penetrating the absorber, in the first radiation length of iron, is the same as that in the first 1.6 radiation lengths of lead; beyond these thicknesses, the iron and lead are equivalent in radiation lengths. Hence, for values of x greater than 1, we have assumed x radiation lengths of iron equivalent to $x+0.6$ radiation lengths of lead.

From the "Mesotron" curve in Fig. 5 we have obtained the counting rate due to mesotrons corresponding to each of the absorbers used in this experiment; in particular for the carbon absorbers, for which the average energy limits set for electrons could be calculated. By subtracting the counting rates due to mesotrons from the total counting rates, we have obtained the counting rates due to electrons, which are given in Table II. The number of electrons penetrating the maximum iron absorber has also been given, for which the approximate energy limit has been calculated with the Snyder-Serber theory.[14]

MESOTRONS DESCENDED FROM A HIGHER ALTITUDE

Under the assumption that practically no electrons penetrate the maximum lead absorber,[13] the counting rate with this absorber gives the intensity of "fast" mesotrons (i.e., mesotrons of momentum above 2.5×10^8 ev/c, the average limit set by this absorber). If the number of mesotrons at Ithaca with momentum below this limit can be calculated, we have an alternative method of obtaining the total number of mesotrons and, hence (by subtraction from the absorption curves), the number of electrons. Provided that no mesotrons are produced between the two elevations, we may calculate the number of low energy mesotrons at Ithaca as the number which have descended from a higher elevation, where they had a greater energy.

Mesotrons of momentum between 0 and 2.5×10^8 ev/c at Ithaca (275-meters elevation) would correspond to mesotrons with momentum between 6.6 and 8.1×10^8 ev/c at Echo Lake (3240-meters elevation), where a differential momentum spectrum of mesotrons, including this range, has been obtained by Rossi, Greisen, Stearns, Froman, and Koontz.[15] By using this momentum spectrum, together with the probability of survival of the mesotrons between the two elevations,[16] we have calculated the number of slow mesotrons which have survived to reach Ithaca from the elevation of Echo Lake. By adding these to the number of fast mesotrons, we have obtained the dashed curves shown in Fig. 5, which should represent the total mesotron intensity. The two curves correspond to calculations made with two different values of the lifetime-to-mass ratio for mesotrons, 8.4×10^{-4} cm-c/ev (upper curve) and 6.7×10^{-4} cm-c/ev (lower curve), between which the correct value probably lies. The value 8.4×10^{-4} cm-c/ev is taken from the measurements of Rossi and collaborators,[15] but may be somewhat too high if mesotron production is an important process at low elevations. A recent direct measurement by Rossi and Nereson[17] indicates that the mesotron lifetime is about 2.2 microseconds; this together with a mesotron mass of 160 electron masses would indicate 8.4×10^{-4} cm-c/ev for the lifetime-to-mass ratio, in agreement with the other measurements, but with a mesotron mass of 200 electron masses indicates 6.7×10^{-4} cm-c/ev for the lifetime-to-mass ratio.

The graphs in Fig. 5 show that this calculation of the number of slow mesotrons is incorrect. In the first place, it yields a graph of total mesotron intensity which is not tangent to the absorption curve in lead at the largest thicknesses. Secondly, it predicts that the number of slow mesotrons is only 3 percent of the total number of mesotrons, while the differences between the absorption curves in iron and lead indicate that the number of slow mesotrons is 8 percent of the total number. From this discrepancy, we may conclude that more than half of the slow mesotrons observed at Ithaca have originated in the air below 3240-meters elevation.

It should be observed that this conclusion has

[14] H. Snyder, Phys. Rev. **53**, 960 (1938); R. Serber, Phys. Rev. **54**, 317 (1938).

[15] B. Rossi, K. Greisen, J. C. Stearns, D. K. Froman, and P. G. Koontz, Phys. Rev. **61**, 675 (1942).

[16] See B. Rossi, Rev. Mod. Phys. **11**, 296 (1939).

[17] B. Rossi and N. Nereson, Phys. Rev. **62**, 417 (1942).

little bearing on the place of origin of the fast mesotrons. If one takes into account not only the decay but also the decrease in rate of mesotron production with increasing atmospheric depth, a rough calculation indicates that most of the high energy mesotrons observed near sea level should have originated near the top of the atmosphere, while most of the low energy mesotrons should have originated near the place of observation.

ABSOLUTE INTENSITIES

From the counting rates given above, it is possible to obtain, by a purely geometrical calculation, the absolute integrated intensities of mesotrons and electrons at Ithaca. The integrated intensity to which the counting rates are most closely related is the one which is connected with the specific ionization, and which gives the number of particles per minute crossing a sphere of unit cross section. In terms of the absolute directional intensity $I(\theta)$ and the zenith angle θ, this integrated intensity is defined as

$$J=2\pi\int_0^{\pi/2}\sin\theta I(\theta)d\theta.$$

Because of the cylindrical shape of the counters, the rates obtained in this experiment do not yield J directly, but yield an elliptic integral of the directional intensity, which may be written as

$$R=2\pi\int_0^{\pi/2}\sin\theta I(\theta)F(\theta)d\theta.$$

$F(\theta)$ is a slowly varying factor, the total variation in which is less than 30 percent of its value at $\theta=0$. Hence we may write $R=KJ$, where K is a constant which depends slightly on the zenith-angle variation of the cosmic-ray intensity, and may be found from a tedious calculation involving the dimensions of the apparatus. In the calculation of K, account is taken of the fact that the outer counters in the present experiment did not completely cover the solid angle above the central counter; however, only a few percent of the particles were missed in this way, because of the small number arriving at large zenith angles. Because the electron intensity has a somewhat steeper zenith-angle dependence than has the mesotron intensity, we have obtained slightly different values of K for electrons and for mesotrons ($K=59.6$ for mesotrons, 61.4 for electrons). The absolute integrated intensities thus calculated are listed in Table III. The errors given include not only the statistical errors but also an estimate of the likely errors which may have arisen in the method of computation.

TABLE III. Absolute integrated intensities of mesotrons and electrons.

Component of cosmic rays	Particles per cm² per min.
Mesotrons above 2.5×10^8 ev/c	1.082 ± 0.007
Mesotrons above 0.5×10^8 ev/c	1.175 ± 0.012
Electrons above 3.4 Mev	0.339 ± 0.015
Electrons above 6.4 Mev	0.287 ± 0.014
Electrons above 10.0 Mev	0.246 ± 0.012
Electrons above 13.6 Mev	0.208 ± 0.014
Electrons above 18.9 Mev	0.176 ± 0.015
Electrons above 350 Mev	0.033 ± 0.008

ELECTRONS ARISING FROM COLLISION PROCESSES OF MESOTRONS

The number of electrons of energy above 10^7 ev in equilibrium with the mesotrons at sea level, as a result of the collision processes, has been calculated accurately by Rossi and Klapman,[7] who obtained the result that the number of electrons was 6.7 percent of the number of mesotrons with momentum above 3×10^8 ev/c. This would be about 6.6 percent of the mesotrons with momentum above 2.5×10^8 ev/c, the limit set by the maximum absorber in the present experiment. Thus the counting rate for collision electrons above 10^7 ev (which corresponds to the energy limit set by one of our carbon absorbers) should be 4.2 per minute.

An approximate method of calculation of the number of collision electrons with energy above other limits has been suggested to the author by Professor Rossi and rests on the conservation of energy. Since the collision electrons are in equilibrium with the mesotrons, the energy given to electrons of energy above E in each g/cm² must be equal to the energy dissipated by them in each g/cm². This energy is lost in two ways: (1) by electrons drifting through the boundary E to lower energies, each taking away an energy E, and (2) by collision and radiation losses of electrons which remain above the boundary E. The last term is very closely approximated by the number of electrons of energy above E times the energy loss of electrons of energy E. The number

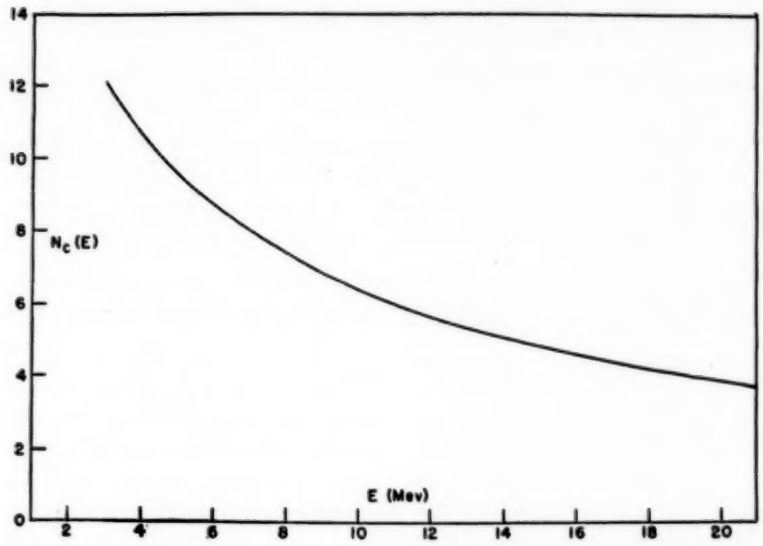

FIG. 6. Electrons arising from collision processes of mesotrons in air. $N_c(E)$ = number of electrons of energy above E in equilibrium with the mesotrons, per 100 mesotrons of momentum above 2.5×10^8 ev/c.

which drift through the boundary to lower energies is equal (under the same approximations) to the number of new electrons added to the group by mesotron collisions. This term, as well as the energy given to the electrons of energy above E, may be calculated from the collision probabilities of mesotrons and integrated over the momentum spectrum of mesotrons given by Blackett.[18] The results of such calculations are presented as a function of E in Fig. 6.

The accuracy of these calculations may be tested by comparing the result for $E=10^7$ ev with the value obtained for this energy by the more accurate calculations of Rossi and Klapman. The present calculations give $N_c(10^7)=6.4$ per 100 fast mesotrons, while those of Rossi and Klapman give $N_c(10^7)=6.6$, in very close agreement.

The counting rates due to collision electrons, corresponding to the carbon absorbers used in this experiment, are listed in Table II.[19] By subtracting the collision electrons from the total electron intensity, we have obtained the electron intensities listed in the last column of that table. The principal source of these remaining electrons must be the decay of mesotrons; but regardless of whether or not some of the electrons have other origins (e.g., primary electrons or radiation by mesotrons), the numbers listed in this column must be *at least* as great as the numbers of electrons arising from mesotron decay.

ELECTRONS ARISING FROM DECAY OF SLOW MESOTRONS

The primary electrons arising from decay of mesotrons with momentum below 2.5×10^8 ev/c have energies of the same order as the critical energy in air; hence the shower theory cannot be applied to calculate the number of electrons to which they give rise. Therefore we have used instead the approximate method of calculation which was used above for the collision electrons. Because the energy spectrum of the decay electrons is not as steep as that of the collision electrons, the approximations are not as good; but because of the small number of slow mesotrons, a slight error in this calculation is of no significance. For the momentum spectrum of slow mesotrons, over which an integration is required, we have used the results deduced in the present paper from the differences between the absorption curves in iron and lead. The results of the

[18] P. M. S. Blackett, Proc. Roy. Soc. **159**, 1 (1937).

[19] These have been obtained from the graph in Fig. 6 by multiplying the number of electrons per fast mesotron by the counting rate due to fast mesotrons in the present experiment. The results have been corrected in the ratio 6.6/6.4 to give exact agreement at $E=10^7$ with the calculations of Rossi and Klapman, which were considered more accurate than the present calculations.

TABLE IV. Electrons arising from mesotron decay.

Energy limit for electrons (Mev)	Assumed decay products: 1 electron, 1 neutrino $\tau_0/\mu=6.7\times10^{-4}$ cm-c/ev S	F	T	$\tau_0/\mu=8.4\times10^{-4}$ cm-c/ev S	F	T	Assumed products: 1 electron, 2 neutrinos $\tau_0/\mu=6.7\times10^{-4}$ T	$\tau_0/\mu=8.4\times10^{-4}$ T
3.4	2.5	19.5	22.0	2.0	15.6	17.6	14.7	11.7
6.4	2.2	17.9	20.1	1.8	14.3	16.1	13.4	10.7
10.0	2.0	16.4	18.4	1.6	13.1	14.7	12.3	9.8
13.6	1.8	15.3	17.1	1.45	12.2	13.7	11.4	9.1
18.9	1.6	14.0	15.6	1.3	11.2	12.5	10.4	8.3
350	0.0	2.3	2.3	0.0	1.8	1.8	1.5	1.2

Legend: S = predicted counting rate due to electrons arising from decay of slow mesotrons; F = predicted counting rate due to electrons arising from decay of fast mesotrons; $T=S+F$ = total predicted counting rate due to electrons arising from mesotron decay.

calculations are listed in Table IV, corresponding to the two values of the lifetime-to-mass ratio with which the calculations have been made (see discussion above in the section on mesotrons descended from a higher altitude). These calculations have been made under the assumption that the decay products of the mesotron are an electron and a neutrino. If the decay products are an electron and a photon, the numbers should be multiplied by approximately 2; while if the mesotron decays into an electron and two neutrinos, the results should be multiplied by $\frac{2}{3}$.

ELECTRONS ARISING FROM DECAY OF FAST MESOTRONS

Since most of the primary electrons arising from the decay of fast mesotrons have energies large compared with the critical energy in air, the shower theory can be applied to calculate the number of electrons to which they give rise. It has been shown by Rossi and Greisen[12] that if one neglects the decrease in the rate of production of the primary electrons over a distance equal to the maximum range of the showers, then the number of electrons of energy above E in equilibrium with the mesotrons is given by the integral track length of all electrons above energy E produced per g/cm² by the mesotrons. In another article,[6] the same authors have shown that the variation in the rate of production of the primary decay electrons can be taken into account by evaluating the track length for the electrons produced per g/cm² at a distance of 130 g/cm² above the place of observation.

The track length for $E=0$ is obtained simply from the conservation of energy as $43\,E_0/\epsilon$, where E_0 is the energy going to decay electrons per g/cm², and $\epsilon/43$ is the ionization loss per g/cm², ϵ being the critical energy, and 43 g/cm² being the radiation length in air. For other energies, we have used the accurately known track length for $E=0$ together with the relative track lengths (or energy distribution at the maximum of a shower) recently calculated by Richards and Nordheim.[8] The track length for $E=10^7$ ev, calculated by Rossi and Klapman,[7] agrees very closely with the corresponding value obtained by Richards and Nordheim, the latter value being higher by about 3 percent.

The energy E_0 going to decay electrons per g/cm², due to the disintegration of fast mesotrons, is given by $E_0=\frac{1}{2}(\mu/\tau_0)(N/\rho)$ (where ρ is the density of air, N is the number of fast mesotrons, and τ_0/μ is the lifetime-to-mass ratio), under the assumption that the disintegration products are an electron and a neutrino. If the mesotron decays into an electron and a photon, E_0 should be twice as large; if into an electron and two neutrinos, E_0 should be $\frac{2}{3}$ as large. E_0 must be evaluated at 130 g/cm² above the place of observation; hence the values of N at 130 g/cm² above Ithaca were read from a graph of mesotron intensity *vs.* elevation recently obtained by the author.[20] Data were available at four different zenith angles, so that an integration over zenith angle could be performed, as was required for comparison with the data of this experiment. Thus we have obtained the numbers in Table IV, which represent the hypothetical counting rates due to electrons arising from decay of fast mesotrons.

CONCLUSIONS

The total numbers of electrons arising from decay, given in Table IV, should be comparable

[20] K. Greisen, Phys. Rev. **61**, 212 (1942).

with the counting rates listed in the last column of Table II; at any rate, they should be *no larger* than those counting rates. Hence it is impossible that the mesotron should decay into a photon and an electron, for in that case the counting rate due to electrons arising from decay would have to be three times what was observed; in fact, it would have to be 50 percent greater than the total difference in counting rate between the minimum absorber (only the counter walls) and the maximum absorber (including 101 g/cm² of lead).

Because of the indirect way in which the counting rates listed in the last column of Table II were obtained, they cannot be considered very accurate. However, considering all the possible sources of error, it is unlikely that any of these numbers should be in error by as much as 3 counts per minute, or that the last of the numbers should be in error by as much as 0.5 counts per minute. Hence we may conclude that the results also discourage the hypothesis that the decay products are an electron and a neutrino. At any rate, if these should be the decay products, the results indicate that the lifetime-to-mass ratio for mesotrons is at least as large as 8.4×10^{-4} cm-c/ev. Thus, if one accepts the value of the lifetime (2.2 microseconds) recently obtained by Rossi and Nereson,[17] the mass of the mesotron must be no larger than 160 electron masses.

In general, however, the results favor the hypothesis that *less* than $\frac{1}{2}$ of the energy of decaying mesotrons goes to the electron component. They would be in agreement with a decay into an electron and two neutrinos, for instance, in which case the spin of the mesotron might be $\frac{1}{2}$ but not 0 or 1, and only $\frac{1}{3}$ of the mesotron energy would go into shower production.

It has been suggested[1,21,22] that some of the mesotrons may disappear by another process other than radioactive decay and, hence, without contributing to the electron component. If this were an important process in the atmosphere, it might reconcile the disintegration into an electron and a neutrino with the small number of electrons observed. However, because of the small density of the atmosphere, and because most of the electrons should arise from disintegration of mesotrons of great momentum, we do not think that the suggested process can affect the conclusions discussed above.

The author wishes to express his gratitude to Professor Bruno Rossi for his invaluable aid in the design and analysis of this experiment.

[21] S. Tomonaga and G. Araki, Phys. Rev. **58**, 90 (1940).
[22] F. Rasetti, Phys. Rev. **60**, 198 (1941).

Meson Theory of the Magnetic Moment of Proton and Neutron

J. M. JAUCH
Palmer Physical Laboratory, Princeton University, Princeton, New Jersey
(Received March 8, 1943)

The magnetic moment of proton and neutron is determined by a second-order perturbation calculation. A new limiting process secures the convergence of the integration in momentum space. The result for both pseudoscalar and vector meson is the same and leads to a positive magnetic moment for the neutron if the magnetic moment of the vector meson is assumed to be one meson magneton ($eh/2\mu c$). Agreement with the known values of the magnetic moment of the heavy particles can only be obtained if we give the vector meson an anomalous magnetic moment of about three meson magnetons.

1.

THE relativistic wave equation of particles with spin $\frac{1}{2}$ leads in a natural way to a value of the magnetic moment of one magneton ($eh/2mc$), where m is the mass and e the charge of the particle. In the case of proton and neutron the magnetic moments differ appreciably from the values which they should have according to this theory. Measured in units of nuclear magnetons the experimental values for these moments are:

$$\mu_p = +2.785 \pm 0.02$$

for the proton[1] and

$$\mu_n = -1.935 \pm 0.02$$

for the neutron.[2] The minus sign in the case of the neutron indicates that the spin points in the opposite direction of the magnetic moment.

It was pointed out by Kemmer[3] and others[4] that the meson theory of nuclear forces would also lead to anomalous magnetic moments of the nucleons, due to the virtual emission and reabsorption of mesons by the nuclear particles. Unfortunately a second-order perturbation calculation leads to divergent integrals. This divergence difficulty was dodged by cutting off the integrals suitably, which is equivalent to introducing a finite size of the nucleon.

This procedure, however, is highly unsatisfactory for two reasons:

(1) It introduces an arbitrary constant into the theory, the physical significance of which is not quite clear.

(2) It destroys the relativistic invariance of the theory.

In spite of these grave objections one feels that the meson theory of the magnetic moment is essentially correct and that a theory of interaction of nucleons with the meson field, formulated in such a way that the divergence difficulties disappear, should give the correct value for these moments.

Recently a theory was proposed by Dirac[5] for the interaction of an electron with the electromagnetic field, which avoids all divergence difficulties for that case. The theory consists of two essentially different parts. The first part is the so-called λ-limiting process, first investigated by Wentzel.[6] It is essentially a classical procedure and consists of using the difference of retarded and advanced potential at the position of the particle. Dirac showed[7] that the λ process may best be introduced in quantum mechanics by a change in the commutators of the field quantities entering into the interaction energy.[8] In this form the procedure may easily be generalized to charged fields with rest mass different from zero.

The integral which causes the divergence of the meson theory of the magnetic moment is the integral

$$\int_0^\infty k^4/(k^2+\mu^2)^2 dk$$

[1] Kellogg, Rabi, Ramsey, and Zacharias, Phys. Rev. **56**, 728 (1939).
[2] L. W. Alvarez and F. Bloch, Phys. Rev. **57**, 111 (1940).
[3] N. Kemmer, Proc. Roy. Soc. **A166**, 127 (1938).
[4] Fröhlich, Heitler, and Kemmer, Proc. Roy. Soc. **A166**, 154 (1938). H. Fröhlich, Phys. Rev. **62**, 180L (1942). The result announced in this note, that the pseudoscalar meson gives no magnetic moment, is incorrect. I am indebted to Professor Fröhlich for correspondence on this point.
[5] P. A. M. Dirac, Proc. Roy. Soc. **A180**, 1 (1942).
[6] G. Wentzel, Zeits. f. Physik **86**, 479, 635 (1933); **87**, 726 (1934).
[7] P. A. M. Dirac, Am. de l'Inst. H. Poincare, **9**, 13 (1939).
[8] For a detailed account see an article by W. Pauli, to be published in the Rev. Mod. Phys.

with μ=meson mass. This integral will be made convergent with the λ process. We must, however, remark that this integral occurs only if a second-order perturbation theory is applied and if the mass m of the heavy particle is infinitely large. In higher approximations in the coupling constant and in μ/m other integrals will appear in addition to this which no longer converge with the λ process alone. In general only integrals which for large values of k behave like

$$\int k^{2n}dk$$

with n integer will be made to converge with this method. A limitation to a second-order perturbation treatment would not be justified if such higher order divergent terms remain.

In order to make the other integrals converge, Dirac has introduced another kind of field oscillator corresponding to states with negative energy and quantized according to an indefinite metric in Hilbert space.[8] Dirac has shown that the two methods lead to the elimination of all divergencies in the quantum theory of fields. Serious interpretation difficulties still remain, however.

It may easily be seen that the higher order terms lead always to integrals of the form[9]

$$\int_0^\infty R(k_0, k)dk$$

with a rational function $R(k_0, k)$ for the integrand containing only even powers of k. The introduction of the negative energy oscillators changes this integral into the form

$$\tfrac{1}{2}\int_0^\infty [R(k_0, k)+R(-k_0, k)]dk$$

and this is sufficient to make all the remaining integrals occurring in this perturbation treatment converge.

The calculation of the magnetic moment due to the meson field with this method leads to a positive value for the neutron both in the pseudoscalar and the vector theory. This is in disagreement with the experimental result. Only by making use of the possibility that the vector meson may have a magnetic moment different from one meson magneton can agreement with the experiment be obtained. The contribution of the meson field to the magnetic moment has then a certain value M which is positive for the proton and negative for the neutron, so that we shall have for the magnetic moment of these particles

$$\mu_p=1+M, \quad \mu_n=-M.$$

By choosing $M\sim+1.9$, agreement with experiment will be obtained within the limits of our approximation.

The objection may be raised that this assumption of an anomalous magnetic moment of the vector meson introduces a new constant into the theory and we stand where we were before. The situation is, however, not quite so bad. We must bear in mind that we have introduced the new parameter in a way which does not destroy the relativistic invariance of the theory. Moreover, the constant has a definite physical meaning, namely, the magnetic moment of the vector meson, which may be checked with an experiment, deciding for or against the theory here presented.

2. THE PSEUDOSCALAR THEORY

In the following we often use one single letter "a" for a four vector with components a_μ. Here $\mathbf{a}=a^k$ is the space part of the vector. The invariant scalar product of two four vectors shall be denoted by $(a, b)=(\mathbf{a}, \mathbf{b})-a^0b^0=a_\mu a^\mu$. ($a_0=-a^0$.)

Charged particles of spin zero are described by a complex field $\psi(x)$ satisfying the field equation

$$\Box\psi-\mu^2\psi=0,$$

where μ is the meson mass in units $\hbar/c$ and $\Box=\partial^2/\partial x^\mu\partial x_\mu$. It is quantized according to the commutation rules

$$i[\psi(x), \psi^*(x')]=D(x-x'), \tag{1}$$

where $D(x)$ is the invariant D function defined by

$$D(\mathbf{x}, x^0)=\frac{1}{(2\pi)^3}\int\frac{d^3k}{k^0}\exp[i(\mathbf{k}, \mathbf{x})]\sin k^0x^0, \tag{2}$$

$$k^0=+(k^2+\mu^2)^{\frac{1}{2}}.$$

The operator for the current density vector is

$$s_\mu=i\left(\frac{\partial\psi^*}{\partial x^\mu}\psi-\frac{\partial\psi}{\partial x^\mu}\psi^*\right) \tag{3}$$

[9] This is not true for the theory of holes, where integrals of the form $\int dk/(k^2+m^2)^{\frac{1}{2}}$ occur, which are logarithmically divergent, even in this theory.

and the total magnetic moment of the field

$$M_{\mu\nu}=\frac{e}{2}\int(x_\mu s_\nu - x_\nu s_\mu)d^3x, \tag{4}$$

where the positive number "e" is the magnitude of the charge of the mesons in units $(\hbar c)^{\frac{1}{2}}$.

For our calculations it is somewhat more convenient to introduce two real fields ψ_1 and ψ_2:

$$\psi=\frac{1}{\sqrt{2}}(\psi_1-i\psi_2),\quad \psi^*=\frac{1}{\sqrt{2}}(\psi_1+i\psi_2),$$

for which we have the commutation rules

$$i[\psi_\alpha(x),\psi_\beta(x')]=\delta_{\alpha\beta}D(x-x'). \tag{5}$$

The spin dependent interaction of the heavy particle with the coordinates z may be written[10]

$$H'=g(4\pi)^{\frac{1}{2}}\tau_\alpha(\boldsymbol{\sigma},\operatorname{grad})\psi_\alpha(z). \tag{6}$$

The τ_α represent the matrices for the isotopic spin and $\boldsymbol{\sigma}=(\sigma_1,\sigma_2,\sigma_3)$ is the ordinary spin vector. They satisfy the equation

$$\tau_1\tau_2=-\tau_2\tau_1=i\tau_3,\ \cdots\sigma_1\sigma_2=-\sigma_2\sigma_1=i\sigma_3,\ \cdots$$
$$\tau_1^2=\cdots=\sigma_3^2=1, \tag{7}$$

together with all the other equations which can be obtained from them by cyclic permutation of the indices. The summation over α is extended over the two indices $\alpha=1,2$. In the symmetrical theory there is a third real field ψ_3 present representing the neutral mesons, and the summation goes then over all three indices. Since neutral particles do not contribute anything to the current and to the magnetic moment, we can restrict ourselves to the first two indices.

The interaction energy contains only the nonrelativistic part of the heavy particles. This approximation can be made since we are only interested in the effects which are of highest order in μ/m, and they are independent of m. This amounts to setting the mass of the heavy particle infinitely large, and then relativistic effects of the heavy particle are of course unimportant. The mesons, however, are treated relativistically all through the calculations. The interaction term in the Hamiltonian leads to an additional term in the current so that the total current now is[11]

$$s_\mu=(\partial\psi_1/\partial x^\mu)\psi_2-(\partial\psi_2/\partial x^\mu)\psi_1$$
$$+g(4\pi)^{\frac{1}{2}}\sigma_\mu(\tau_2\psi_1-\tau_1\psi_2)\delta(\mathbf{x}-\mathbf{z}). \tag{8}$$

We develop the field operators into eigenstates in momentum space

$$\psi_\alpha(x)=\frac{1}{\sqrt{2}(2\pi)^{\frac{1}{2}}}\int\frac{d^3k}{k^0}\{\varphi_\alpha(\mathbf{k})e^{i(k,x)}$$
$$+\varphi_\alpha^*(\mathbf{k})e^{-i(k,x)}\}. \tag{9}$$

This definition of the $\varphi_\alpha(k)$ and $\varphi_\alpha^*(k)$ is useful since they are constant operators if there is no interaction between heavy particles and field. In case of an interaction they are slowly varying according to the law[12]

$$d\varphi_\alpha/dx^0=i[H',\varphi_\alpha]. \tag{10}$$

From (1), (2), and (9) it follows that the commutation rules for the $\varphi_\alpha(k)$ are

$$[\varphi_\alpha(\mathbf{k}),\varphi_\beta^*(\mathbf{k}')]=k^0\delta_{\alpha\beta}\delta(\mathbf{k}-\mathbf{k}'), \tag{11}$$

from which it follows in the well-known way that

$$N_\alpha(\mathbf{k})=(1/k^0)\varphi_\alpha^*(\mathbf{k})\varphi_\alpha(\mathbf{k})$$

has the eigenvalues 0, 1, 2, $\cdots$ and represents the number of mesons in the state $(\alpha,\mathbf{k})$.

The interaction energy is

$$H'=if\tau_\alpha\int\frac{d^3k}{k^0}(\boldsymbol{\sigma},\mathbf{k})$$
$$\times\{\varphi_\alpha(\mathbf{k})e^{i(k,z)}-\varphi_\alpha^*(\mathbf{k})e^{-i(k,z)}\} \tag{12}$$

with

$$f=g/2\pi.$$

The λ process may be introduced, as Dirac[13] has shown, by a change in the commutation rules of the field operators which enter into the interaction energy. In x space these commutation rules may be written

$$i[\tilde{\psi}_\alpha(x),\tilde{\psi}_\beta(x')]=\delta_{\alpha\beta}D_\lambda(x-x'), \tag{13}$$

where

$$D_\lambda(x)=\tfrac{1}{2}\{D(x+\lambda)+D(x-\lambda)\}. \tag{14}$$

$\lambda=\{\boldsymbol{\lambda},\lambda^0\}$ is a time-like four vector, $(\lambda,\lambda)<0$, (15)

[10] In the complex notation this term corresponds to the expression

$$H'=g(8\pi)^{\frac{1}{2}}[\tau_-(\boldsymbol{\sigma},\operatorname{grad})\psi^*+\tau_+(\boldsymbol{\sigma},\operatorname{grad})\psi]$$

with $\tau_\pm=1/2(\tau_1\pm i\tau_2)$. Our g is therefore $\sqrt{2}$ times the coupling constant which is usually used in the literature.

[11] See W. Pauli and S. M. Dancoff, Phys. Rev. **62**, 105 (1942). There would be a third term in the total current due to the proton which, however, in our approximation is zero, since the velocity (although not the momentum) of the nucleons is zero.

[12] See W. Pauli, Rev. Mod. Phys. **13**, 210 (1942).

[13] P. A. M. Dirac, Ann. de l'Inst. Henri Poincaré **9**, 13 (1939).

which ultimately goes to zero in such a way that the inequality (15) is always satisfied. If λ transforms like a four vector, then the scheme is evidently relativistically invariant. In k space the introduction of the λ process shows itself in the commutation rules

$$[\tilde{\varphi}_\alpha(\mathbf{k}), \tilde{\varphi}_\beta^*(\mathbf{k}')] = k^0\delta_{\alpha\beta}\delta(\mathbf{k}-\mathbf{k}')\cos(k,\lambda) \quad (16)$$

which follow from (13).

A possible representation of the $\tilde{\varphi}_\alpha(\mathbf{k})$ in terms of the $\varphi_\alpha(\mathbf{k})$ is given by

$$\tilde{\varphi}_\alpha(\mathbf{k}) = \varphi_\alpha(\mathbf{k})\left\{\cos\frac{(k,\lambda)}{2} - \sin\frac{(k,\lambda)}{2}\right\},$$

$$\tilde{\varphi}_\alpha^*(\mathbf{k}) = \varphi_\alpha^*(\mathbf{k})\left\{\cos\frac{(k,\lambda)}{2} + \sin\frac{(k,\lambda)}{2}\right\}.$$

The quantities which depend on the field alone remain unchanged.[14] For instance, the magnetic moment may be written

$$M_{\mu\nu} = M_{\mu\nu}^{(1)} + M_{\mu\nu}^{(2)}, \quad (17)$$

$$M_{\mu\nu}^{(1)} = \frac{e}{2}\int\left\{x_\mu\left(\frac{\partial\psi_1}{\partial x^\nu}\psi_2 - \frac{\partial\psi_2}{\partial x^\nu}\psi_1\right) - x_\nu\left(\frac{\partial\psi_1}{\partial x^\mu}\psi_2 - \frac{\partial\psi_2}{\partial x^\mu}\psi_1\right)\right\}d^3x$$

$$= \frac{ei}{4(2\pi)^3}\int d^3x\left\langle x_\mu\int\int\frac{d^3l}{l_0}\frac{d^3l'}{l_0'} \times[\{\varphi_1(\mathbf{l})e^{i(l,x)} - \varphi_1^*(\mathbf{l})e^{-i(l,x)}\} \times\{\varphi_2(\mathbf{l}')e^{i(l',x)} + \varphi_2(\mathbf{l}')e^{-i(l',x)}\} - \text{sym. } (12)] - \text{sym. } (\mu\nu)\right\rangle, \quad (18)$$

where sym. $(\mu\nu)$ stands for the preceding expression with the indices μ and ν interchanged.

$$M_{\mu\nu}^{(2)} = \frac{e}{2}g(4\pi)^{\frac{1}{2}}(z_\mu\sigma_\nu - z_\nu\sigma_\mu)\frac{1}{\sqrt{2}(2\pi)^{\frac{1}{2}}} \times\int\frac{d^3k}{k^0}[\tau_2\{\tilde{\varphi}_1(\mathbf{k})e^{i(k,x)} + \tilde{\varphi}_1^*(\mathbf{k})e^{-i(k,x)}\} - \text{sym. } (1,2)]. \quad (19)$$

The first of these two expressions may be simplified by replacing x_μ by a differentiation of the exponential and subsequent integration by parts

$$M_{\mu\nu}^{(1)} = -\frac{e}{4(2\pi)^3}\int d^3x\int\frac{d^3l}{l_0}\frac{d^3l'}{l_0'} \times\left\langle l_\nu\left[\left\{\frac{\partial\varphi_1(\mathbf{l})}{\partial l^\mu}e^{i(l,x)} + \frac{\partial\varphi_1^*(\mathbf{l})}{\partial l^\mu}e^{-i(l,x)}\right\} \times\{\varphi_2(\mathbf{l}')e^{i(l',x)} + \varphi_2^*(\mathbf{l}')e^{-i(l',x)}\} - \text{sym. } (12)\right] - \text{sym. } (\mu\nu)\right\rangle. \quad (20)$$

Using

$$\frac{1}{(2\pi)^3}\int\exp[i(\mathbf{l},\mathbf{x})]d^3x = \delta(\mathbf{l})$$

we find

$$M_{\mu\nu}^{(1)} = \frac{e}{4}\int\frac{d^3l}{l_0^2}\left[l_\nu\left\{\left(\frac{\partial\varphi_2(\mathbf{l})}{\partial l^\mu}\varphi_1(-\mathbf{l})e^{-2il_0x_0} + \frac{\partial\varphi_2^*(\mathbf{l})}{\partial l^\mu}\varphi_1(\mathbf{l}) + \text{compl. conj.}\right) - \text{sym. } (1,2)\right\} - \text{sym. } (\mu\nu)\right]. \quad (21)$$

The Schrödinger functional Ω satisfies the Schrödinger equation

$$i(\partial\Omega/\partial x^0) = H'\Omega. \quad (22)$$

We look for stationary solutions of this equation which are correct up to the second order in g. For that purpose we write

$$\Omega = \Omega_0 + \Omega_1 + \Omega_2 + \cdots,$$

where $\Omega_0, \Omega_1, \Omega_2, \cdots$ represent those parts of the functional with 0, 1, 2, $\cdots$ mesons present. The leading terms of these functionals will then be of zeroth, first, second, $\cdots$ order in the coupling constant g.

Let u represent the state of the nucleon which we choose in such a way that $\sigma_3 u = u$. The spin then points in the positive z direction. Furthermore, let ω represent that state of the field in which no mesons are present, so that

$$\varphi_\alpha(\mathbf{k})\omega = 0. \quad (23)$$

Then we have for $\Omega_0 = u\omega$.

We then write the equations for the Ω's

$$i(d\Omega_1/dx^0) = H'\Omega_0, \qquad i(d\Omega_2/dx^0) = H'\Omega_1. \quad (24)$$

[14] This definition of the adjoint operators of the $\bar{\varphi}$ is a generalization of the Hermitian conjugate, similar to the one described by Pauli in a paper to be published in the Rev. Mod. Phys.

If we can integrate these equations, we can use the Ω's to calculate the expectation value of $M_{12} \equiv M_3$.

$$\bar{M}_3 = \Omega^* M_3 \Omega = 2\Omega_0^* M_3^{(1)} \Omega_2 + \Omega_1^* M_3^{(1)} \Omega_1 + 2\Omega_0 M_3^{(2)} \Omega_1 \quad (25)$$

since M_3 is Hermitian.

It is seen from the last equation that only terms of zero order in g which occur in Ω_0 will contribute anything to the magnetic moment in our approximation. With this remark in mind we can integrate the equations (24) approximately. The first one with the help of (22) and (23) reads

$$i\frac{d}{dx^0}\Omega_1 = -if\tau_\alpha \int \frac{d^3k}{k^0}(\sigma, \mathbf{k})\tilde{\varphi}_\alpha^*(\mathbf{k})e^{-i(k,x)}u\omega$$

or

$$\Omega_1 = if\tau_\alpha \int \frac{d^3k}{k_0^2}(\sigma, \mathbf{k})\tilde{\varphi}_\alpha^*(\mathbf{k})e^{-i(k,x)}u\omega \quad (26)_1$$

and from this and the second equation of (22) we get

$$\begin{aligned} i\frac{d}{dx^0}\Omega_2 &= f^2\tau_\alpha\tau_\beta \int \frac{d^3k'}{k^{0\prime}}(\sigma, \mathbf{k}')\tilde{\varphi}_\alpha^*(\mathbf{k}')e^{-i(k',x)} \\ &\quad \times \int \frac{d^3k}{k_0^2}(\sigma, \mathbf{k})e^{-i(k,x)}u\omega, \\ \Omega_2 &= -\tau_\alpha\tau_\beta f^2 \int \frac{d^3k'}{k_0'(k_0+k_0')}\frac{d^3k}{k_0^2}(\sigma, \mathbf{k}')(\sigma, \mathbf{k}) \\ &\quad \times \tilde{\varphi}_\alpha^*(\mathbf{k}')\tilde{\varphi}_\beta^*(\mathbf{k})e^{-i(k'+k,x)}u\omega. \end{aligned} \quad (26)_2$$

These integrations are only approximately correct since the operators φ_α and φ_α^* are slowly varying according to (10). But this variation would lead to a correction term to Ω_0 of the second order and a similar term in Ω_1 of the third order. Another term of the second order has been neglected by including in the expression $H'\Omega_1$ only those terms which correspond to two mesons present. In view of the above remark, we may, for our approximation, neglect all these terms. With these wave functions we can now calculate the expectation value of the magnetic moment. First we prove that the last term in (25) does not contribute anything in this approximation. This term is proportional to

$$u^*\omega^*(z_1\sigma_2 - z_2\sigma_1)\int \frac{d^3k}{k^0}\{\tau_2\tilde{\varphi}_1(\mathbf{k})e^{i(k,x)} - \text{sym. (12)}\} \times \tau_\alpha \int \frac{d^3k'}{k_0'^2}(\sigma, \mathbf{k}')\tilde{\varphi}_\alpha^*(\mathbf{k}')e^{-i(k',x)}u\omega,$$

which is equal to

$$-iu^*(z_1\sigma_2 - z_2\sigma_1)\tau_3 \int \frac{d^3k}{k_0^2}(\sigma, \mathbf{k})u\cos(k, \lambda)$$

when we use the commutation relations. The integral vanishes and therefore

$$\Omega_0^* M_3^{(2)} \Omega_1 = 0.$$

Of the remaining terms let us first calculate $\Omega_1^* M_3 \Omega_1 = \bar{M}_3^{\mathrm{I}}$. We notice at once that only the part in M_3 which contains an emission and an absorption operator can give a contribution to this expression. The remaining part may be simplified by adding to it the expression

$$\left(k_2\frac{\partial}{\partial k_1} - k_1\frac{\partial}{\partial k_2}\right)\{\varphi_1^*\varphi_2 + \varphi_1\varphi_2^*\}$$

which vanishes when integrated over k space. In this way we obtain for the part M_3^{I} of M_3 [15]

$$\begin{aligned} M_3^{\mathrm{I}} &= \frac{e}{2}\int \frac{d^3k}{k_0^2}\Big[k_\nu\Big(\varphi_1^*(\mathbf{k})\frac{\partial\varphi_2(\mathbf{k})}{\partial k_x} + \varphi_1(\mathbf{k})\frac{\partial\varphi_2^*(\mathbf{k})}{\partial k_x}\Big) - \text{sym. } (x\nu)\Big], \\ \bar{M}_3^{\mathrm{I}} &= \frac{e}{2}f^2u^*\omega^*\tau_\alpha\tau_\beta \int\int \frac{d^3k}{k_0^2}\frac{d^3k'}{k_0'^2}(\sigma, \mathbf{k})(\sigma, \mathbf{k}') \\ &\quad \times e^{i(k-k',x)}\tilde{\varphi}_\alpha(k)\int \frac{d^3l}{l_0^2}\Big[l_\nu\Big(\varphi_1^*(\mathbf{l})\frac{\partial\varphi_2(\mathbf{l})}{\partial l_x} + \varphi_1(\mathbf{l})\frac{\partial\varphi_2^*(\mathbf{l})}{\partial l_x}\Big) - \text{sym. } (x\nu)\Big] \\ &\quad \times \tilde{\varphi}_\beta^*(\mathbf{k}')u\omega. \end{aligned} \quad (27)$$

This expression may be simplified by using the commutation rules (11). We have

$$\begin{aligned} &\omega^*\tau_\alpha\tau_\beta\tilde{\varphi}_\alpha(\mathbf{k})\Big[l_\nu\Big(\varphi_1^*(\mathbf{l})\frac{\partial\varphi_2(\mathbf{l})}{\partial l_x} + \varphi_1(\mathbf{l})\frac{\partial\varphi_2^*(\mathbf{l})}{\partial l_x}\Big) - \text{sym. } (x\nu)\Big]\tilde{\varphi}_\beta^*(\mathbf{k}')\omega \\ &= \tau_1\tau_2 l_0^2\Big[l_\nu\Big(\delta(\mathbf{k}-\mathbf{l})\frac{\partial}{\partial l_x}\delta(\mathbf{l}-\mathbf{k}') - \delta(\mathbf{l}-\mathbf{k}')\frac{\partial}{\partial l_x}\delta(\mathbf{k}-\mathbf{l}) - \text{sym. } (x\nu)\Big]\cos(l, \lambda), \end{aligned}$$

[15] In order to avoid ambiguity we have put $\mu = x$, $\nu = y$.

so that after a partial integration[16]

$$\bar{M}_3^{\mathrm{I}}=-if^2u^*\tau_3\int\frac{d^3k}{k_0^4}\{\sigma_1k_2-\sigma_2k_1\}(\boldsymbol{\sigma},\mathbf{k})u\cos(k,\lambda).$$

If we choose a special coordinate system for which the space part of λ is zero, we may first carry out the integration over the angles and obtain

$$\bar{M}_3^{\mathrm{I}}=\frac{8\pi}{3}f^2u^*\tau_3u\int\left(\frac{k}{k_0}\right)^4\cos k_0\lambda_0dk.$$

The integral may be evaluated in the following way

$$\int\left(\frac{k}{k_0}\right)^4\cos k_0\lambda_0dk=\int\cos k_0\lambda_0dk-\int\frac{k_0^4-k^4}{k_0^4}\cos k_0\lambda_0dk.$$

The first integral is zero in the limit $\lambda_0=0$, as is shown in the appendix, and for the second we get $-(3\pi/4)\mu$, by going to the limit $\lambda_0=0$ before carrying out the integration so that finally

$$\bar{M}_3^{\mathrm{I}}=\mp2\pi^2f^2e\mu=\mp(g\mu)^2(e/2\mu). \tag{28}$$

The upper sign is for the proton and the lower for the neutron.

For the calculation of $2\Omega_0^*M_3\Omega_2$ we need only to consider that part in M_3 which contains two absorption operators

$$M_3^{\mathrm{II}}=\frac{e}{4}\int\frac{d^3k}{k_0^2}\left[k_\nu\left(\varphi_1(-\mathbf{k})\frac{\partial\varphi_2(\mathbf{k})}{\partial k_x}-\text{sym. (12)}\right)-\text{sym. }(xy)\right]e^{-2ik_0z_0},$$

$$\bar{M}_3^{\mathrm{II}}=-\frac{e}{2}f^2u^*\omega^*\tau_\alpha\tau_\beta\int\frac{d^3l}{l_0^2}\left[l_\nu\left(\varphi_1(-1)\frac{\partial\varphi_2(1)}{\partial l_x}\times e^{-2il_0z_0}-\text{sym. (12)}\right)-\text{sym. }(xy)\right]\times\int\int\frac{d^3k'}{k_0(k_0+k_0')}\frac{d^3k}{k_0^2}(\boldsymbol{\sigma},\mathbf{k}')(\boldsymbol{\sigma},\mathbf{k})\times\tilde{\varphi}_\alpha^*(\mathbf{k}')\tilde{\varphi}_\beta^*(\mathbf{k})e^{-i(k+k',z)}u\omega.$$

[16] We have dropped terms which arise from the differentiation of the cos-factor and which tend to zero as λ goes to zero and terms coming from the differentiation of the exponential function which leads to an expression of the form $\sigma_1z_2-\sigma_2z_1$ and which is zero after averaging over z.

Again applying the commutation rules we have

$$u^*\omega^*\tau_\alpha\tau_\beta\left[l_\nu\left(\varphi_1(-1)\frac{\partial\varphi_2(1)}{\partial l_x}-\text{sym. (12)}\right)-\text{sym. }(xy)\right]\varphi_\alpha^*(\mathbf{k}')\varphi_\beta^*(\mathbf{k})u\omega$$

$$=2iu^*\tau_3l_0^2\left[\delta(1+\mathbf{k}')\left(l_\nu\frac{\partial}{\partial l_x}\delta(1-\mathbf{k})-l_x\frac{\partial}{\partial l_\nu}\delta(1-\mathbf{k})\right)-\delta(1+\mathbf{k}')\left(l_\nu\frac{\partial}{\partial l_x}\delta(1-\mathbf{k}')-l_\nu\frac{\partial}{\partial l_x}\delta(1-\mathbf{k}')\right)\right]\cos(k,\lambda),$$

$$\bar{M}_3^{\mathrm{II}}=2ief^2u^*\tau_3\int\int\frac{d^3k'}{k_0(k_0+k_0')}\frac{d^3k}{k_0^2}\times(\sigma_1k_2'-\sigma_2k_1')(\boldsymbol{\sigma},\mathbf{k})\delta(\mathbf{k}+\mathbf{k}')u$$

$$=\frac{8\pi}{3}ef^2\int\left(\frac{k}{k_0}\right)^4\cos(k,\lambda)dku^*\tau_3u=\mp(g\mu)^2\frac{e}{2\mu}. \tag{29}$$

The total magnetic moment due to the pseudoscalar meson field is

$$\bar{M}_3=\mp2(g\mu)^2(e/2\mu) \tag{30}$$

for the proton and neutron, respectively.

3. THE VECTOR THEORY

The mesons of spin 1 are described by a complex vector field ψ_μ satisfying the equations

$$\Box\psi_\mu-\mu^2\psi_\mu=0,\quad\partial\psi_\mu/\partial x_\mu=0. \tag{31}$$

It is quantized according to

$$i[\psi_\mu(x),\psi_\nu^*(x')]=\left(g_{\mu\nu}-\frac{1}{\mu^2}\frac{\partial^2}{\partial x^\mu\partial x^\nu}\right)\times D(x-x'). \tag{32}$$

The current is defined in terms of the quantities ψ_μ and $\psi_{\mu\nu}=(\partial\psi_\nu/\partial x^\mu)-(\partial\psi_\mu/\partial x^\nu)$.

$$s_\mu=i(\psi_{\mu\nu}^*\psi^\nu-\psi^{*\nu}\psi_{\mu\nu}) \tag{33}$$

and the magnetic moment is then again given by Eq. (4) of the preceding section.

We decompose the field again in the real fields by

$$\psi_\mu=\frac{1}{\sqrt{2}}(\psi_\mu{}^1-i\psi_\mu{}^2),\quad\psi_{\mu\nu}=\frac{1}{\sqrt{2}}(\psi_{\mu\nu}^1-i\psi_{\mu\nu}^2).$$

We put $\psi=\{\psi_k\}(k=1, 2, 3)$ and write for the interaction energy

$$H'=g(4\pi)^{\frac{1}{2}}\tau_\alpha(\sigma, \text{curl})\psi^\alpha(z), \tag{34}$$

with this interaction present the current is

$$s_\mu=(\psi^1_{\mu\nu}\psi^{2\nu}-\psi^2_{\mu\nu}\psi^{1\nu}) + g(4\pi)^{\frac{1}{2}}\{\sigma\times(\psi^1\tau_2-\psi^2\tau_1)\}_\mu\delta(\mathbf{x}-\mathbf{z}). \tag{35}$$

The second part corresponds to the second part in (8) in the scalar theory. It will give rise to an additional term in the magnetic moment. A consideration similar to the one given above will show that this term does not contribute anything to the expectation value of the magnetic moment within the limits of our approximation.

We develop $\psi_\mu{}^\alpha$ and $\psi^\alpha_{\mu\nu}$ in eigenstates in momentum space

$$\psi_\mu{}^\alpha(x)=\frac{1}{\sqrt{2}(2\pi)^{\frac{1}{2}}}\int\frac{d^3k}{k^0} \times\{\varphi_\mu{}^\alpha(\mathbf{k})e^{i(k,x)}+\varphi_\mu{}^{*\alpha}(\mathbf{k})e^{-i(k,x)}\} \tag{36}$$

and

$$\psi_{\mu\nu}{}^\alpha(x)=\frac{1}{\sqrt{2}(2\pi)^{\frac{1}{2}}}\int\frac{d^3k}{k^0} \times\{(k_\mu\varphi_\nu{}^\alpha(\mathbf{k})-k_\nu\varphi_\mu{}^\alpha(\mathbf{k}))e^{i(k,x)} -(k_\mu\varphi_\nu{}^{*\alpha}(\mathbf{k})-k_\nu\varphi_\mu{}^{*\alpha}(\mathbf{k}))e^{-i(k,x)}. \tag{37}$$

Because of the subsidiary condition $\partial\psi_\mu/\partial x^\mu=0$ the $\varphi_\mu{}^\alpha(\mathbf{k})$ satisfy the equations

$$(\varphi^\alpha, k)=(\varphi^{*\alpha}, k)=0.$$

From the commutation relations (32) it follows that

$$[\varphi_\mu{}^\alpha(\mathbf{k}), \varphi_\nu{}^{*\beta}(\mathbf{k}')] =k^0\left(g_{\mu\nu}+\frac{1}{\mu^2}k_\mu k_\nu\right)\delta(\mathbf{k}-\mathbf{k}')\delta_{\alpha\beta}. \tag{38}$$

The $\varphi_\mu{}^\alpha$, $\varphi_\mu{}^{*\alpha}$ again are defined in such a way that they are slowly varying according to

$$\frac{d\varphi_\mu{}^\alpha}{dx^0}=i[H', \varphi_\mu{}^\alpha]. \tag{39}$$

For H' we get from (34) in momentum space

$$H'=if\tau_\alpha\int\frac{d^3k}{k^0}\{(\sigma, [\mathbf{k}\times\boldsymbol{\phi}^\alpha])e^{i(k,x)} -(\sigma, [\mathbf{k}\times\boldsymbol{\phi}^\alpha])e^{-i(k,x)}\}, \tag{40}$$

$f=g/2\pi$.

The λ process is again introduced by defining the operators $\tilde{\varphi}_\mu{}^\alpha$ and $\tilde{\varphi}_\mu{}^{*\alpha}$ as was done in the scalar theory. As before this is equivalent to replacing the D function in (32) by the D_λ function. This alters the commutation relations (38) in momentum space to

$$[\tilde{\varphi}_\mu{}^\alpha(\mathbf{k}), \tilde{\varphi}_\nu{}^{*\beta}(\mathbf{k}')]=k^0\delta_{\alpha\beta}\left(g_{\mu\nu}+\frac{1}{\mu^2}k_\mu k_\nu\right) \times\delta(\mathbf{k}-\mathbf{k}')\cos(k, \lambda). \tag{41}$$

The magnetic moment operator

$$M_{\mu\nu}=\frac{e}{2}\int\{x_\mu(\psi^1_{\nu\rho}\psi^{2\rho}-\psi^2_{\nu\rho}\psi^{1\rho}) -x_\nu(\psi^1_{\mu\rho}\psi^{2\rho}-\psi^2_{\mu\rho}\psi^{1\rho})\}d^3x \tag{42}$$

may be transformed with a calculation exactly analogous to that which led to the expression (21) in the scalar theory to give

$$M_{\mu\nu}=\frac{e}{4}\int\frac{d^3l}{l_0{}^2}\Big\langle\Big\{\Big[\Big(l_\nu\frac{\partial\varphi_\rho{}^2(\mathbf{l})}{\partial l^\mu}-l_\rho\frac{\partial\varphi_\nu{}^2(\mathbf{l})}{\partial l^\mu}\Big) \times\varphi^{1\rho}(-\mathbf{l})e^{-2il_0x_0} +\Big(l_\nu\frac{\partial\varphi_\rho{}^{*2}(\mathbf{l})}{\partial l^\mu}-l_\rho\frac{\partial\varphi_\nu{}^{*2}(\mathbf{l})}{\partial l^\mu}\Big)\varphi^{1\rho}(\mathbf{l}) +\text{compl. conj.}\Big]-\text{sym. (12)}\Big\}-\text{sym. }(\mu\nu)\Big\rangle. \tag{43}$$

The solutions of the equations

$$i(d/dx^0)\Omega_1=H'\Omega_0, \quad i(d/dx^0)\Omega_2=H'\Omega_1, \tag{44}$$

corresponding to the solutions (26) in the scalar theory are then

$$\begin{aligned}\Omega_0&=u\omega,\\ \Omega_1&=if\tau_\alpha\int\frac{d^3k}{k_0{}^2}(\sigma, [\mathbf{k}\times\tilde{\boldsymbol{\phi}}^{*\alpha}])e^{-i(k,x)}u\omega,\\ \Omega_2&=-f^2\tau_\alpha\tau_\beta\int\frac{d^3k}{k_0(k_0+k_0')}\frac{d^3k}{k_0'{}^2}(\sigma, [\mathbf{k}\times\tilde{\boldsymbol{\phi}}^{*\alpha}]) \times(\sigma, [\mathbf{k}'\times\tilde{\boldsymbol{\phi}}^{*\beta}])e^{-i(k+k',x)}u\omega.\end{aligned} \tag{45}$$

The part $\bar{M}_3^{\mathrm{I}}$ corresponding to (27) is

$$\bar{M}_3^{\mathrm{I}}=\tfrac{1}{2}ef^2u^*\omega^*\tau_\alpha\tau_\beta\int\int\frac{d^3k}{k_0^2}\frac{d^3k'}{k_0'^2}\times(\boldsymbol{\sigma},[\mathbf{k}\times\tilde{\boldsymbol{\phi}}^\alpha])e^{i(k-k',z)}\int\frac{d^3l}{l_0^2}\times\left\{\left[\left(l_y\frac{\partial\varphi_\rho^{*2}}{\partial l_x}-l_\rho\frac{\partial\varphi^{*2}}{\partial l_x}\right)\varphi^{1\rho}+\text{compl. conj.}\right]-\text{sym. }(xy)\right\}\times(\boldsymbol{\sigma},[\mathbf{k}'\times\tilde{\boldsymbol{\phi}}^{*\beta}])u\omega. \quad (46)$$

Writing

$$(\boldsymbol{\sigma},[\mathbf{k}\times\tilde{\boldsymbol{\phi}}^\alpha])=-i\sigma_r\sigma_s k_r\tilde{\varphi}_s{}^\alpha \quad (r\neq s)$$

we can simplify the expression (46) considerably by using the commutation rules (37)

$$-\omega^*\tau_\alpha\tau_\beta\sigma_r\sigma_s k_r k_s\varphi_s{}^\alpha\left\{\left[\left(l_y\frac{\partial\varphi_\rho^{*2}}{\partial l_x}-l_\rho\frac{\partial\varphi_y^{*2}}{\partial l_x}\right)\varphi^{1\rho}+\text{compl. conj.}\right]-\text{sym. }(xy)\right\}\sigma_t\sigma_h k_t'\varphi_h^{*\beta}\omega \quad \begin{matrix}r\neq s\\ t\neq h\end{matrix}$$

$$=-2\tau_\alpha\tau_\beta\sigma_r\sigma_s k_r k_0\left\{\left[l_y\delta_{\alpha 2}\left(\delta_{s\rho}+\frac{1}{\mu^2}k_s k_\rho\right)\frac{\partial}{\partial l_x}\times\delta(\mathbf{k}-1)-l_\rho\delta_{\alpha 2}\left(\delta_{sy}+\frac{1}{\mu^2}k_s k_y\right)\frac{\partial}{\partial l_x}\delta(\mathbf{k}-1)\right]\times l_0\delta_{1\beta}\left(\delta_{\rho h}+\frac{1}{\mu^2}l_\rho l_h\right)-\text{sym. }(xy)\right\}\times\delta(1-\mathbf{k}')\sigma_t\sigma_h k_t'\cos(k,\lambda). \quad \begin{matrix}r\neq\rho\\ t\neq\rho\end{matrix}$$

After multiplying with

$$(d^3k'/k_0'^2)\exp[i(k-k',z)]$$

and integrating over k' we get by using

$$\sum_{r\neq s}\sigma_r\sigma_s k_r k_s=0$$

$$2i\tau_3(\sigma_r k_r)\frac{k_0}{l_0}\left[(l_y\sigma_\rho-l_\rho\sigma_y)(\sigma_t l_t)\sigma_\rho\frac{\partial}{\partial l_x}\delta(\mathbf{k}-1)-\text{sym. }(xy)\right]e^{i(k-l,z)}\cos(k,\lambda), \quad \begin{matrix}r\neq\rho\\ t\neq\rho\end{matrix}$$

so that (46) becomes

$$eif^2u^*\tau_3\int\frac{d^3k}{k_0}\frac{d^3l}{l_0^3}(\sigma_r k_r)\left[(l_y\sigma_\rho-l_\rho\sigma_y)(\sigma_t l_t)\sigma_\rho\times\frac{\partial}{\partial l_x}\delta(\mathbf{k}-1)-\text{sym. }(xy)\right]e^{i(k-l,z)}\cos(k,\lambda). \quad (47)$$

$$r\neq\rho,\ t\neq\rho$$

Integrating by parts over 1 first we get a term from the differentiation of $1/l_0^3$ which, however, is zero just as in the scalar theory because it contains a factor $\sigma_t\sigma_\rho l_t l_\rho=0$ since $t\neq\rho$.

The other part gives a term

$$(\sigma_2k_2+\sigma_3k_3)\sigma_2(\sigma_2k_2+\sigma_3k_3)\sigma_1-(\sigma_1k_1+\sigma_3k_3)\sigma_1(\sigma_1k_1+\sigma_3k_3)\sigma_2+(\sigma_1k_1+\sigma_2k_2)(k_3\sigma_2-k_2\sigma_3)\sigma_1\sigma_3-(\sigma_1k_1+\sigma_2k_2)(k_3\sigma_1-k_1\sigma_3)\sigma_2\sigma_3.$$

Most of these terms will give zero after the integration over the angles. The only term different from zero is

$$-i\sigma_3(k_1^2+k_2^2);$$

introducing this in (47) we get

$$\bar{M}_3^{\mathrm{I}}=\pm ef^2\frac{8\pi}{3}\int\left(\frac{k}{k_0}\right)^4\cos k_0\lambda_0 dk=\mp 2\pi^2ef^2\mu.$$

The term $\bar{M}_3^{\mathrm{II}}$ is

$$\bar{M}_3^{\mathrm{II}}=-f^2eu^*\omega^*\tau_\alpha\tau_\beta\int\int\frac{d^3k}{k_0(k_0+k_0')}\frac{d^3k'}{k_0'^2}\times e^{-i(k+k',z)}\int\frac{d^3l}{l_0^2}\left[\left(l_y\frac{\partial\varphi_\rho{}^2}{\partial l_x}-l_\rho\frac{\partial\varphi_y{}^2}{\partial l_x}\right)\times\varphi^{1\rho}(-1)e^{-2il_0x_0}-\text{sym. }(xy)\right]\times(\boldsymbol{\sigma},[\mathbf{k}\times\tilde{\boldsymbol{\phi}}^{*\alpha}])(\boldsymbol{\sigma},[\mathbf{k}'\times\tilde{\boldsymbol{\phi}}^{*\beta}]).$$

A calculation similar to the one above leads to

$$2eif^2u^*\tau_3\int\int\frac{d^3kd^3l}{k_0(k_0+l_0)l_0^2}(\sigma_r k_r)\times\left[(l_2\sigma_\rho-l_\rho\sigma_2)(\sigma_t l_t)\sigma_\rho\frac{\partial}{\partial l_1}\delta(\mathbf{k}-1)-\text{sym. }(12)\right]\cos(k,\lambda). \quad \begin{matrix}r\neq\rho\\ t\neq\rho\end{matrix}$$

In comparing this with (47) we find that again we have

$$\bar{M}_3^{\mathrm{II}}=\mp 2\pi^2ef^2\mu,$$

so that the total magnetic moment in the vector theory is

$$\bar{M}_3=\bar{M}_3^{\mathrm{I}}+\bar{M}_3^{\mathrm{II}}=\mp 2(g\mu)^2(e/2\mu).$$

The upper sign is for the proton and the lower for the neutron. This is the same result as for the pseudoscalar meson.

4. A VECTOR MESON WITH AN ARBITRARY MAGNETIC MOMENT

The Lagrangian for a vector meson field is not unique insofar as it is possible to introduce terms in the Lagrange-function which are proportional to the external electromagnetic field.[17] Such a term makes itself felt in an altered expression for the current density and consequently a change in the magnetic moment. The additional current density is

$$s_\mu' = -iK\frac{\partial}{\partial x_\rho}(\psi_\rho^*\psi_\mu - \psi_\mu^*\psi_\rho), \tag{48}$$

where K is a dimensionless and arbitrary constant. The change in the magnetic moment operator is then from Eq. (4)

$$\begin{aligned} M'_{\mu\nu} &= ieK\int(\psi_\mu^*\psi_\nu - \psi_\nu^*\psi_\mu)d^3x \\ &= eK\int(\psi_\mu'\psi_\nu^2 - \psi_\nu'\psi_\mu^2)d^3x \\ &= \tfrac{1}{2}eK\int\frac{d^3k}{k_0^2}\{[(\varphi_\mu^1(\mathbf{k})\varphi_\nu^2(-\mathbf{k})e^{-2ik_0x_0} \\ &\quad + \varphi_\mu^1(\mathbf{k})\varphi_\nu^{*2}(\mathbf{k})) - \text{compl. conj.}] \\ &\quad - \text{sym. } (\mu\nu)\}. \end{aligned} \tag{49}$$

We have, therefore,

$$\begin{aligned} \bar{M}_3'^{\,I} &= 2eKf^2u^*\omega^*\tau_\alpha\tau_\beta\int\frac{d^3k}{k_0^2}\frac{d^3k'}{k_0'^2}(\sigma,[\mathbf{k}\times\tilde{\boldsymbol{\phi}}^\alpha]) \\ &\quad\times e^{i(k-k',x)}\int\frac{d^3l}{l_0^2}\varphi_1^1(\mathbf{l})\varphi_2^{*2}(\mathbf{l}) \\ &\quad\times[\sigma,[\mathbf{k}'\times\tilde{\boldsymbol{\phi}}^{*\beta}])u\omega, \\ &= -2eKf^2u^*\tau_3\sigma_3\frac{4\pi}{3}\int\left(\frac{k}{k_0}\right)^4\cos(k_0\lambda_0)dk \\ &= \pm K(g\mu)^2(e/2\mu). \end{aligned} \tag{50}$$

[17] See H. C. Corben and J. Schwinger, Phys. Rev. **58**, 953 (1940).

A similar calculation for $\bar{M}_3'^{\,II} = 2\Omega_0^* M_3\Omega_2$ leads to the same result so that

$$\bar{M}_3' = \bar{M}_3'^{\,I} + \bar{M}_3'^{\,II} = \pm 2K(g\mu)^2(e/2\mu). \tag{51}$$

The total magnetic moment in the vector theory is then

$$\bar{M}_3 = \pm 2(K-1)(g\mu)^2(e/2\mu) \tag{52}$$

for the proton and neutron, respectively.

Taking the two theories together and assuming for the vector meson twice the mass of the scalar meson, but the same coupling constant, we find

$$M = \pm 2(g\mu)^2\{2(K-1)-1\}(e/2\mu) \tag{53}$$

for $(g\mu)^2 \sim 0.1$, $\mu \sim \frac{1}{10}m$, $K \sim 2$,

$$M \sim \pm 2,$$

for the magnetic moment of proton and neutron, respectively, due to the meson field only. If we add to that the magnetic moment of the nucleons (0 for the neutron and $+1$ for the proton), we find agreement with the experiment within the limits of our calculation.

This problem was suggested to me by Professor W. Pauli of the Institute for Advanced Study. I am very grateful to him for his generosity in taking time for discussion and helpful advice.

APPENDIX

The integral $I = \int_0^\infty \cos k_0\lambda_0 dk$ may be evaluated in the following way. With the substitution $k = \mu i \sin v\lambda_0\mu = \alpha$, we have

$$I = \frac{i\mu}{4}\int_{-i\infty}^{+i\infty}\cos v(e^{i\alpha\cos v} + e^{-i\alpha\cos v})dv.$$

For the second integral we substitute v by $\pi - v$.

$$I = \frac{i\mu}{4}\left\{\int_{-i\infty}^{+i\infty}\cos ve^{i\alpha\cos v}dv + \int_{+i\infty+\pi}^{-i\infty+\pi}\cos ve^{i\alpha\cos v}dv\right\}.$$

The paths of integration have to be taken in the regions for which $Im(\cos v) > 0$, in order to secure the convergence of the integrals. They may be chosen in such a way that the contribution from the branches leading to infinity cancel, and we are then left with the expression

$$I = -\frac{i\mu}{2}\int_0^{2\pi}\cos ve^{i\alpha\cos v}dv = -\frac{\mu}{2\pi}J_1(\alpha) \quad \lim_{\alpha\to 0} I(\alpha) = 0.$$

PHYSICAL REVIEW VOLUME 63, NUMBERS 9 AND 10 MAY 1 AND 15, 1943

Ultra-High Frequency Oscillations of Cylindrical Cavity Resonators Containing Two and Three Dielectric Media

DAVID MIDDLETON
Cruft Laboratory and the Research Laboratory of Physics, Harvard University, Cambridge, Massachusetts
(Received October 26, 1942)

The mathematical problem of the perfectly conducting cylindrical cavity resonator containing two and three dielectrics is set up, and solved in terms of the electric and magnetic Hertzian vector potentials. The relations between the various natural frequencies and resonant lengths are determined and discussed, in particular for a cylindrical resonator containing a movable slab of dielectric. It is shown that modes of the form E_{np0} and H_{np0} are not excitable if there is more than one dielectric present in the resonator. The band transmission characteristics of such resonators are considered briefly, and a simple and convenient absolute method for the measurement of dielectric constants at microwave frequencies is suggested. Experimental measurements were made at 3070 megacycles per sec., for the H_{111} mode, and the results were found to agree well with the theory. Experimental and theoretical curves illustrating various points of the discussion are included.

I. INTRODUCTION

IT has been known for a long time that, if the frequency is sufficiently high, electromagnetic waves can be propagated inside conducting tubes of various cross sections, rectangular, circular, elliptical, etc.[1] Any closed, highly conducting chamber, practically not more than a few wavelengths long, may serve as a cavity resonator, inside of which standing wave patterns may be set up. Such resonators may oscillate in a large number of different modes,[2–4] the mode of oscillation depending on the manner of excitation.[5] By varying the dimensions of the cavity, one can tune the resonator to different frequencies; dielectrics (other than air), also, have a considerable effect on the resonant dimensions. In earlier work, King[6] and Lamont[7] have discussed this property of a dielectric of shifting resonant positions, with particular emphasis on the measurement of dielectric constants at ultra-high frequencies. King's paper describes a parallel wire method for measuring the dielectric constant of fluids and solids at wave-lengths around 2 meters, based on the solution of the telegraphist's equations for the parallel wire system. The measurement depends on a simple mathematical expression involving the dielectric constant, the frequency at which the measurement is made, the dielectric thickness for both liquids and solids, and a bridge shift measured along the parallel wires in air. Lamont extends the theory to include the hollow pipe or waveguide.[8] Both works emphasize the importance of the change in resonant length of the particular system used due to the presence of a dielectric medium, particularly for the measurement of the dielectric constant of the sample under test.

This paper, however, is concerned primarily with the problem of determining the relations between the natural modes and resonant lengths of a cylindrical cavity resonator containing several dielectrics. Some of the properties of such resonators as tunable circuit elements, and as wave filters, are discussed and finally, as a special case of the general theory, a simple method of measuring dielectric constants is suggested. This method differs from those described by King[6] and Lamont[7] in that a single resonance position is determined with the sample under test at one end of the resonator; the advantages are that the calculations are somewhat simplified and less

[1] Lord Rayleigh, Phil. Mag. **43**, 125–132 (1897).
[2] W. L. Barrow, Proc. I.R.E. **24**, 1298–1328 (1936).
[3] J. R. Carson and S. P. Schelkunoff, Bell Sys. Tech. J. **15**, 310–333 (1936).
[4] S. P. Schelkunoff, Proc. I.R.E. **25**, 1457–1492 (1937).
[5] G. C. Southworth, Proc. I.R.E. **25**, 807–832 (1937).
[6] R. King, Rev. Sci. Inst. **8**, 201–209 (1937).
[7] H. R. L. Lamont, Phil. Mag. **29**, 521–540 (1940).

[8] A distinction should be made between a cavity resonator and a waveguide. The waveguide is considerably longer, in fact, is treated mathematically as having infinite length; infinitely long waveguides are equivalent in the practical case to a finite guide terminated in its characteristic impedance. The waveguide may in general be treated analytically as a two-dimensional problem, whereas for cavity resonators the entire configuration, including the ends, must be considered.

experimental data are required, and in the case of fluids the data may be more conveniently taken, as no container is necessary. The disadvantage, however, is that the method is less sensitive because the maximum shift conditions are not necessarily satisfied.

It is the purpose, then, of this work to examine some of the resonant properties of cylindrical cavity resonators containing two and three dielectric media. The results indicate a new and convenient absolute method for the measurement of dielectric constants of good dielectrics, for wave-lengths around 10 cm. They show also that the resonator behaves like a band transmission filter for the particular mode excited, and further the analysis yields formulae involving the resonant lengths and frequencies, which, it is hoped, may be of use in future experimental measurements and in the design of tunable ultra-high frequency resonators. The theory applies generally for all modes and resonant dimensions of a tube containing three different dielectrics. Specifically, we will discuss the E_{011} and H_{111} modes and corresponding resonant lengths of

(a) a cylindrical resonator of fixed over-all length containing a movable slab of dielectric,
(b) a cylindrical resonator of variable over-all length containing a movable dielectric slab, and
(c) a resonator of variable total length containing a slab of dielectric at one end.

Solutions for the electric and magnetic fields, **E** and **H**, will be obtained in terms of Hertzian vector potentials,[9] and application of the various boundary conditions will then give us expressions involving the resonant lengths and frequencies.

II. MATHEMATICAL ANALYSIS

If we assume that the media considered are homogeneous and isotropic and if the disturbance is periodic with angular frequency $\omega=2\pi f$, we may express the wave equations in the following form:

$$\nabla\cdot\nabla\mathbf{\Pi}^{(s)}+\mu\epsilon'\omega^2\mathbf{\Pi}^{(s)}=0, \quad s=1, 2, \qquad (1)$$

where $\mathbf{\Pi}^{(1)}$ and $\mathbf{\Pi}^{(2)}$ denote, respectively, the electric and magnetic Hertzian vector potentials,

[9] J. A. Stratton, *Electromagnetic Theory* (McGraw-Hill, New York, 1941), p 28.

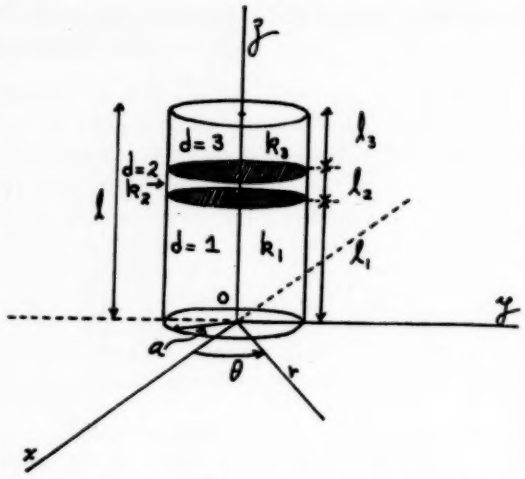

FIG. 1. Cylinder containing three dielectric media with constants ϵ_d, μ_d, $d=1, 2, 3$.

which are related to the field vectors by the formulas:

$$\mathbf{E}=\nabla\nabla\cdot\mathbf{\Pi}^{(1)}-\mu\epsilon'\ddot{\mathbf{\Pi}}^{(1)}-\mu\nabla\times\dot{\mathbf{\Pi}}^{(2)}, \qquad (2)$$

$$\mathbf{H}=\nabla\nabla\cdot\mathbf{\Pi}^{(2)}-\mu\epsilon'\ddot{\mathbf{\Pi}}^{(2)}+\epsilon'\nabla\times\dot{\mathbf{\Pi}}^{(1)}, \qquad (3)$$

and as usual, ϵ, μ, and σ are the dielectric constant, permeability, and conductivity, and ϵ' is given by

$$\epsilon'=\epsilon-i\sigma/\omega. \qquad (4)$$

Equations (1) may be converted into scalar wave equations,[10] and the solutions may be easily obtained. For cylindrical coordinates it can be shown that for our problem a complete set of solutions of Eq. (6) is made up of

$$J_n(\nu_{np}^{(s)}r)\begin{pmatrix}\cos\gamma_m^{(s)}z\\ \sin\gamma_m^{(s)}z\end{pmatrix}\cos n\theta;\ \begin{matrix}n=0, 1, 2\cdots\\ m=0, 1, 2\cdots\\ p=1, 2\cdots,\end{matrix} \qquad (5)$$

in various combinations to satisfy the boundary conditions. Choosing potentials having a z component only, we have for the E, or transverse magnetic modes alone ($s=1$):

$$\mathbf{E}_z=\mathbf{i}_1\frac{\partial^2\Pi_z^{(1)}}{\partial r\partial z}+\mathbf{i}_2\frac{\partial^2\Pi_z^{(1)}}{r\partial\theta\partial z}+\mathbf{i}_3(\nu_{np}^{(1)})^2\Pi_z^{(1)}, \qquad (6)$$

$$\mathbf{H}_z=\mathbf{i}_1\left(\frac{i\omega\epsilon+\sigma}{r}\right)\frac{\partial\Pi_z^{(1)}}{\partial\theta}-\mathbf{i}_2(i\omega\epsilon+\sigma)\frac{\partial\Pi_z^{(1)}}{\partial r}, \qquad (7)$$

and for the H, or transverse electric modes

[10] See reference 9, page 349 *et seq.*

alone, we have, $(s=2)$:

$$\mathbf{E}_z=-\mathbf{i}_1\frac{\omega\mu i\partial\Pi_z^{(2)}}{r\partial\theta}+\mathbf{i}_2\omega\mu i\frac{\partial\Pi_z^{(2)}}{\partial r}, \tag{8}$$

$$\mathbf{H}_z=\mathbf{i}_1\frac{\partial^2\Pi_z^{(2)}}{\partial r\partial z}+\mathbf{i}_2\frac{\partial^2\Pi_z^{(2)}}{r\partial\theta\partial z}+\mathbf{i}_3(\nu_{np}^{(2)})^2\Pi_z^{(2)}. \tag{9}$$

The quantities $\mathbf{i}_1$, $\mathbf{i}_2$, $\mathbf{i}_3$ are unit vectors in the r, θ and z directions, respectively; see Fig. 1 above; the values of $d=1$, 2, 3 designate the various media. Henceforth we will omit the subscript z on the field vectors, etc.

We shall assume that the cylinder is perfectly conducting and that the dielectrics are perfect. Then $\sigma=\infty$ for the cylinder, and $\sigma=0$ for the dielectrics.

For both the electric and magnetic modes, the boundary conditions[11] require that the $\mathbf{B}(=\mu\mathbf{H})$ and $\mathbf{D}(=\epsilon\mathbf{E})$ vectors vanish everywhere outside the inner boundaries of the cylinder since it is a perfect conductor, and that the normal components of the $\mathbf{B}$ field and the tangential components of the $\mathbf{E}$ field also vanish there, as well as at the interfaces of the dielectric. The surface charge density η and the surface current density $\mathbf{I}$ are determined from the remaining boundary conditions:

$$\mathbf{n}\cdot\mathbf{D}=\eta, \tag{10}$$

$$\mathbf{n}\times\mathbf{H}=\mathbf{I}, \tag{11}$$

where $\mathbf{n}$ is a unit vector normal to the surface under consideration. Since the dielectrics are assumed to be perfect, homogeneous, and isotropic, the surface current density $\mathbf{I}$ is zero at the dielectric interfaces, and the charge density η must be also.

In obtaining solutions of the scalar wave equations we will need one arbitrary constant $A_{mn1}^{(s)}$ for the first region, $0\leqq z\leqq l_1$, two constants, $A_{mn2}^{(s)}$ and $B_{mn2}^{(s)}$, for the second region, $l_1\leqq z\leqq l_1+l_2$, and finally one more constant $A_{mn3}^{(s)}$ for the third medium, $l_1+l_2\leqq z\leqq l$. In the separation of variables the following relations may be shown to hold:

$$(k_{mnp}^{(s)})^2=(\omega_{mn}^{(s)})^2\mu_d\epsilon_d=(\gamma_{md}^{(s)})^2+(\nu_{np}^{(s)})^2, \tag{12}$$

and it can also be shown that $\omega_{mnp}^{(s)}$ is the same for each dielectric, i.e., the system as a whole has but one resonant frequency for the particular mode excited.

The complete solutions then are, for medium one:

$$\Pi_1^{(s)}=\sum\begin{pmatrix}\cos\gamma_{m1}z\\ \sin\gamma_{m1}z\end{pmatrix}\times\exp(i\omega_{mnp}^{(s)}t), \tag{13}$$

for medium two:

$$\Pi_2^{(s)}=\sum\left(A_{mn2}^{(s)}\begin{matrix}\cos\gamma_{m2}z\\ \sin\gamma_{m2}z\end{matrix}+B_{mn2}^{(s)}\begin{matrix}\sin\gamma_{m2}z\\ \cos\gamma_{m2}z\end{matrix}\right)\times J_n(\nu_{np}^{(s)}r)\cos n\theta\exp(i\omega_{mnp}^{(s)}t), \tag{14}$$

and for medium three:

$$\Pi_3^{(s)}=\sum\begin{pmatrix}\cos\gamma_{m3}(l-z)\\ \sin\gamma_{m3}(l-z)\end{pmatrix}\times\exp(i\omega_{mnp}^{(s)}t). \tag{15}$$

The upper or lower line in the cos, sin applies according as $s=1$ or $s=2$.

The possible natural modes are described by the parameters n, p, m, in that order; where $n=0, 1, 2, \cdots$ is the order of $J_n(\nu_{np}^{(s)}r)$, p is the particular root for a given order n, and m depends on the length of the resonator; the parameters p and m may also take on any positive integral values. Thus, the E_{011} mode may be obtained from Eqs. (13)–(15) above by letting $n=0$, $p=1$, and $m=1$.

The expressions $\nu_{np}^{(s)}$ are determined from the equations

$$J_n(\nu_{np}^{(1)}a)=0;\quad J_n'(\nu_{np}^{(2)}a)=0, \tag{16}$$

where a is the radius of the cylindrical resonator.[12]

The following equations, obtained from the boundary conditions, suffice to determine the γ's and $\omega_{mn}^{(s)}$:[13]

$$\frac{(\gamma_1^{(s)})^2+(\nu^{(s)})^2}{\mu_1\epsilon_1}=\frac{(\gamma_2^{(s)})^2+(\nu^{(s)})^2}{\mu_2\epsilon_2}=\frac{(\gamma^{(s)})^2+(\nu^{(s)})^2}{\mu_3\epsilon_3}=(\omega^{(s)})^2, \tag{17}$$

$$c_d=1/(\mu_d\epsilon_d)^{\frac{1}{2}},$$

[11] See reference 9, pages 34–38, for a general discussion of boundary conditions.

[12] It is interesting to note that Eqs. (16) have p-infinite, discrete, positive roots, all of which are mutually distinct.

[13] Henceforth we shall omit subscripts wherever there is no ambiguity in so doing.

where the subscripts refer to the medium, and the superscripts distinguish between the electric and magnetic modes, as before, with c_d as the velocity of electromagnetic waves in medium d. The fourth equation is

$$\alpha_2^{(s)} \tan \gamma_3^{(s)} l_3 = \frac{\alpha_1^{(s)} \tan \gamma_1^{(s)} l_1 + \tan \gamma_2^{(s)} l_2}{\alpha_1^{(s)} \tan \gamma_1^{(s)} l_1 \tan \gamma_2^{(s)} l_2 - 1}; \quad s = 1, 2, \tag{18}$$

where the following abbreviations are used, for $s=1$:

$$\alpha_2^{(1)} = \epsilon_2 \gamma_3^{(1)} / \epsilon_3 \gamma_2^{(1)}; \quad \alpha_1^{(1)} = \epsilon_2 \gamma_1^{(1)} / \epsilon_1 \gamma_2^{(1)}. \tag{19}$$

and for $s=2$:

$$\alpha_2^{(2)} = \mu_3 \gamma_2^{(2)} / \mu_2 \gamma_3^{(2)}; \quad \alpha_1^{(2)} = \mu_1 \gamma_2^{(2)} / \mu_2 \gamma_1^{(2)}. \tag{20}$$

An important special case is that of two dielectric media enclosed by the perfectly conducting cylinder. To obtain the boundary condition equations, allow l_3 (or l_1) to approach zero. Then (17 and 18) become

$$\frac{(\gamma_1^{(s)})^2 + (\nu^{(s)})^2}{\mu_1 \epsilon_1} = \frac{(\gamma_2^{(s)})^2 + (\nu^{(s)})^2}{\mu_2 \epsilon_2} = (\omega^{(s)})^2, \tag{21}$$

and

$$\tan \gamma_2^{(s)} l_2 = -\alpha_1^{(s)} \tan \gamma_1^{(s)} l_1. \tag{22}$$

Expressions for the fields may be obtained by substituting (13)–(15) into (6)–(9), and the charge and current densities are then determined by (10) and (11). The relative field amplitudes in the various media may also be obtained without difficulty from the boundary conditions. The above analysis is easily generalized to include cross sections of the resonator other than circular, the only modification occurring for the terms involving the transverse dimensions.

III. CALCULATION OF THE RESONANT LENGTHS AND NATURAL MODES

Equations (18) are the expressions relating the resonant lengths l_1, l_2, l_3 for the E and H modes. It is immediately obvious that one possible set of solutions is

$$\gamma_{md}^{(s)} = \pi m / l_d, \quad m \neq 0, \quad d = 1, 2, 3. \tag{23}$$

This will be so only if

$$c_1^2[(m\pi/l_1)^2 + (\nu^{(s)})^2] = c_2^2[(m\pi/l_2)^2 + (\nu^{(s)})^2] = c_3^2[(m\pi/l_3)^2 + (\nu^{(s)})^2] \tag{24}$$

hold simultaneously.

For $m>0$ we have modes higher than the fundamental.* (In the calculations and discussion of the experimental work that follows we shall be concerned primarily with the modes for which $m=1$, and hence the subscripts for m on the γ's, may be omitted.) If m were equal to zero, then the propagation constants $\gamma_d^{(s)}$ for the three media would also be zero, which is immediately obvious from Eq. (23). Now $\omega^{(s)}$ does not depend on any particular medium, and generally the various velocities, $1/(\mu_d \epsilon_d)^{\frac{1}{2}}$, are different, so we see at once from Eq. (17) that $\gamma_d^{(s)}$ must be different from zero, and hence we conclude that *if there is more than one dielectric present in the resonator, it is not possible to excite modes of the type* E_{np0}, H_{np0}. This is physically plausible since we would not expect to be able to excite modes independent of the thickness and position of the dielectrics. Such modes may be excited, of course, if there is only one dielectric in the cylinder.

The set (23) is special in that (24) must hold also. But in general, the restrictions on l_1, l_2, l_3 are such that (24) will not be satisfied. The procedure is to choose any two of the lengths l_1, l_2, l_3 and a frequency, whence the third resonant length is determined from Eq. (18) for $s=1, 2$, depending on the type of mode excited. The quantities $\gamma_d^{(s)}$ are determined from (17) and are the same for the three media as well as for the two. The upper limit on $\gamma_{md}^{(s)}$ is given by $\pi m/l_d$, and the lower cut-off limit occurs when

$$\gamma_{md}^{(s)} = [(\omega_{mnp}^{(s)}/c_d)^2 - (\nu_{np}^{(s)})^2]^{\frac{1}{2}} = 0, \quad d = 1, 2, 3. \tag{25}$$

The lower cut-off frequency is determined by the medium having the lowest dielectric constant, i.e., for the value of $\omega_{mnp}^{(s)}/c_d$ which is smallest and still satisfies (25), which becomes

* *Note:* In the simple case of a resonant hollow pipe containing only one dielectric medium, the wave-length is given by $\lambda = 2\pi[(\gamma_m^{(s)})^2 + (\nu_{np}^{(s)})^2]^{-\frac{1}{2}}$, and the propagation constant $\gamma_m^{(s)}$ is determined from $\gamma_m^{(s)} m\pi/l$, where $m=0, 1, 2, \cdots$, and 1 is the over-all length of the resonator. When the pipe contains several different dielectrics, however, we can no longer use the term wave-length in the pipe, and $\gamma_m^{(s)}$ is then not in general equal to $m\pi/l$. This is because there are now as many different wave-lengths, and fractions thereof, in the tube, as there are different dielectric media and dielectric interfaces. In order to carry over symbolically the dependence of the higher modes on $\gamma_m^{(s)}$, in analogy with the one-dielectric case, we have used Eq. (23) to set the upper and lower limits on the propagation constant; for example, for the mode in which we have $m=3$, we have $2\pi/l_d < \gamma_{3d}^{(s)} \leqq 3\pi/l_d$. Additional half-wave-lengths in the various media now no longer define the modes, as far as dependence on the axial, or z direction is concerned.

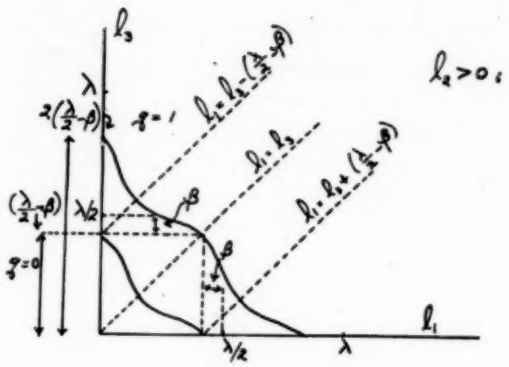

FIG. 2. Resonant length of one air space, $l_3^{(s)}$, as a function of $l_1^{(s)}$, a chosen resonant length of the other air space, for a given thickness of dielectric l_2, for one and two half-wave-lengths in the tube, $q=0$, 1, respectively.

simply

$$\omega_{mnp}^{(s)}(\text{cut-off}) = \nu_{np}^{(s)} c_d. \tag{26}$$

(a). Cavity Resonator of Constant Over-All Length Containing a Movable Slab of Dielectric

For three dielectric media an important case to be considered is that for which medium one is the same as medium three, with a thickness l_2 of dielectric separating them. The total length of the resonator is kept constant, and the position of the dielectric plug is varied.

For a constant tube length, l, and since medium one is the same as three, we have

$$\epsilon_1=\epsilon_3; \quad \mu_1=\mu_3; \quad \gamma_1^{(s)}=\gamma_3^{(s)}, \tag{27}$$

and

$$\alpha_2^{(s)}=\alpha_1^{(s)}\equiv\alpha^{(s)}; \tag{28}$$

let

$$l_3^{(s)}=(l-l_2)-l_1^{(s)}=\delta-l_1^{(s)}, \tag{29}$$

where l_2 and δ are constant. Substituting these values into (18) and solving for $l_1^{(s)}$, we obtain finally

$$l_1^{(s)}=\frac{1}{\gamma_1^{(s)}}\left[\tan^{-1}\left(\frac{-B^{(s)}\pm([B^{(s)}]^2-4A^{(s)}C^{(s)})^{\frac{1}{2}}}{2A^{(s)}}\right)+\pi q\right] \tag{30}$$

$$q=0, 1, 2, \cdots,$$

where integral values of $q>0$ correspond to additional half-wave-lengths, q, of course, being such that $l_1^{(s)}+l_2+l_3^{(s)}=l$, which is fixed. We have also

$$\begin{aligned} A^{(s)}&=\alpha^{(s)}\tan\gamma_1^{(s)}\delta+(\alpha^{(s)})^2\tan\gamma_2^{(s)}l_2,\\ B^{(s)}&=[1-(\alpha^{(s)})^2]\tan\gamma_1^{(s)}\delta\tan\gamma_2^{(s)}l_2,\\ C^{(s)}&=\alpha^{(s)}\tan\gamma_1^{(s)}\delta+\tan\gamma_2^{(s)}l_2. \end{aligned} \tag{31}$$

Thus there are two values of the resonant length l_1, as might be expected, one for a position near one end of the tube, the other near the other end. The sum of these two values is constant and equal to δ, and the variation of $l_1^{(s)}$ with frequency is symmetrical about $l_1^{(s)}$ equal to $l_3^{(s)}$, as can easily be shown (see Fig. 13). This indicates that the greatest effect of the dielectric on changing the resonant frequency occurs, as one would expect, at an anti-node of the **E** field, or in the middle of the tube, as shown in Fig. 13, if the resonator is a half-wave-length long ($q=0$). When $l_1^{(s)}=l_3^{(s)}$, we have $(B^{(s)})^2=4A^{(s)}C^{(s)}$, and this condition becomes

$$1+\left(\frac{\tan\gamma_1^{(s)}\delta}{\tan\gamma_2^{(s)}l_2}\right)^2+\left(\frac{1+(\alpha^{(s)})^2}{\alpha^{(s)}}\right)\left(\frac{\tan\gamma_1^{(s)}\delta}{\tan\gamma_2^{(s)}l_2}\right)=\left[\left(\frac{1-(\alpha^{(s)})^2}{2\alpha^{(s)}}\right)\tan\gamma_1^{(s)}\delta\right]^2. \tag{32}$$

Equation (32) is a complicated function of frequency, but the frequency at which $l_1^{(s)}$ equals $l_3^{(s)}$ can be obtained fairly readily by graphical methods. An upper limit to resonance for the particular modes excited is given when $l_3^{(s)}$ (or $l_1^{(s)}$) is zero; then the problem reduces to that of two dielectric media.

It was not possible to test (30) directly by experiment because an oscillator variable over a wide enough frequency range was not available.

(b). Cavity Resonator of Variable Over-All Length Containing a Movable Slab of Dielectric

It was found most convenient for the experimental work to select $l_1^{(s)}$ as the independent variable in (18), $l_3^{(s)}$ as the dependent, for a given dielectric thickness l_2, and a given constant frequency. The over-all resonant length varies as $l_1^{(s)}$ and l_2 are changed, while the resonant frequency remains at some constant value; in the case of the theoretical curves (Fig. 14), this frequency was chosen as 3000 mc/sec., or a 10-cm wave-length; in the actual experimental work it

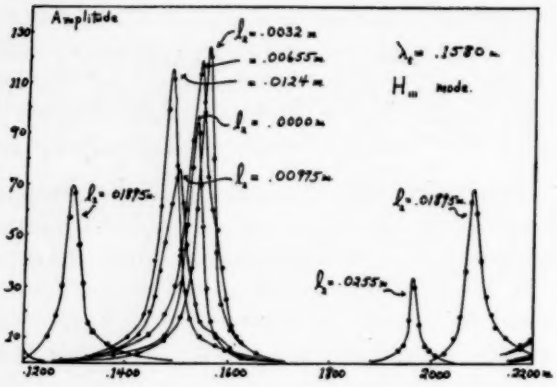

FIG. 3. Amplitude of the standing wave pattern *vs.* position in the resonator.

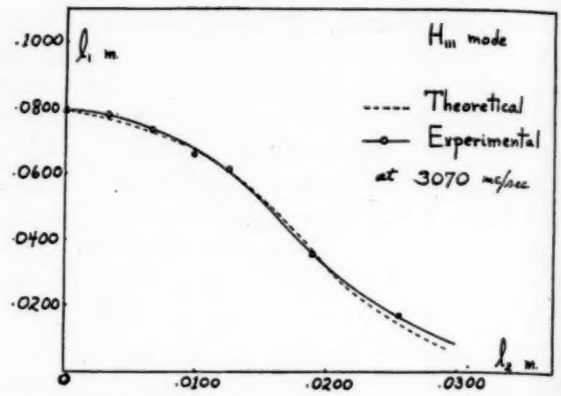

FIG. 4. Resonant length $l_1^{(2)}$ as a function of dielectric thickness l_2 at 3070 mc/sec., experimental and theoretical curves for the H_{111} mode, with the dielectric at one end of the resonator.

was 3070 mc/sec., or about 9.78 cm. Let

$$\phi^{(s)}=\tan^{-1}(\alpha^{(s)}\tan\gamma_1^{(s)}l_1^{(s)}); \qquad (33)$$

then from (18) we have

$$l_3^{(s)}=\frac{1}{\gamma_3^{(s)}}\left[\tan^{-1}\left(\frac{-\tan[\phi^{(s)}+\gamma_2^{(s)}l_2]}{\alpha_2^{(s)}}\right)+\pi q\right]. \qquad (34)$$

These equations (34) are general for three different media.

The important case is as before, that media one and three be the same, a condition which simplified the experimental work. Then $\gamma_1^{(s)}=\gamma_3^{(s)}$, etc., and (34) is symmetrical about $l_1^{(s)}=l_3^{(s)}$. (To test this, replace $l_1^{(s)}$ by $l_3^{(s)}$ in the above.) Again the greatest effect of the dielectric occurs when the slab is symmetrically placed with respect to the ends of the tube, if it is half a wave-length long, as shown in Fig. 14. When the resonator is more than a half-wave-length long, the maximum effect is obtained as before at antinodes of the **E** field. Figure 2 shows this for a full wave-length in the resonator.

(c). Cavity Resonator of Variable Total Length Containing a Slab of Dielectric at One End

This is the case of two dielectric media; if we let $l_3=0$, then Eq. (22) is easily solved for $l_1^{(s)}$; l_2 is as before the thickness of the dielectric slab.

When the resonator is $\lambda/2$ cm long and when $l_1^{(s)}$ is zero, or equivalently when

$$l_2^{(s)}=\pi[(\omega^{(s)}/c_2)^2-(\nu^{(s)})^2]^{-\frac{1}{2}};\ \text{or}\ \gamma_2^{(s)}=\pi/l_2, \qquad (35)$$

then this sets an upper limit to the frequency obtainable for a given size of dielectric and for a given mode (see Fig. 9). When this upper limit is equal to the lower cut-off frequency, we have the maximum value of $l_2^{(s)}$ possible and still excite (in this instance) the E_{011} or H_{111} mode. This means that $\gamma_1^{(s)}=0$ at cut-off, and $c_1>c_2$; putting this into (22) we obtain

$$l_2^{(s)}(\text{max.})=(q+1)\pi/\gamma_2^{(s)}$$
$$=(q+1)\pi/\nu_{11}^{(s)}[(c_1/c_2)^2-1]^{\frac{1}{2}}, \qquad (36)$$

and $q>0$ for more than one-half wave-length in the tube. The lower cut-off frequency is the same for all thicknesses of dielectric equal to or less than $l_2^{(s)}$ (max.). If we combine Eqs. (26) and (35), letting $\Delta f^{(s)}$ be the band of frequencies for which a given mode may be excited, we find that

$$\Delta f^{(s)}=c_2[(m\pi/l_2^{(s)})^2+(\nu_{np}^{(s)})^2]^{\frac{1}{2}}-c_1\nu_{np}^{(s)}, \qquad (37)$$

which depends on the dielectric thickness; thus, by inserting different lengths of dielectric, the transmission band for a particular mode may be adjusted between the upper limit, given by Eq. (35), and the lower cut-off limit, given by Eq. (26). Under these conditions the resonator acts like a band transmission filter, for the given mode excited.

IV. RESULTS

The general theory has been developed in Section II, and the analysis for three special cases has been given in Section III. A brief discussion of the experimental and theoretical results follows. See Figs. 3–14.

(a). Experimental Procedure and Results

With a dielectric plug of thickness l_2 at one end of a hollow cylinder and a movable piston at the other, the resonant air length $l_1^{(s)}$ was determined for several values of l_2. A klystron oscillator, loosely coupled to avoid forced coupled-circuit effects, was used to excite the resonator. Because of the presence of the antenna and detector, as well as a small longitudinal slot down which the antenna and detector could be moved, and because of the fact that the resonator was not a perfect conductor, the fields were slightly distorted, and the maximum and minimum values of the **E** and **H** fields did not occur quite at the ends of the cylinder, as predicted by theory. The effect of these factors was to decrease the over-all resonant length by 0.48 cm, the correction which was added to $l_1^{(s)}$ to obtain the first calculated half-wave-length value of 7.89 cm. The calculations for this case were made from Eq. (22). The average experimental value of $\lambda/2$ in the tube was found to be 7.90 cm, good agreement with the theory. The dielectric used was a cylindrical, tightly-fitting slab of polystyrene, and the measurements were made at a wave-length of 9.78 cm, corresponding to a frequency of 3070 megacycles/sec. for the H_{111} mode.

Figure 3[14] shows part of the resonance curve obtained for the H_{111} mode in the hollow cylinder, of radius $a=3.65$ cm, at a frequency of 3070 mc/sec. Figure 4 compares the experimental and theoretical values of $l_1^{(2)}$ *vs.* l_2, for various values of l_2, at 3070 mc/sec.; the theoretical curve was calculated from Eq. (22) for $\epsilon_2=2.41\epsilon_0$, which was the experimentally determined value for the

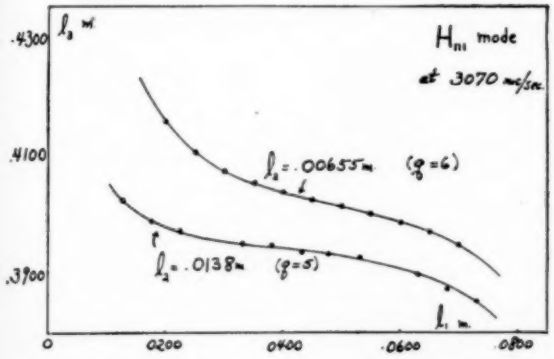

FIG. 5. Resonant length $l_2^{(2)}$ as a function of a chosen resonant air length $l_1^{(2)}$ for two different thicknesses of dielectric l_2, at 3070 mc/sec., for a tube length greater than $\lambda_{tube}/2$.

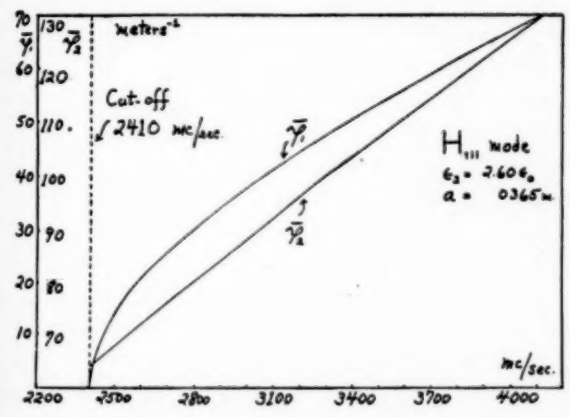

FIG. 6. Propagation constants, $\gamma_1^{(2)}$, $\gamma_2^{(2)}$ *vs.* frequency, with $\epsilon_1=\epsilon_0$ (air), $\epsilon_2=2.60\epsilon_0$, H_{111} mode.

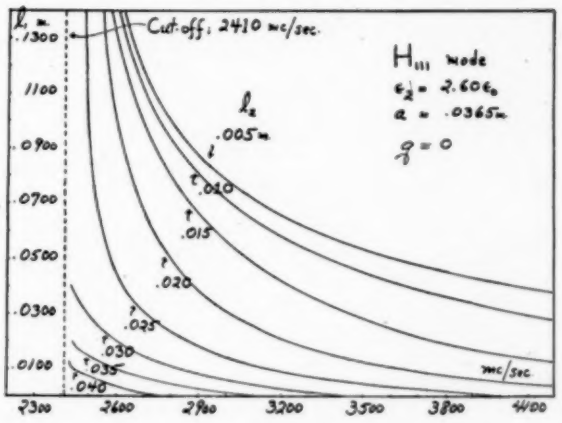

FIG. 7. Resonant air-length $l_1^{(2)}$ as a function of frequency for different thicknesses of dielectric l_2, for a half-wave-length in the tube, H_{111} mode.

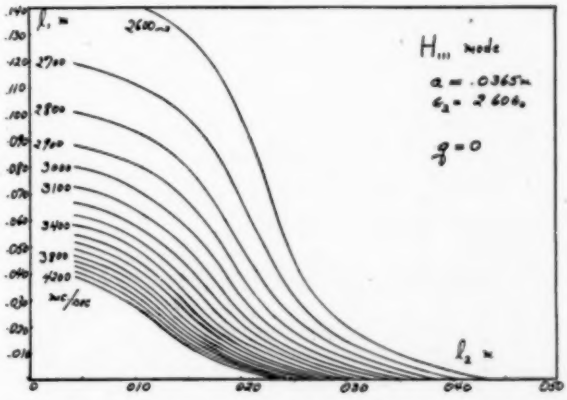

FIG. 8. Resonant air length $l_1^{(2)}$ as a function of dielectric thickness l_2 for various resonant frequencies, for a half-wave-length in the tube, H_{111} mode.

[14] Note: the bar, (—), appearing over any symbol in the figures, denotes the value of that quantity for the H_{111} or magnetic mode, $s=2$.

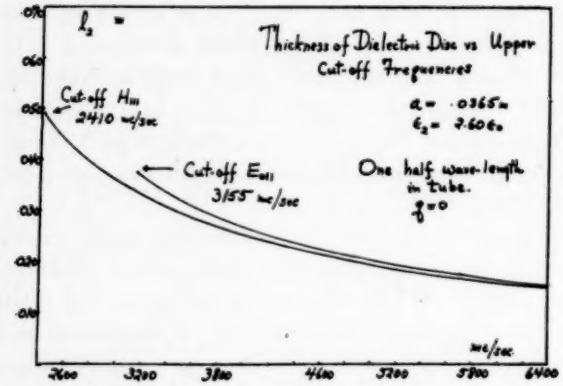
Thickness of Dielectric Disc vs Upper Cut-off Frequencies
Cut-off H_{111} 2410 mc/sec
Cut-off E_{011} 3155 mc/sec
One half wave-length in tube.
$a = .0365$ m
$\epsilon_2 = 2.60\epsilon_0$
$g = 0$
mc/sec

FIG. 9. Thickness of dielectric as a function of the upper cut-off frequency for one-half wave-length in the tube.

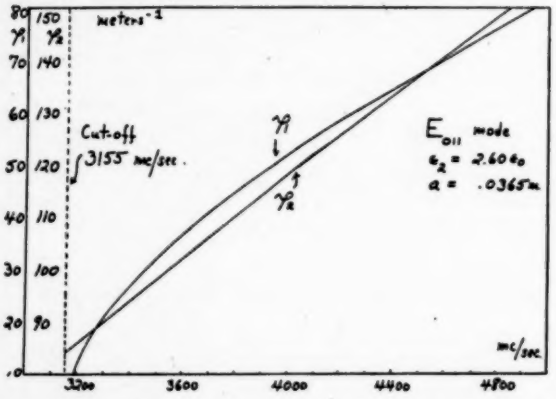

FIG. 10. Propagation constants $\gamma_1^{(1)}$, $\gamma_2^{(1)}$ as a function of frequency, with ϵ_1 (air) $= \epsilon_0$, $\epsilon_2 = 2.60\epsilon_0$, E_{011} mode.

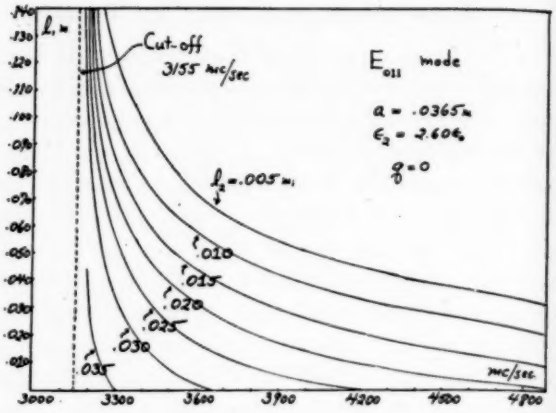

FIG. 11. The same as Fig. 7, E_{011} mode.

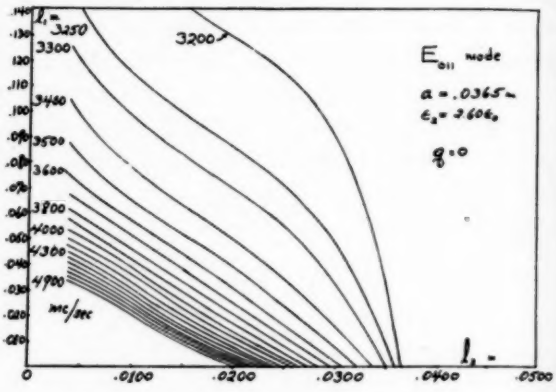

FIG. 12. The same as Fig. 8, E_{011} mode.

dielectric used. The experimental work is seen to be in good agreement with the theory.

Figure 5 below shows typical experimental curves for the three dielectric case (medium one the same as medium three), where the air length $l_3^{(2)}$ is plotted *vs.* $l_1^{(2)}$, for a dielectric of thickness l_2 at various distances $l_1^{(2)}$ from one end. These curves are similar to the theoretical ones shown in Figs. 2 and 14. Figure 14 was obtained by calculation from Eq. (42).

(b). Properties of The Cylindrical Resonator

Equations involving the resonant lengths and frequencies of cylindrical cavity resonators containing two and three dielectric media have been developed in Sections II and III. The properties of such resonators indicate their usefulness as ultra-high frequency resonant circuits which are tunable by varying the length of the air space or by shifting a dielectric plug. Figure 13, calculated from (32) for the H_{111} mode, shows the variation of resonant length $l_1^{(2)}$ with frequency, a cylinder of dielectric being moved about within the tube, whose total length is constant. As we have seen, a half-wave-length resonator containing a dielectric at one end or at some position about the middle of the cylinder acts like a filter, for a given mode, whose frequency transmission band width is adjustable by varying the dielectric thickness. Figure 9, calculated from Eq. (35), shows the variation of dielectric thickness l_2 as a function of the upper cut-off frequency, for one-half wave-length in a tube of radius $a = 3.65$ cm, for both the E_{011} and H_{111} modes; from such a curve it is a simple matter to obtain the thickness of dielectric needed for a given band width, and vice versa. Resonators containing a greater number of half-wave-lengths may also serve as band transmission filters, but may be impractical because of their size and the length of dielectric required for a given passband.

(c), Measurement of Dielectric Constants at 10 cm

The tube containing two different dielectrics, for example, polystyrene at one end, the rest of the interior filled with air, suggests a simple absolute method for measuring the dielectric constants at microwave frequencies, in this case approximately 10 cm.

Figure 8 shows calculated curves of the resonant air length $l_1^{(2)}$ as a function of the dielectric thickness l_2, for one-half wave-length in the tube, with frequency as a parameter, and $\epsilon_2 = 2.60\epsilon_0$; these calculations were made from Eq. (22). Figure 7 is obtained from this curve, where the parameter is now l_2 and the resonant air length $l_1^{(2)}$ varies as a function of the natural frequency of the resonator.

To find the dielectric constant of a sample of the unknown, thickness l_2, all that is required is to place the sample at one end of the tube, and to determine the new resonant air length $l_1^{(2)}$, then determine the resonant length with air only, and plot $\gamma_2^{(2)} \tan \gamma_1^{(2)} l_1^{(2)}/\gamma_1^{(2)}$ and $-\tan \gamma_2^{(2)} l_2$ as a function of $\gamma_2^{(2)}$. The point of intersection of these two curves determines $\gamma_2^{(2)}$, while $\gamma_1^{(2)}$ is readily calculated for air from (21) and the frequency at which the data are taken. The H_{111} mode was the one used experimentally, though any physically possible mode will do. Equation (21) becomes

$$[(\gamma_2^{(2)})^2 + (\nu_{11}^{(2)})^2]/(\omega_{111}^{(2)})^2 \mu_2 = \epsilon_2 = \epsilon_2' \epsilon_0$$

$$(\mu_2 \epsilon_0)^{-\frac{1}{2}} = c = 3 \cdot 10^8 \text{ meters/sec.}, \quad (38)$$

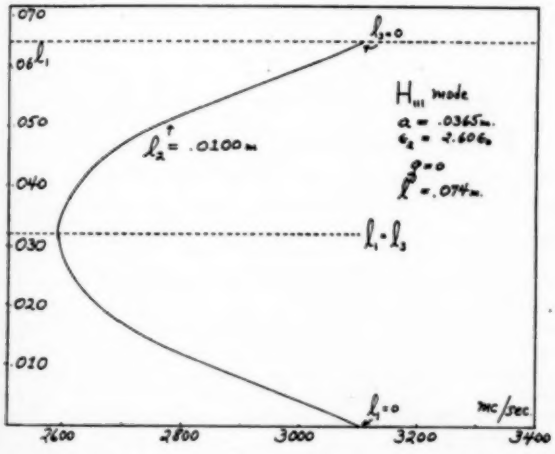

FIG. 13. Resonant air length $l_1^{(2)}$ as a function of frequency, $l_2 = 1.0$ cm, in a resonator of constant total length $l = .074$ m, for one-half wave-length of the H_{111} mode.

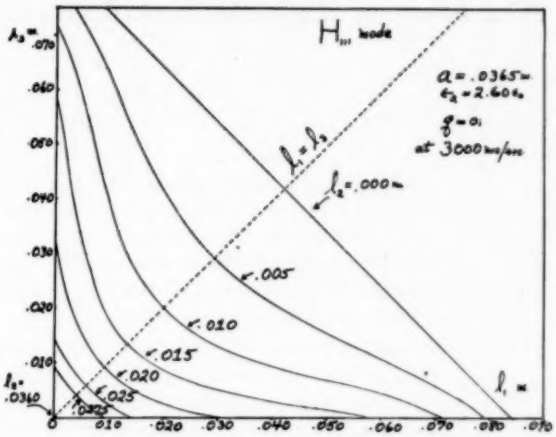

FIG. 14. Same as Fig. 5: calculated curves for one-half wave-length in the tube, at 3000 mc/sec.

from which ϵ_2 is readily found. The method is absolute, as it depends only on the dimensions of the resonator, the sample, and on the wave-length in the tube. By this method, with data taken from Fig. 4, ϵ_2 for polystyrene was found to have the value $2.41\epsilon_0$, which is in fairly close agreement with Lamont's value[15] of $2.47\epsilon_0$, the difference being due to the fact that different samples of polystyrene have different dielectric constants, because of variation in purity and polymerization.

This method of measurement is convenient for solids, as only a thin sample, $1.0 < l_2 < 8.0$ cm, is needed in most cases, and the larger the dielectric constant the thinner the sample. As may be seen from Fig. 8, the sample should be of the order of thickness of a quarter-wave-length or greater, so that an appreciable resonance shift will occur. With a little adaptation, ϵ of liquids can also be measured, one possibility being to place the resonator in a vertical position, with the bottom end sealed to prevent the escape of any fluid; this does away with the need of a separate fluid container; here, too, a few centimeters or so of liquid should be sufficient.

The author wishes to express his sincere appreciation to Professors Ronold King and J. H. Van Vleck for their generous encouragement and many helpful suggestions in the preparation of this manuscript, and to Professor King also, for the use of his apparatus in the experimental work.

[15] H. R. L. Lamont, Phil. Mag. 30, 15 (1940).

The Effect of High Electrostatic Fields upon the Vaporization of Molybdenum*

G. B. ESTABROOK**
University of Pittsburgh, Pittsburgh, Pennsylvania
(Received March 6, 1943)

It has been found for wires of varying diameters, (1) that, for field strengths of about 0.52×10^6 volts/cm or less at the wire surface, there was no change in the rate of change of resistance with time and hence the rate of vaporization upon application of the field; (2) that, for field strengths above approximately 0.52×10^6 volts/cm, as successively higher fields were applied, the rate of vaporization first decreased slowly, then more rapidly, and finally asymptotically toward zero at field strengths over 1.8×10^6 volts/cm; (3) that, with increasing temperatures, the same field strength applied at the surface of a wire produced progressively smaller decreases in the rate of vaporization; (4) that, when there was an effect upon the rate of vaporization, sudden increases in resistance occurred when the field was applied, and sudden decreases when it was removed. Worthing has reported similar results for tungsten except that the sudden increases and decreases were opposite to those of platinum and molybdenum.

INTRODUCTION

THE filament of a tungsten lamp operated at its normal temperature of about 2450°K is known to decrease in cross-sectional area with time. Evidence of this change may be seen by the deposition of metal upon the sides of the lamp. This change, because of vaporization of the metal, is accompanied by an increase in resistance of the wire.

In an investigation of the effects of high electrostatic fields upon the vaporization of small heated tungsten wires Worthing[1] has found that for a wire 0.020 mm in diameter, operated at 2500°K, a radial field of strength 2.7×10^6 volts per cm at the wire surface reduced the rate of increase of resistance, and hence the rate of vaporization, to 45 percent of the value without the field. He further observed that, upon applying the field, there was a sudden decrease in resistance of the wire and that, upon removing

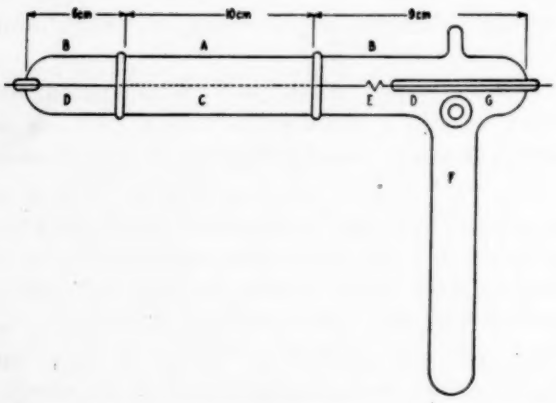

FIG. 1. Tube used for mounting molybdenum wires. *A*, copper tube, 2.8 cm I.D., walls 0.2 cm thick; *B*, Nonax glass tubing; *C*, molybdenum wire; *D*, 20-mil tungsten lead wires; *E*, small spring of 5-mil tungsten wire to provide slight tension; *F*, liquid-air tube; *G*, side tubes containing tungsten electrodes, on either side of main tube, for "cleaning up" residual gases.

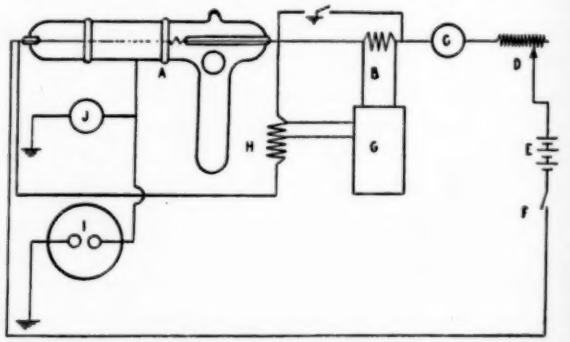

FIG. 2. Electrical arrangement for measuring the rates of vaporization of molybdenum wires. *A*, tube containing molybdenum wire; *B*, standard resistance; *C*, milliammeter; *D*, variable rheostat; *E*, storage batteries; *F*, switch; *G*, potentiometer; *H*, voltage multiplier; *I*, Wimshurst machine; *J*, electrostatic voltmeter; *K*, single pole double throw switch for grounding the circuit containing the molybdenum wire.

* This work was carried out during the year 1931–32. Publication has been delayed because of an apparent discrepancy with data on the vaporization of molybdenum already published. Now that an explanation of this discrepancy has been found (see following paper), it is offered for publication.

** Now at the Department of Physics, University of Maryland, Baltimore, Maryland.

[1] A. G. Worthing, Phys. Rev. **17**, 418 (1921).
[2] E. H. Greibach, Phys. Rev. **33**, 844 (1929).

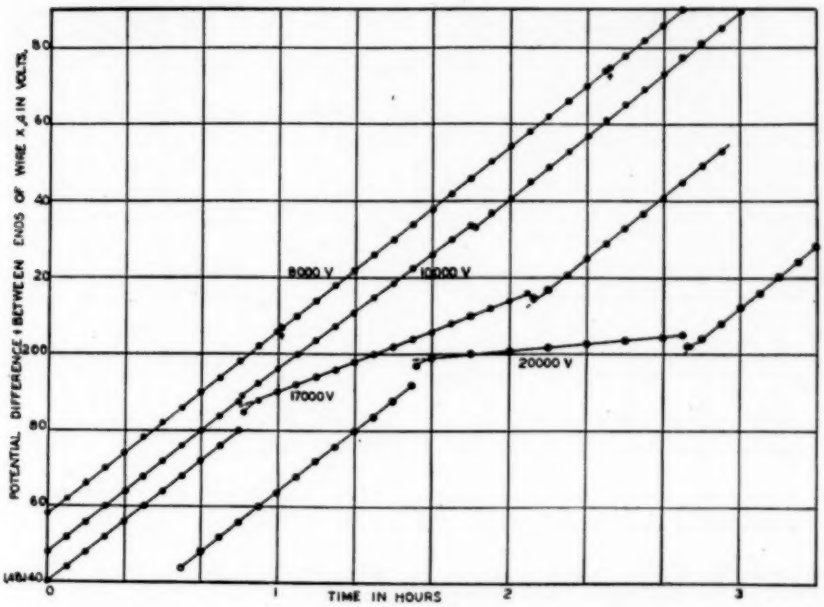

FIG. 3. Change in the rate of vaporization of a molybdenum wire ($r=0.00243$ cm, $T=1462°K$) upon application of four different electrostatic potentials. (Ordinate scales differ by a constant.)

the field, there was a sudden increase. Greibach[2] has predicted, on the basis of classical theory, that the effect of an electric field, such as used by Worthing, should be to decrease the rate of vaporization by less than one percent.

The present investigation was undertaken to obtain information on the behavior of small molybdenum wires under conditions somewhat similar to those described for tungsten. Prior to using molybdenum wires, a similar study of small platinum wires was attempted. A decrease in the rate of vaporization was observed when they were under the influence of the electric field. Contrary to the case for tungsten, a sudden increase in the resistance of the wire took place at the instant of applying the field and a decrease when the field was removed. However, the data were not consistent, probably on account of the difficulty in out-gassing the platinum; and so the work on platinum was dropped temporarily.

APPARATUS

The molybdenum used was obtained from the Cleveland Wire Works of the General Electric Company at Cleveland, Ohio, in the form of wires 0.00486 cm, 0.00684 cm, and 0.00762 cm in diameter. While no analyses of the particular samples used were available, the Cleveland Wire Works reported that analysis of powdered metal, similar to that from which the wires were made, ran 99.9 percent molybdenum. A fourth size wire used was obtained by electrolytically etching the 0.00486-cm wire to 0.00458 cm. The wires were examined under a microscope and initially found to have polished surfaces with no pits. Their diameters were determined by weighing a measured length on a microbalance. Approximately 10-cm lengths of these wires were mounted in highly evacuated tubes, as indicated in Fig. 1. During the evacuation, which took about 18 hours, the tubes were heated in a furnace at about 425°C.

Figure 2 represents the electrical arrangement for measuring the change in resistance of the wire while keeping the current constant. For convenience of measuring potential differences, a Leeds and Northrup potentiometer, modified to operate as a limited double potentiometer, as described by Worthing and Forsythe,[3] was used. The electrostatic potential difference was measured by means of an electrostatic voltmeter as described by Shrader.[4]

[3] A. G. Worthing and W. E. Forsythe, J. Opt. Soc. Am. **10**, 599 (1925).
[4] J. E. Shrader, J. Opt. Soc. Am. **6**, 273 (1922).

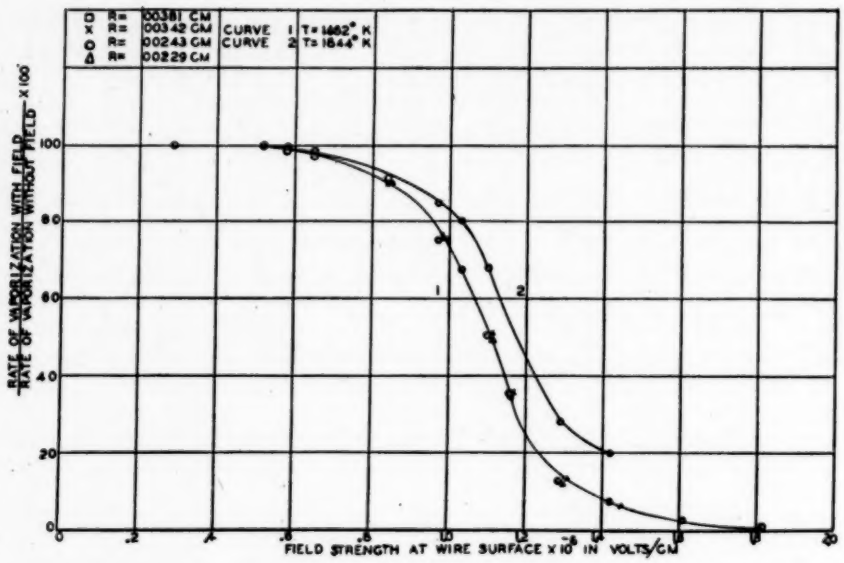
R= .00381 CM
R= .00342 CM
R= .00243 CM
R= .00229 CM
CURVE 1 T= 1662° K
CURVE 2 T= 1644° K
RATE OF VAPORIZATION WITH FIELD / RATE OF VAPORIZATION WITHOUT FIELD — X 100
FIELD STRENGTH AT WIRE SURFACE X 10⁻⁸ IN VOLTS/CM

FIG. 4. Variation in the rate of vaporization of molybdenum wires with electrostatic field strength applied at the surface of the wires.

PROCEDURE AND RESULTS

Before making the initial run on any sample, the wire in the tube was first aged for a period of several hours, at a temperature above 2000°K, and then run at the desired temperature for approximately two hours, or until conditions became steady. Following this, by repeated adjustments, the current in the wire was kept constant to about one part in 200,000 and differences in potential between the ends of the wire measured every five minutes. By use of the limited double potentiometer mentioned above, it was possible, once adjustments were made, by merely throwing a single switch, to change directly from the current balance to the potential balance without disturbing the galvanometer. Thus the two measurements could be made in rapid succession, a condition essential in this work.

Figure 3 contains a typical set of curves showing the changes in the rates of increase of voltage with time, for a wire 0.00486 cm in diameter operated at an average temperature of about 1462°K, upon the application of several high potentials between the cylinder and the wire. To obtain a single curve, three steps are necessary. Consider the curve for 17,000 volts. After the preliminary heating, the wire was operated at constant current for a period of 50 min., with a potential of 45 volts only between the wire and the cylinder, to eliminate thermionic emission effects. During this time, the potential difference between the ends of the wire was found to increase regularly, so that when voltage was plotted against time, the slope of the curve, that is, the rate of increase of potential difference, was constant, and in this instance had a value 8.00

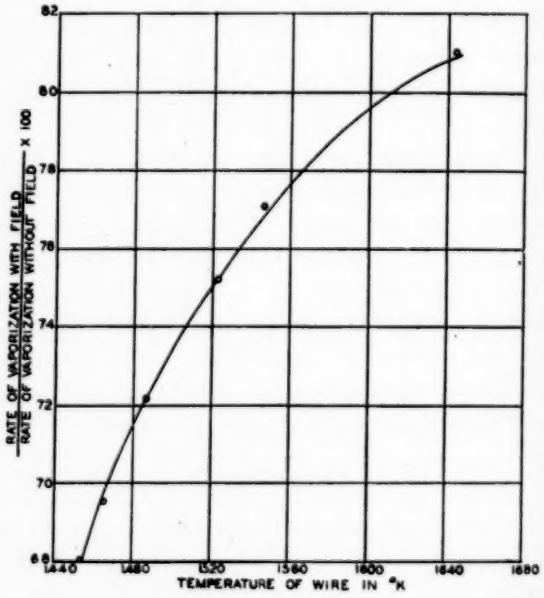

FIG. 5. Relative change of vaporization rate of a molybdenum wire ($r=0.00243$ cm) with temperature. Electrostatic field 1.03×10^6 volts/cm.

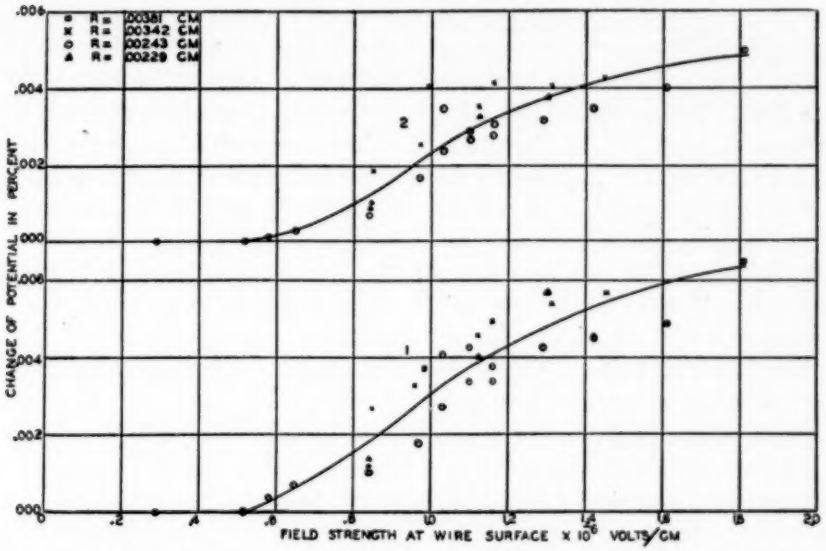

FIG. 6. Sudden changes in potential difference between the ends of molybdenum wires upon application and removal of high electrostatic fields.

$\times 10^{-6}$ volt per min. The 45-volt potential difference then was changed suddenly to 17,000 volts and the changes in potential drop along the wire followed for one hour and 15 min., the rate being 4.00×10^{-6} volt per min. Finally the high potential was removed, the 45 volts reapplied, and again changes in potential drop along the wire were followed for 50 min. The slope of the curve returned to 8.00×10^{-6} volt per min. In many cases, this procedure was continued through two more steps, making five in all. Since in each run the current was kept constant, the slope of the curve is proportional to the rate of change of resistance of the wire. Now as a wire evaporates, its cross-sectional area diminishes; and, since this varies inversely with resistance, a change in the rate of increase of resistance is interpreted as a change in the rate of vaporization. As appears later in the discussion, there is a disturbing factor in this interpretation.

The slopes of the curves before and after the application of the high potentials were always the same for any one run. For the runs graphed in Fig. 3, the application of a potential of 8000 volts resulted in no change of slope. A slight change of slope was observed for 10,000 volts, more of a change for 17,000 volts, and for 20,000 volts the curve became almost horizontal. In addition, for all potentials above 8000 volts, a sudden increase in potential difference between the ends of the wire was observed when the high potential was applied, and a decrease, though not quite so great in magnitude, when it was removed.

Similar runs to those just described were made on the same wire with other high potentials and at other temperatures, and on other wires of different diameters. Curve 1 of Fig. 4 is a composite curve showing the results obtained from four sizes of wire operated at about 1462°K. In this curve, the percentage variation in the rate of vaporization is plotted against field strength at the wire surface. For reasons appearing later under "Discussion," field strength has been chosen as abscissas rather than potentials. As is evident from the curve, for a given field strength, the change in rate of vaporization is independent of the size of the wire. No change of rate of vaporization was found for field strengths of 0.52×10^6 volts per cm or less. However, for increasing field strengths above this value, the rates of vaporization, upon applying the field, decreased, at first slowly, then more rapidly, and finally asymptotically toward zero at field strengths above 1.8×10^6 volts per cm. Curve 2 shows similar results for an average temperature of 1644°K. As for 1462°K, no change was found for field strengths of 0.52×10^6 volts per cm or less. At higher field strengths, the vaporization rates are higher for the higher temperature.

Figure 5 represents the variation of the rate of vaporization for the 0.00486-cm wire with temperature, the field in all cases being the same. Again, the higher the temperature of the wire, the less the field decreases the vaporization rate.

In Fig. 6, curve 1, the sudden increase in resistance of the wire upon application of a field is plotted against field strength at the wire surface, and in curve 2, the sudden decrease upon removing the field. The values in the former case are somewhat larger than those in the latter. Both curves, however, have similar shapes. In neither case was an effect observed for field strengths of 0.52×10^6 volts per cm or less.

To determine whether or not the change in resistance could be ascribed to vaporization, approximately 20-cm lengths of the wires were mounted in tubes and operated for 50 hours or more at an average temperature of 1462°K, the average temperature used in most of the runs just described. From the weights of a measured length of wire before and after the prolonged heating, the amount of metal vaporized was calculated and compared with that expected from the resistance changes in the runs on the wire from which the data of Fig. 3 were obtained. For a 0.00486-cm wire, which had first been aged at a temperature above 2000°K for about an hour and then weighed and put in operation, the ratio of the loss in weight of the wire to its original weight was 0.0253, while for the same sized wire for which resistance variations were followed the rate of change of resistance (dR/dt) was 114.3×10^{-6} ohm per min. In this latter case, the average value of $(1/R)(dR/dt)$ was 6.16×10^{-6} min.$^{-1}$, and the value of $(1/R)(dR/dt)t$ was 0.0211, where t is the total time of operation of the wire. On the assumption of no pitting or roughening of the surface during operation, this value is subject to a correction for change in temperature. This is necessary to give the fractional change in resistance had the initial and final resistance measurements been made at the same temperature. When thus corrected, a value of 0.0147 is obtained. (See Appendix.) If one considers the uncertainties resulting from (1) the difficulty in obtaining small differences in weight with a microbalance (the difference was 0.068 mg), (2) the end losses (the vaporization rate was less at the cooled ends of the wire than at the center), (3) the slight roughening of the surface of the wire with operation (the roughening of a surface by increasing the radiating area cuts down the increase in temperature which normally follows operation of such a wire on constant current), and (4) the possible decrease in resistivity, or in radiancy, or both (this follows a decrease in V^3I, which Worrell[5] has shown to be true for a molybdenum wire mounted in a highly evacuated tube), the ratio 0.0253 seems not inconsistent with the ratio 0.0147, and it seems reasonable to attribute the change in resistance to vaporization.

It is interesting to compare the rate of vaporization which may be obtained from the above with that reported by Langmuir and Mackay.[6] They give for molybdenum the following expression:

$$\log m = 17.11 - 38600/T - 1.76 \log T,$$

where m is the rate of vaporization in g/(cm² sec.), and T the temperature in °K. On the scale of temperature used by Langmuir and Mackay, 1462°K becomes 1443°K. Substituting this temperature in the formula, one obtains a value of 6.31×10^{-17} g/(cm² sec.) for m. The value obtained from the above run is 1.36×10^{-9} g/(cm² sec.). This difference is discussed in the following paper by Reid.

DISCUSSION

To account for the decrease in the rate of vaporization of the various sizes of wire with the application of a strong electrostatic field, it may be assumed that the atoms which have left the surface of the wire in a high electrostatic field become dipoles and that many of them are forced back by the field to the surface of the wire where the field is strongest. Consider a dipole of length l and charge e in a radial field of strength R between two concentric cylinders, the inner cylinder having a radius a, and the outer cylinder a radius b.

$^{+}e \quad ^{-}e$
$\cdot\leftarrow l\rightarrow\cdot$
$\leftarrow r\rightarrow$ to positively charged wire.

[5] F. T. Worrell, Phys. Rev. **61**, 520 (1942).
[6] I. Langmuir and G. M. J. Mackay, Phys. Rev. **4**, 377 (1914).

The force on the dipole is accordingly

$$F=[R+\tfrac{1}{2}l(\partial R/\partial r)]e-[R-\tfrac{1}{2}l(\partial R/\partial r)]e$$
$$=le(\partial R/\partial r).$$

Let us assume, as is usually done, that the dipole moment le is related to the field strength R, thus

$$\alpha R=le,$$

where α is the polarizibility. Now the work done by a vaporized atom at the expense of its kinetic energy against the field in moving from the wire to the cylinder is

$$W=\int_a^b Fdr,$$

or substituting the above values, we have

$$W=\int_a^b le(\partial R/\partial r)dr=\alpha\int_a^b R(\partial R/\partial r)dr.$$

Substituting for R and $\partial R/\partial r$ the values

$$R=-V_b/r\ln(b/a)$$

and

$$\partial R/\partial r=(1/r^2)[V_b/\ln(b/a)],$$

where V_b is the potential at the outer cylinder, the inner cylinder being grounded, we obtain

$$W=\frac{-\alpha V_b^2}{\left(\ln\frac{b}{a}\right)^2}\int_a^b\frac{dr}{r^3}=\frac{\alpha V_b^2}{2\left(\ln\frac{b}{a}\right)^2}\left[\frac{1}{b^2}-\frac{1}{a^2}\right].$$

To produce equal decreases in the rates of vaporization for two wires of different radii, at the same temperature and placed concentrically in cylinders of the same size, requires the same work per dipole for the transfer from a to b. Thus, where W_1 is the work in the case of a wire of radius a_1, and W_2 the work for the same effect upon the rate of vaporization in case of a wire of radius a_2,

$$\frac{W_1}{W_2}=1=\frac{V_{b_1}[\ln(b_2/a_2)][(1/a_1^2)-(1/b_1^2)]}{V_{b_2}[\ln(b_1/a_1)][(1/a_2^2)-(1/b_2^2)]}.$$

Neglecting the b^2 term since b is large compared with a, it follows that

$$W_1/W_2=R_{a_1}/R_{a_2}=1,$$

where R_{a_1} is the field strength at the surface of the wire of radius a_1, and R_{a_2} that for a wire of radius a_2. Hence for equal field strengths at the surfaces of the wires, equal decreases in the rates of vaporization are expected. This is in accord with Fig. 4. It is to be noted that though the rate of vaporization is proportional to the field strengths, the existence of a dR/dr is the characteristic of the field which produces the change.

In the case of the sudden increase in resistance observed when the field was applied, or decrease when it was removed, it was first thought that this might result from a current between the wire and the surrounding cylinder due to either a positive ion current from the wire or a leakage current over the surface of the glass. To test for such a current, the effect of switching the ground connection from one terminal of the standard resistance B, Fig. 2, to the other was investigated. No indication of such a current was found. If a current had been present, due to its inclusion or exclusion from that passing through the standard resistance, it would have been detected in the potential measurements. While potential differences could be read to about one part in 200,000 and a sudden increase in resistance caused a change of as much as one part in 10,000, the change in the ground connection never produced any detectable effect. Further, since the introduction of grounded guard rings did not alter the sudden increase and decrease of resistance, the possibility of leakage currents seemed excluded. Again since a positive ion current, if present, would be expected at fields lower than that which just produced the sudden changes in resistance, the possibility of such a current being present seemed likewise excluded.

As mentioned above, there is a disturbing factor in the interpretation of the rate of increase of resistance as proportional to the rate of vaporization. It is the difference in the sudden changes of resistance when applying and removing the electric field. During a run of three steps, as described earlier, the total change in resistance is not equal to the sum of those occurring during the individual steps, the difference being that between the two sudden changes.

Increases and decreases of resistance in the same direction were observed for platinum, but for tungsten Worthing reported opposite changes.

These changes are further discussed in the following paper.

APPENDIX. CORRECTION OF OBSERVED $(1/R)(dR/dt)$ FOR CHANGE IN TEMPERATURE

Consider the resistance of an electrically heated wire in vacuum as a function of its temperature T, and its radius r, thus

$$R=f(T, r).$$

As the wire evaporates, its resistance changes with time t, and

$$dR/dt=(\partial R/\partial T)_r(dT/dt)+(\partial R/\partial r)_T(dr/dt). \quad (1)$$

Let

$$[(\partial R/R)/(\partial T/T)_r]=(T/R)(\partial R/\partial T)_r=\beta.$$

Multiplying (1) by $(1/R)$ and substituting, we obtain

$$\frac{1}{R}\frac{dR}{dt}=\frac{\beta}{T}\frac{dT}{dt}-\frac{2}{r}\frac{dr}{dt}=\frac{\beta d(\ln T)}{dt}-2\frac{d(\ln r)}{dt}. \quad (2)$$

Now the energy dissipated from a wire of length l, carrying a current I, is

$$I^2R=\rho l I^2/\pi r^2=2\pi r l\,\mathfrak{R} \quad (3)$$

where ρ is the resistivity, and $\mathfrak{R}$ the radiancy expressed in watts/cm^2. Then

$$\rho/\mathfrak{R}=2\pi^2r^3/I^2=(\rho_0/\mathfrak{R}_0)(T/T_0)^{(\beta-x)}, \quad (4)$$

where $\rho=\rho_0(T/T_0)^\beta$; $\mathfrak{R}=\mathfrak{R}_0(T/T_0)^x$ and ρ_0 and $\mathfrak{R}_0$ are fixed values at T_0. The terms β and x are taken as constant values for the small interval of temperature considered. From (4)

$$r^3=[(I^2/2\pi^2)(\rho_0/\mathfrak{R}_0)](T/T_0)^{(\beta-x)} \quad (5)$$

and

$$d(\ln r)/dt=(\beta-x/3)[d(\ln T)/dt]. \quad (6)$$

Substitution in (2) gives

$$1/R(dR/dt)=[\beta-\tfrac{1}{3}(\beta-x)](1/T)(dT/dt). \quad (7)$$

For $(T/R)(\partial R/\partial T)_r=\beta$, and for $(T/\mathfrak{R})(\partial\mathfrak{R}/\partial T)_r=x$, at 1466°K, Worthing[7] gives, for molybdenum, 1.145 and 5.14, respectively. Substitution in (7) and multiplication by t gives

$$(1/R)(dR/dt)t=3.80(1/T)(dT/dt)t. \quad (8)$$

Since for the region considered (dR/dt) and (dT/dt) are constant, except for minor fluctuations, we may replace $(1/R)(dR/dt)t$ and $(1/T)(dT/dt)t$ by $\Delta R/R$ and $\Delta T/T$ where ΔR and ΔT are the changes in R and T during the interval t.

For the run described in "Procedure and Results,"

$$(t/R)(dR/dt)=(\Delta R/R)_0=0.0211, \quad (9)$$

the observed value which is to be corrected for variation in temperature during the run to give the fractional changes in resistance had the initial and final resistance measurements been made at the same temperatures.

Substitution of the value 0.0211 in (8) gives $\Delta T/T=0.0056$. From this it follows that the average temperature is equal to the final observed temperature times $[1-\frac{1}{2}(\Delta T/T)]$, and in this case the final observed temperature of 1466°K yields an average temperature of 1462°K.

Upon applying this correction to $(\Delta R/R)_0$, the corrected value $(\Delta R/R)$ becomes

$$(\Delta R/R)_c=\frac{R_b(1-0.0028\beta)-R_0(1+0.0028\beta)}{\frac{1}{2}(R_b+R_0)}, \quad (10)$$

where R_b is the final resistance and R_0 the initial resistance of the wire. Substitution in (10) yields for $\Delta R/R$ (corrected for temperature variation during the run) 0.0147 in place of the uncorrected value 0.0211.

The writer wishes to express his indebtedness to Dr. A. G. Worthing, who suggested this problem, for his help and encouragement during the course of the work.

---

[7] A. G. Worthing, Phys. Rev. **28**, 190 (1926).

The Effect of High Electrostatic Fields upon the Vaporization and Resistance of Molybdenum Filaments*

WALTER P. REID**
University of Pittsburgh, Pittsburgh, Pennsylvania
(Received March 6, 1943)

This paper endeavors to show that equations can be obtained to fit Estabrook's observed variation of vaporization rate with electric field strength at wire surface if we consider the vaporization decrease as due to the formation of an adsorbed gas layer on the filament. It is mentioned that electric field strengths of the magnitudes used can be shown to have no appreciable effect upon the motion of the gas particles or metallic atoms in the region between filament and cylinder, and that time lags of the size observed can be approximately accounted for by the times required for formation and removal of the gas layer when the field is applied or withdrawn. The following postulates are proposed: (1) the resistance changes were due to temperature changes resulting from small changes in emissivity; (2) resistance changes in different directions were due to spectral variation in the behavior of the emissivity of a filament when it is coated with gas; (3) Estabrook's vaporization rate was higher than that calculated from an equation given by Jones, Langmuir, and Mackay because the wires used by the latter were more coated with gas; and (4) Jones did not observe any effect of an electric field upon resistance or vaporization because his tube did not contain enough oxygen. These hypotheses remain of course to be proved or disproved by appropriate experiments.

INTRODUCTION

SUPPOSE that we had a fine wire supported along the axis of a metallic cylinder, the whole being in a vacuum. If the wire were heated to incandescence by means of an electric current, its resistance would gradually increase because of vaporization of its atoms. This much is well known. In addition however, Worthing[1] and Estabrook[2] found that the application of a sufficiently high potential difference between filament and the concentric cylinder reduced the rate of increase of resistance of the filament. Their cylinders were made negative with respect to the filaments in order that there would be no emission of electrons. In addition to the change in slope of the resistance *versus* time curve, there was also a change in the actual resistance itself at the instant the field was applied, and a change in the opposite direction when the field was removed. These two effects were found with Pt, W, and Mo filaments, and presumably would exist also with other metals. Estabrook found that for Mo and Pt there was an increase in resistance when the field was applied, and a decrease when it was removed. Worthing found changes in the opposite direction with W. Both observers, however, found a decrease in the rate of resistance change when a radial field was applied. Figure 1 of this article, and Fig. 3 of Estabrook's article illustrate the above. In the graphs it is seen that there is a rounding of the corners indicating that the resistance and vaporization changes do not take place instantaneously.

It seems reasonable to attribute the steady increase in resistance of a wire with time to a gradual vaporization of its atoms. If such is the case, then the applied radial field must decrease the rate of vaporization. The ratio of the rate of vaporization after the field is applied to that

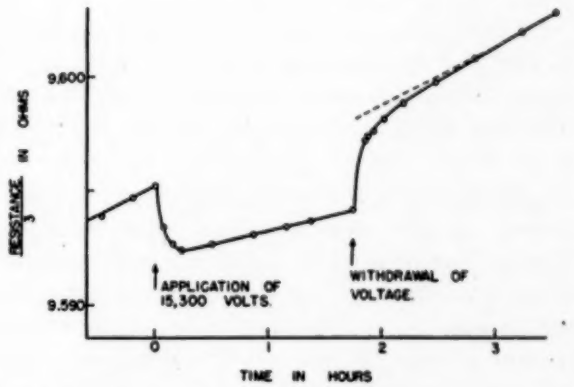

FIG. 1. This curve shows how the resistance of a tungsten wire was affected by the application of a high potential difference between it and a concentric cylinder. The temperature was 2500°K, and the wire radius 0.010 mm. [Taken from A. G. Worthing, Phys. Rev. **17**, 419 (1921).]

* Submitted to the Graduate School of the University of Pittsburgh in partial fulfillment of the requirements for the degree of Doctor of Philosophy.
** Now at the United States Rubber Company, Detroit, Michigan.
[1] A. G. Worthing, Phys. Rev. **17**, 418 (1921).
[2] See preceding paper.

before is given by the ratio of the two corresponding slopes of the resistance *versus* time curve. Figure 2 shows how this ratio varies with the field at the surface of the filament.

In Fig. 3 we see how the resistance change is affected by the field strength. This figure differs from Estabrook's Fig. 6 only in that the ordinates have been doubled, and a different curve has been chosen. Note that in it, as in Fig. 2, there is no apparent effect for fields of less than 0.5

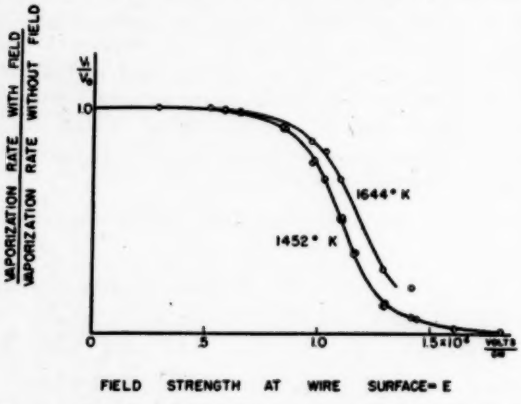

FIG. 2. These curves show the variation in rate of vaporization of molybdenum wires with the electrostatic field at the wire surface. The circles are from Estabrook's data. The solid lines are calculated values.

$\times 10^6$ volts/cm. Both Worthing and Estabrook found the resistance change to go more or less hand in hand with the vaporization change, although the former change has also been found to occur at temperatures where there is no appreciable vaporization at all. Vissat[3] has studied such resistance changes at room temperature and above.

In this paper we wish to propose a theory to account for the phenomena mentioned. Any such theory should provide an explanation for the following features of the problem as well as those cited above: (1) The vaporization rate observed by Estabrook was much larger than that predicted by the work of Jones, Langmuir, and Mackay,[4] and (2) Lloyd Jones (results unpublished), working with a very good vacuum, did not observe either the resistance or the vaporization change. Before undertaking our treatment, let us consider the dipole theory. This is done because the latter is apparently the explanation which occurs first to a person confronted with the problem.

THE DIPOLE THEORY

The metallic atoms leaving the filament were found to be uncharged, and so it is not easy to see why an electric field should have any effect upon them unless they become dipoles under its influence. If they do become dipoles, then each atom upon evaporation will experience a force tending to return it to the filament. This force arises, of course, from the fact that we have a radial rather than a uniform field. Greibach[5] studied thermodynamically the problem of evaporation of dipoles into an electric field, but was able thereby to account for but one percent of the effect observed.

At first it appears plausible to consider the decrease in vaporization rate as being due to the influence of the electric field upon evaporating metallic dipoles. A closer investigation, however, reveals that an unreasonably large value must be taken for the dipole moment of the metallic atom at the wire surface in order to produce decreases in vaporization of the magnitudes observed. It is also found that many phases of the problem cannot be explained suitably with such a physical picture, as, for example, the fact that quite large fields must be applied before there is any appreciable effect on the vaporization rate. These and other features make the dipole theory untenable.

THE ADSORBED GAS THEORY

It has been quite well established[6] that at least some of the gas particles striking a surface stick to it for a while before leaving again. The process of reflection of gas from a surface consists, therefore, at least in part, of a continual condensation and subsequent reevaporation of the particles. Since some of the molecules linger for a while, it follows that the surface will at all times be partially covered with an adsorbed gas film. The extent to which it is covered will

[3] P. L. Vissat, Ph.D. Thesis, University of Pittsburgh (1941).

[4] I. Langmuir and G. M. Mackay, Phys. Rev. **4**, 377 (1914). H. A. Jones, I. Langmuir, and G. M. Mackay, Phys. Rev. **30**, 201 (1927).

[5] E. H. Greibach, Phys. Rev. **33**, 844 (1929).

[6] See, for example, L. B. Loeb, *The Kinetic Theory of Gases* (New York, McGraw Hill, 1934), second edition, 338ff.

of course depend upon the conditions. In general gas films are driven off at temperatures much lower than that of 1452°K at which Estabrook worked, but chemisorbed films can adhere quite tenaciously even at temperatures considerably higher. The layer of atomic oxygen on the surface of tungsten filaments has, for example, been studied quite extensively, and is known to persist up to temperatures in the neighborhood of 2000°K. Since Mo is quite similar to W, we can perhaps safely assume that an atomic layer of oxygen could adhere to it too at temperatures such as those used by Estabrook.

Let us get an expression for the fraction of the wire surface covered by gas.[7] We shall do this first for the case where there is no electric field, and on the basis of Langmuir's physical picture. We denote by f_0 the fraction of the total number of adsorbable gas particles striking the filament that stick to it. These molecules upon condensing will dissociate. The separate atoms will remain upon the surface for a while, but will subsequently leave singly, and with a heat of desorption of ϕ_0 per atom. Let ν_0 be the number of adsorbed atoms per unit area; η the number of Mo atoms per unit area; θ_0 the fraction of the surface covered by gas; N_0 the rate at which gas molecules strike per unit area; and N_0' the rate at which molecules of the type being adsorbed strike the surface per unit area. Then $N_0'(1-\theta_0)$ will be the rate per unit area at which the latter strike that portion not covered by gas, and $N_0'f_0(1-\theta_0)$ will be the rate per unit area at which they stick. Since each gas molecule consists of two atoms, it follows that the number of atoms being adsorbed per unit area and per unit time will be given by

$$2N_0'f_0(1-\theta_0). \tag{1}$$

To get the number of atoms leaving[8] per unit area of the surface per unit time, let us first consider the case of a gas escaping through a small opening into a vacuum. Assuming a Maxwellian distribution of velocities for the gas particles, we get as the total number leaving the hole per unit area and per unit time with velocities greater than v_0:

$$[\sigma(\tfrac{1}{2}mv_0^2+kT_0)/(2\pi mkT)^{\frac{1}{2}}] \times\exp(-mv_0^2/2kT_0). \tag{2}$$

If, as in our case, we have gas particles escaping from a surface rather than through an opening in a container, then we can use the above expression for the number leaving provided that we let $\phi_0=\frac{1}{2}mv_0^2$ be the amount of work required to remove a gas particle, and replace σ, the number of molecules per unit volume in the container by something proportional to the surface concentration of gas atoms, or let $\sigma\rightarrow C\nu_0$. This gives

$$[C\nu_0(\phi_0+kT_0')/(2\pi mkT_0')^{\frac{1}{2}}] \times\exp(-\phi_0/kT_0') \tag{3}$$

as the number of gas atoms leaving per unit area and unit time. The prime is used on the T_0 because the effective temperature of the gas departing from the filament may not be the same as that of the surface.

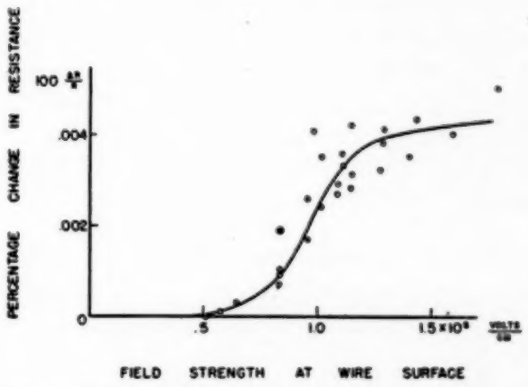

FIG. 3. This graph shows the percentage changes in resistance obtained by Estabrook for the case when the field is removed. The data were obtained with molybdenum wires of radii 0.00229, 0.00243, and 0.00342 cm at 1452°K. Similar changes occur upon application of the field.

It has been found that the number of atoms of oxygen in a complete chemisorbed layer on W is about equal to the number of W atoms on that surface. If the same is true for the gas adsorbed on Mo, then η will be a maximum value for ν_0, and we shall have

$$\theta_0=\nu_0/\eta. \tag{4}$$

Since the rate at which atoms leave must, in the steady state, be the same as the rate at which

[7] See Neil K. Adam, *The Physics and Chemistry of Surfaces* (Oxford, Clarendon Press, 1938), second edition, p. 264f.

[8] From J. K. Roberts, Trans. Faraday Soc. **31**, part 2, 1710 (1935).

they stick, we set expressions (1) and (3) equal to each other. Upon doing so, and using (4), we get

$$1-\theta_0=\left[1+\frac{2N_0'f_0(2\pi mkT_0')^{\frac{1}{2}}}{C\eta(\phi_0+kT_0')}\times\exp\left(\phi_0/kT_0'\right)\right]^{-1} \quad (5)$$

as the fraction of the surface not covered by gas before the field is applied. The fraction $1-\theta_1$ of the surface not covered after the field is applied is obtained from the last equation by changing the subscripts from 0 to 1 throughout.

If we let V be the rate of vaporization of Mo per unit area of the filament, and assume that it is proportional to the fraction of the surface not covered by gas, we have

$$V_1/V_0=(1-\theta_1)/(1-\theta_0) \quad (6)$$

as the ratio of vaporization after field is applied to that before. Let us apply this equation to Fig. 2. θ_1 is equal to θ_0 when the field E at the filament surface is zero. It seems reasonable to imagine that θ_1 steadily increases as E increases, but yet in Fig. 2 we see that V_1/V_0 remains equal to unity until E is about 0.5×10^6 volts/cm. Hence θ_0 must be essentially equal to zero if Eq. (6) is to apply to Fig. 2, and so Eq. (6) becomes

$$V_1/V_0\doteq1-\theta_1. \quad (7)$$

We next consider the number N_1' of adsorbable molecules striking the filament per unit area and per unit time after the field is applied. Because of the fact that the gas molecules probably become dipoles under the influence of the field, it follows that they would experience forces tending to move them toward the filament. The motion of such dipoles in a radial field was studied mathematically, and led to the result

$$N_1'\doteq N_3'[1+\gamma E^2/2kT_3+\cdots], \quad (8)$$

where N_3' is the number of the molecules striking the cylinder wall per unit area and time after field is applied. γ is the polarizability of a gas molecule. Let us consider it to be about 10^{-24} cm^3, or 1.1×10^{-29} erg cm^2/volt^2. The largest value of E used by Estabrook was about 1.8×10^6 volts/cm. T_3 is the temperature of the cylinder, and was probably just a shade above room temperature, or about 310°K. Using these values, together with the Boltzmann constant k, we obtain

$$(\gamma E^2/2kT_3)_{\text{maximum}}\doteq0.00042. \quad (9)$$

Hence

$$N_1'\doteq N_3'. \quad (10)$$

This means that when the field is on, the number of gas molecules striking the filament per unit area and time is essentially the same as the number striking the cylinder, or that field strengths of the magnitude used have no appreciable effect upon the motion of the gas particles. Since N_3' is known from the kinetic theory of gases, we have

$$N_1'\doteq N_3'=p_3'/(4\pi mkT_3)^{\frac{1}{2}}, \quad (11)$$

where $2m$ is the mass of a gas molecule and p_3' is the partial pressure at the cylinder of whichever gas is being adsorbed.

If we evaluate Eq. (7) by means of Eqs. (5) and (11), we get

$$V_1/V_0\doteq1-\theta_1=\left[1+\frac{p_3'f_1(2T_1')^{\frac{1}{2}}\exp\left(\phi_1/kT_1'\right)}{C\eta(T_3)^{\frac{1}{2}}(\phi_1+kT_1')}\right]^{-1}. \quad (12)$$

In order to use this equation, we should know how all of the various terms in it vary with the electric field strength at the wire surface. A study of Fig. 2, however, reveals that the data can most easily be fitted by a linear increase of ϕ_1/kT_1' with the applied electric field. T_1' is known from the experiment to have remained about constant, and so it is a linear increase in ϕ_1 which best fits Eq. (12) to the data. f would probably also increase with E if ϕ_1 increased, but for simplicity let us assume it to be constant.

We shall next put numerical values into Eq. (12). T_1' is the average temperature upon leaving the filament of those gas atoms which have adhered to it for a while, and hence is probably about equal to the temperature of the filament, or 1452°K for the first curve. As before, let us take $T_3\doteq310$°K. η is the number of Mo atoms per unit area of the surface. Assuming that the 110 plane is the one most likely to be along the wire surface, we get $\eta\doteq(14.4)10^{14}$ atoms/cm^2. The constant C, which was originally defined as

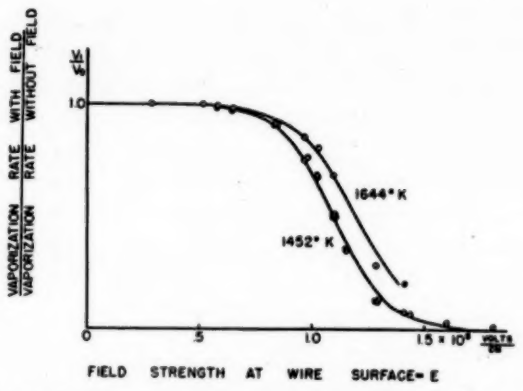

FIG. 4. This graph shows the curves obtained when the heat of desorption of the adsorbed gas is assumed to vary linearly with the field strength at the wire surface. The circles are from Estabrook's data.

the proportionality constant in expression (3), can be found from an equation for the rate of evaporation of adsorbed atoms and molecules given by J. K. Roberts.[8] The constant in his relationship was obtained from some of Langmuir's data on the rate of evaporation of oxygen atoms from a tungsten surface and leads to the value

$$C=(2.56)\times 10^{17} \text{ dynes/calorie.}$$

According to Roberts, this value for C should be the same for all substances. By comparison with experiment, he found his equation to apply accurately to a considerable range of atomic films. Hence we shall use the above value for C. For f we can use the following equation given by Langmuir:[9]

$$\log_{10} f_0 = 1.76 - 5940\text{K}^\circ/T \qquad (13)$$

for $1000^\circ\text{K} < T < 2000^\circ\text{K}$. This expression was obtained for oxygen atoms striking a W wire, but might perhaps hold for our case too. For 1452°K, we get $f_0 = 0.0047 (= f_1)$.

Experiments dealing with the interaction between gas molecules and solid surfaces have led to many conflicting theories and contradictory experimental results. This is due primarily to the fact that the results are quite sensitive to particular conditions existing at the surface, and to the practical impossibility of knowing the nature of the surfaces.[10] Hence the above value for f is quite likely to be in error.

[9] I. Langmuir, J. Am. Chem. Soc. **35**, 105ff (1913).
[10] L. B. Loeb, reference 6, p. 347f.

The partial pressure p_3' at the cylinder of whichever gas was coating the wire is not known. We must guess at it, and because of the uncertainty in f_1, let us consider the product $p_3' f_1$ as being unknown, and perhaps within the range covered below:

Case 1. Assume $p_3' f_1 = (10^{-8} \text{ mm Hg})(0.0047)$,
Case 2. Assume $p_3' f_1 = (10^{-7} \text{ mm Hg})(0.0047)$,
Case 3. Assume $p_3' f_1 = (10^{-6} \text{ mm Hg})(0.0047)$.

Upon putting the values above into Eq. (12), and applying the latter to the data at 1452°K in Fig. 2, we find that the equation will fit the data if

$$\phi_1 = \phi_0 + (4.02)10^{-26} E \text{ cal. cm/atom volt,} \qquad (14)$$

where ϕ_0 is about $(18.3)10^{-20}$ cal./atom for Case 1, 17.2 for Case 2, and 16.1 for Case 3. The coefficient of E is approximately the same for the three cases. In curve 1 of Fig. 4, we see the graph of Eq. (12) when the values given above are used for the various quantities in it. The graph turns out to be about the same for each of the three cases and is essentially the same for an even wider range of values chosen for $p_3' f_1$. Thus the coefficient of E in Eq. (14) and the graph of Eq. (12) are not greatly influenced by errors in the choices for constants in Eq. (12). This is the case because the changes in $\phi_1 + kT_1'$ with ϕ_1 are small compared to the changes in $\exp(\phi_1/kT_1')$ in Eq. (12).

When we consider the data at 1644°K, we again find that a linear variation of ϕ_1 with E will give fair agreement between Eq. (12) and the experimental results. The slope of the ϕ_1 *versus* E line turns out to be about the same as at 1452°K, and as before the value for ϕ_0 depends upon our choice of the constants. If we take $p_3' = 10^{-7}$ mm Hg, $T_1' = 1644^\circ\text{K}$, f from Eq. (13) as 0.014, and C, η, and T_3 as before, we get

$$\phi_{1\,(\text{at } 1644^\circ\text{K})} \doteq [19.0 + (4.02)10^{-6} E \text{ cm/volt}] \times 10^{-20} \text{ cal./atom.}$$

Using this last equation in Eq. (12), we get the second curve in Fig. 4.

From above we see that ϕ_0 appears to be in the neighborhood of 16 to 19×10^{-20} cal. per atom. By way of comparison we find that Roberts[11] gives a mean value of 128 kilogram

[11] J. K. Roberts, Proc. Roy. Soc. **A152**, 464 (1935).

calories per gram atom, or 21×10^{-20} cal. per atom for the heat of desorption of oxygen from W filaments. Other values in the literature are of the same magnitude. Our values for ϕ_0 seem, therefore, to be reasonable ones and are of a size which seems to indicate that the adsorbed gas on Estabrook's filaments was oxygen.

AN EXTENSION OF THE ADSORBED GAS THEORY

In Fig. 4 we see that the previous treatment does not give perfect agreement with Estabrook's data. We wish now to show how better correlation can be obtained.

We have assumed that only those Mo atoms which were not covered by the gas layer were capable of evaporating. It is reasonable however to suppose that a Mo atom might be able to leave the surface along with the oxygen atom on top of it. In fact, Langmuir has found that the combination of a W and an oxygen atom does indeed evaporate from the surface of a W filament, and has used this fact to explain the clean-up of oxygen by an incandescent W wire. He showed it to be WO_3 which evaporates, but the molecule is formed by the combination of an impinging O_2 molecule and a WO group from the wire surface. Hence as far as the surface is concerned, it is W plus O which leaves. By analogy, therefore, we shall assume that Mo plus O is capable of leaving the wire surface, perhaps combining with an O_2 molecule to form MoO_3, although it does not matter for our considerations how it leaves.

Let us take the rate at which Mo plus O leaves the wire to be directly proportional to the fraction of the surface covered by gas. Since we have previously assumed that Mo alone leaves at a rate proportional to the fraction of the surface not coated, it follows that the total number of Mo atoms leaving the surface per unit area and time after the field is applied will be given by

$$V_{1T}=A(1-\theta_1)+B\theta_1,$$

and

$$V_{1T}/V_{0T}=[A(1-\theta_1)+B\theta_1]/[A(1-\theta_0)+B\theta_0]\doteq[A(1-\theta_1)+B\theta_1]/A,$$

or

$$V_{1T}/V_{0T}\doteq1-\theta_1+s\theta_1, \tag{16}$$

where A, B, and s are assumed to be constants depending upon the temperature of the filament, but not upon the electric field applied. Substituting for θ_1 from Eq. (12), we get

$$\frac{V_{1T}}{V_{0T}}=\frac{1+s\dfrac{p_3'f_1(2T_1')^{\frac{1}{2}}\exp(\phi_1/kT_1')}{C\eta(T_3)^{\frac{1}{2}}(\phi_1+kT_1')}}{1+\dfrac{p_3'f_1(2T_1')^{\frac{1}{2}}\exp(\phi_1/kT_1')}{C\eta(T_3)^{\frac{1}{2}}(\phi_1+kT_1')}}. \tag{17}$$

As E gets larger, θ_1 approaches unity, and hence we see by Eq. (16) that V_{1T}/V_{0T} approaches s as a limiting value at high fields. Thus $V_{1T}/V_{0T}=s$ is an asymptote for our curve. If we are to apply Eq. (17) to Estabrook's data, we will have to know s at temperatures of 1452°K and 1644°K. From the data at 1452°K, it seems to be about 0.01. Since the data at 1644°K do not extend to high enough fields, it is difficult to determine a value of s for that temperature. By trial, it was found that a curve which fit the data best would be obtained if s were about 0.12. This seems too large in comparison with the asymptote at 1452°K. The choice of 0.12 was needed because of the last point on the curve. Upon throwing out the latter, it becomes quite impossible to determine an asymptote from Estabrook's data. By developing an approximate expression for s, and substituting into it the best numerical values we could find, we obtained $s\doteq0.017$ at 1644°K. This seems more reasonable, and so we shall use it.

When we use the above values for s in Eq. (17) and apply the latter to the data, we again find that ϕ_1 must vary approximately linearly with E in order to give agreement. In order to get completely satisfactory correlation between theory and experiment, however, it is found to be desirable to have ϕ_1 increase linearly with the fraction of the surface covered as well as with the electric field. The equation, therefore, is of the general form

$$\phi_1=\phi_0+gE+j\theta_1, \tag{18}$$

and if we substitute for θ_1 from Eq. (16), we get

$$\phi_1=\phi_0+gE+j(V_{1T}/V_{0T}-1)/(s-1). \tag{19}$$

When this relationship is put into Eq. (17), we obtain an expression in terms of V_{1T}/V_{0T} and E

which we shall use as the equation for the curves in Fig. 2. Values for the constants ϕ_0, g, and j can be determined by making the equation fit the data. If we choose $p_s' = 10^{-7}$ mm of Hg, we get for ϕ_0, g, and j, respectively, the values $(17.92)10^{-20}$ cal./atom, $(2.86)10^{-26}$ cal. cm/atom volt, and $(0.90)10^{-20}$ cal./atom at 1452°K, and $(19.42)10^{-20}$ cal./atom, $(3.40)10^{-26}$ cal. cm/atom volt and $(0.70)10^{-20}$ cal./atom at 1644°K. The curves shown in Fig. 2 were obtained by using these values in Eq. (19), and the latter in Eq. (17). They are seen to fit the data quite well except for the last point on the curve at 1644°K, which we decided to ignore, as mentioned before.

The fact that it is necessary to include the term $j\theta_1$ in Eq. (18) is not at all surprising. The heats of desorption of gases are known to change markedly with the fraction of the surface coated. Roberts,[12] for example, found the heat of desorption of H from W wires to decrease from 45 kilocalories per mole for a bare surface to 18 for a surface covered with gas. This change is presumably due to interaction energy between the adsorbed atoms.

The question then is not one of why a variation of ϕ_1 with the fraction of the surface covered was found, but instead—why was the change in our case so small? The answer to this is found in a theoretical treatment by Miller[13] of the problem of adsorption of dipoles. Quoting from his paper, we have ". . . the electrostatic and van der Waals forces give contributions to the variation of the heat of adsorption which are of opposite sign, and almost counterbalance one another, so that the resultant variation in the heat of adsorption is very much less than would be expected from consideration of forces of one type only."

CONSIDERATION OF THE TIME LAGS, RESISTANCE CHANGES, ETC.

As has been mentioned before, the resistance and vaporization changes do not take place instantaneously. This is apparent because of the rounding of the corners in Fig. 1. On the basis of the theory proposed, the explanation for the time lags becomes quite simple. Upon applying an electric field, a gas layer begins to form on the filament. It is not until the fraction of the surface covered reaches a maximum, constant value that the resistance *versus* time curve can have a steady slope. In like manner, we must wait for the gas layer to leave the wire before we can expect the slope of the curve to return to the value that it had before the field was applied.

When we calculate the lags to be expected on the assumption that they are due to the time required for gas layers to form and leave, we find that the magnitudes observed can be accounted for quite easily. It must be assumed, however, that f_1 increases with the electric field if we are to explain the lags with exactly the same numerical values that were used in the treatment of the vaporization change.

By comparing Figs. 2 and 3, we see that the resistance and vaporization changes apparently go hand in hand. Note, for example, that both effects begin at about the same field strength, and that if the curve in Fig. 3 were inverted, it would have the same general appearance as that in Fig. 2. In Worthing's work at 2500°K he also found the two effects to begin at about the same field strength and to increase together. It would seem, therefore, that the theory which has been presented to explain the decrease in vaporization rates should also be able to account for the resistance changes.

Any such explanation must be consistent with the following experimental facts. (a) Worthing and Estabrook found resistance changes in opposite directions. These findings were not contradictory, because different metals were used, and at different temperatures. It means, however, that any theory must be able to account for a change in resistance in either direction depending upon the conditions. (b) Vissat observed resistance changes at room temperature. Thus the changes can occur even when there is no appreciable vaporization. (c) Vissat found that his resistance changes were influenced by vacuum conditions, and were accompanied by a leakage current. (d) Lloyd Jones, working with a very good vacuum, did not observe any resistance or vaporization changes.

Let us attribute the resistance changes to variations in the temperature of the wire resulting from its being coated with gas when a field is applied, and uncoated when field is withdrawn. If the temperature changes are pro-

[12] J. K. Roberts, Proc. Roy. Soc. **A152**, 445 (1935).
[13] A. R. Miller, Proc. Camb. Phil. Soc. **36**, 69 (1940).

duced by changes in emissivity, and if the emissivity in turn varies linearly with the fraction of the surface covered with gas, then it is not hard to show that the percentage change in resistance would be directly proportional to the change in the fraction of the wire surface covered with gas, or

$$\Delta R/R \doteq (\text{constant})(\theta_1-\theta_0) \doteq (\text{constant})\theta_1. \quad (22)$$

With this relationship, the curve in Fig. 3 would look the same as the 1452°K curve in Fig. 2 turned upside down. This is seen to be approximately the case.

The fact that Worthing observed a decrease in resistance of his W filament when a field was applied at 2500°K, while Estabrook and Vissat, using Mo and W wires, found increases at lower temperatures can be understood if we imagine that there is a spectral variation in the behavior of the emissivity when a filament is coated with gas. The results are explainable if the presence of a gas layer decreases the long wave-length emissivity below that for a bare wire, but increases the short wave-length emissivity so that at high temperatures there is a resultant increase in the total emissivity, but at lower temperatures a resultant decrease.

Another feature of this work that must be considered is the fact that Estabrook obtained a vaporization rate for Mo at 1452°K which was very much greater than that predicted by an equation set forth by Jones, Langmuir, and Mackay.[4] Estabrook's value was 1.4×10^{-9} g/cm² sec., while from J., L., and M., we get 8.0×10^{-15} g/cm² sec. Because of this discrepancy, Norris[14] also studied the vaporization of Mo. His work gives 1.9×10^{-13} g/cm² sec. as the vaporization rate for Mo at 1452°K, and hence does not agree with either of the above values. Thus the question of what the correct vaporization rate is remains unsettled.

It may be that the variation in values obtained was due to differences in extent to which the filaments were covered with gas. If such is the case, then Estabrook's value should be the best because it is the highest. This is in agreement with our treatment above, in which we found his filament to be essentially uncoated before the field was applied (i.e., $\theta_0 \doteq 0$). The vaporization rate of Mo as given by Jones, Langmuir, and Mackay would then seem to be in error. As a partial corroboration of this, we note that Wahlen and Whitney[15] were forced to discard the vaporization rates of W as predicted by equations of J., L., and M. In so doing, they say ". . . but their (J., L., and M.) calculations are based on evaporation data obtained at a time when vacuum conditions had not been developed to the present extent; so this value is somewhat questionable."

At the beginning of this paper we mentioned that Lloyd Jones, working with a very good vacuum, had failed to observe either the resistance or the vaporization change. Such a fact would of itself lead one to suspect that the phenomena were in some way due to the gas in the tube. Since we have attributed the effects observed to an adsorbed gas layer, presumably oxygen, on the wire, we can easily account for Jones' failure to find anything by assuming that he had removed too much of the gas from his tube.

ACKNOWLEDGMENT

The author wishes to express his appreciation to Dr. A. G. Worthing, who suggested this problem and under whose supervision it was conducted. He is grateful also to Dr. Estabrook who sent him more data when he needed it, and to Dr. James Tipping for his continued interest and encouragement.

[14] L. A. Norris, M.S. Thesis, University of Pittsburgh (1933).

[15] H. B. Wahlin and L. V. Whitney, Phys. Rev. **50**, 735 (1936).

PHYSICAL REVIEW VOLUME 63, NUMBERS 9 AND 10 MAY 1 AND 15, 1943

Theory of Complex Spectra. III

GIULIO RACAH
The Hebrew University, Jerusalem, Palestine
(Received February 8, 1943)

The consideration of the phases of the fractional-parentage coefficients allows the extension of the matrix methods to configurations with more than two equivalent electrons. Tables are given for the parentages of the terms of p^n and d^n. Applications are made to the spin-orbit interaction of the d^n terms and to the electrostatic interaction between the configurations d^n, $d^{n-1}s$, and $d^{n-2}s^2$. Errata in Part II are indicated.

§1. INTRODUCTION

THIS paper deals chiefly with the application of matrix methods to calculations within configurations with more than two equivalent electrons.

It is known that the eigenfunctions built up with the usual vector-coupling formulas[1] are not antisymmetrical as required from the exclusion principle and they must be antisymmetrized afterwards. But if certain of the electrons are equivalent, these antisymmetrized states are no longer normalized and some of them are linearly dependent, so that the calculations become very complicated.

An escape from these difficulties was proposed by Gray and Wills[2] who started from the nlm_lm_l scheme with antisymmetrized eigenfunctions and computed the SL eigenfunctions using angular-momentum operators and orthogonality considerations. This method leads to an orthonormal system of eigenfunctions, but since it gives up the vector-coupling formulas, the matrix of each operator must at first be calculated in the nlm_lm_l scheme and then transformed to the SL scheme, and no use may be made of the powerful matrix methods developed in Chapter III of TAS[1] and also extended in a previous paper of the author.[3]

In order to make full use of the above-mentioned methods, we shall calculate the eigenfunctions of the configuration l^n as linear combinations of the eigenfunctions obtained by the addition of a further electron l to the configuration l^{n-1}. This possibility was already indicated by Goudsmit and Bacher,[4] who introduced the concept of fractional parentage; but they were interested only in the squares of the coefficients of these linear combinations and calculated them with a procedure which, being based on a diagonal-sum method, did not permit them to separate the fractional parentages of duplicated terms.[5] The consideration of the phases of the coefficients of fractional parentage will enable us to calculate them separately also for terms of the same kind occurring in a given configuration and to calculate the matrix elements of every symmetrical operator between configurations containing equivalent electrons.

The fractional parentages of the configurations p^n and d^n are calculated in §3 and §4, whilst §2 contains a lemma on which these calculations are based and §5 deals with the matrices of symmetrical operators. In §6 an analysis is made of the structure of the configurations l^n in connection with the appearance of more terms of the same kind, and §7 contains an application to configuration interactions.

§2. TRANSFORMATIONS BETWEEN THE DIFFERENT COUPLING SCHEMES OF THREE ANGULAR MOMENTA

If we add two angular momenta j_1 and j_2, the magnitude J of the resulting vector and its z-component M characterize completely the states of the system; but if we add three angular momenta, several states may occur with the

[1] E. U. Condon and G. H. Shortley, *Theory of Atomic Spectra* (Cambridge, 1935) (which we shall denote by TAS), §14[3].
[2] N. M. Gray and L. A. Wills, Phys. Rev. **38**, 248 (1931); TAS §5[4].
[3] G. Racah, Phys. Rev. **62**, 438 (1942) (which we shall denote by II). We refer to this paper and to TAS for definitions, notations, and bibliographical indications.
[4] S. Goudsmit and R. F. Bacher, Phys. Rev. **46**, 948 (1934).
[5] D. H. Menzel and L. Goldberg, Astrophys. J. **84**, 1 (1936).

TABLE I. $(p^3SL[p^2(S'L')pSL)$. The different rows are normalized separately, and N is the normalization factor of each linear combination.

		p^2		
p^3	N	^1S	^3P	^1D
^4S	1	0	1	0
^2P	$18^{-\frac{1}{2}}$	2	−3	$-5^{\frac{1}{2}}$
^2D	$2^{-\frac{1}{2}}$	0	1	−1

same J and M and a complete characterization of the states needs the specification of the type of coupling of the vectors.

We may for instance couple at first j_1 and j_2 and then add j_3 to their resultant J': In this case the eigenfunctions are

$$\psi(_1jj_2(J')j_3JM)=\sum_{m_3M'}\psi(j_1j_2J'M')\phi(j_3m_3)\cdot(J'j_3M'm_3|J'j_3JM)$$
$$=\sum_{m_1m_2m_3M'}\phi(j_1m_1)\phi(j_2m_2)\phi(j_3m_3)\cdot(j_1j_2m_1m_2|j_1j_2J'M')\cdot(J'j_3M'm_3|J'j_3JM);\quad(1)$$

but we may also couple at first j_2 and j_3 and then add their resultant J'' to j_1, and in this case the eigenfunctions are

$$\psi(j_1, j_2j_3(J''), JM)=\sum_{m_1m_2m_3M''}\phi(j_1m_1)\phi(j_2m_2)\phi(j_3m_3)\cdot(j_2j_3m_2m_3|j_2j_3J''M'')\cdot(j_1J''m_1M''|j_1J''JM).\quad(2)$$

The unitary transformation which connects these two representations of the same system is

$$(j_1j_2(J')j_3J|j_1, j_2j_3(J''), J)=\sum_{m_1m_2m_3M'M''}(J'j_3JM|J'j_3M'm_3)\cdot(j_1j_2J'M'|j_1j_2m_1m_2)\cdot(j_2j_3m_2m_3|j_2j_3J''M'')\cdot(j_1J''m_1M''|j_1J''JM);\quad(3)$$

introducing the expression (16′)II for the transformation coefficients for the addition of two angular momenta and using Eqs. (19)II and (37)II we obtain

$$(j_1j_2(J')j_3J|j_1, j_2j_3(J''), J)=[(2J'+1)(2J''+1)]^{\frac{1}{2}}W(j_1j_2Jj_3; J'J''),\quad(4)$$

where W is the function defined by (36′)II.

It is sometimes useful to consider the changing of the coupling together with a change in the order of the vectors; the same way as before yields

$$(j_1j_2(J')j_3J|j_1j_3(J'')j_2J)=[(2J'+1)(2J''+1)]^{\frac{1}{2}}W(J'j_3j_2J''; Jj_1).\quad(5)$$

If we have three electrons or groups of electrons, the transformations between the different parentages in SL coupling are obvious extensions of (4) and (5): For instance,

$$(s_1l_1s_2l_2(S'L')s_3l_3SL|s_1l_1, s_2l_2s_3l_3(S''L''), SL)=[(2S'+1)(2S''+1)(2L'+1)(2L''+1)]^{\frac{1}{2}}\cdot W(s_1s_2Ss_3; S'S'')W(l_1l_2Ll_3; L'L'');\quad(6)$$

a particular case of this transformation was considered in TAS 6[8] 14.

§3. THE EIGENFUNCTIONS OF GROUPS OF EQUIVALENT ELECTRONS

If we couple two equivalent electrons with the usual vector-coupling formulas, we obtain antisymmetric or symmetric eigenfunctions according to whether $S+L$ is even or odd (TAS, p. 231); the eigenfunctions of the states with $S+L$ even are therefore the normalized eigenfunctions of the allowed states of l^2.

If we add in the same way to the allowed states of l^2 a third l electron, the obtained eigenfunctions are in general antisymmetric only with respect to the first two electrons, but not with

TABLE II. $(d^2vSL[d^2(v'S'L)dSL)$.

		d^2				
d^2	N	^1S	^3P	^1D	^3F	^1G
$_2{}^3P$	$30^{-\frac{1}{2}}$	0	$7^{\frac{1}{2}}$	$15^{\frac{1}{2}}$	$-8^{\frac{1}{2}}$	0
$_3{}^4P$	$15^{-\frac{1}{2}}$	0	$-8^{\frac{1}{2}}$	0	$-7^{\frac{1}{2}}$	0
$_1{}^3D$	$60^{-\frac{1}{2}}$	4	−3	$-5^{\frac{1}{2}}$	$-21^{\frac{1}{2}}$	−3
$_3{}^3D$	$140^{-\frac{1}{2}}$	0	−7	$45^{\frac{1}{2}}$	$21^{\frac{1}{2}}$	−5
$_3{}^3F$	$70^{-\frac{1}{2}}$	0	$28^{\frac{1}{2}}$	$-10^{\frac{1}{2}}$	$7^{\frac{1}{2}}$	−5
$_3{}^4F$	$5^{-\frac{1}{2}}$	0	−1	0	2	0
$_3{}^3G$	$42^{-\frac{1}{2}}$	0	0	$-10^{\frac{1}{2}}$	$21^{\frac{1}{2}}$	$11^{\frac{1}{2}}$
$_3{}^3H$	$2^{-\frac{1}{2}}$	0	0	0	−1	1

respect to the third. If we apply in effect to $\psi(l^2(S'L')lSL)$ the transformation[6]

$$\psi(l^2(S'L')lSL)=\sum_{S''L''}\psi(l,\,l(S''L''),\,SL)\cdot(l,\,l(S''L''),\,SL\,|\,l^2(S'L')lSL),\quad(7)$$

where the transformation matrix is given by (6), we obtain in general in the sum (7) allowed and forbidden values of $S''L''$ and, therefore, $\psi(l^2(S'L')lSL)$ cannot be an eigenfunction of l^3.

Only such a linear combination

$$\Psi(l^3\alpha SL)=\sum_{S'L'}\psi(l^2(S'L')lSL)\cdot(l^2(S'L')lSL]\,l^3\alpha SL)\quad(8)$$

may be the eigenfunction of l^3 for which the coefficients of $\psi(l,\,l(S''L''),\,SL)$ vanish for every forbidden value of $S''L''$ after the application of the transformation (7); the "coefficients of fractional parentage" $(l^2(S'L')lSL]\,l^3\alpha SL)$ must therefore satisfy the equation system

$$\sum_{S'L'}(l,\,l(S''L''),\,SL\,|\,l^2(S'L')lSL)\cdot(l^2(S'L')lSL]\,l^3\alpha SL)=0\quad(S''+L''\text{ odd}).\quad(9)$$

Since a function antisymmetric with respect to the electrons 1 and 2 and also with respect to the electrons 2 and 3 is antisymmetric with respect to all three electrons, the condition (9) is necessary and sufficient for the determination of the coefficients of fractional parentage of the terms of l^3, and the number of independent non-vanishing solutions of (9) for a given SL equals the number of allowed terms of this kind in l^3; if this number is greater than one, the different terms may be distinguished by a parameter α.

As an illustration of this method let us calculate the eigenfunction of the term $p^3\,{}^2D$. It follows from (6) that

$$\psi(p^2({}^3P)p\,{}^2D)=(3/16)^{\frac{1}{2}}\psi(p,\,pp({}^3D),\,{}^2D)-(3/16)^{\frac{1}{2}}\psi(p,\,pp({}^1P),\,{}^2D)+(3/4)\psi(p,\,pp({}^1D),\,{}^2D)-(1/4)\psi(p,\,pp({}^3P),\,{}^2D),$$

[6] Since we shall mostly consider transformations and operators which are diagonal with respect to M_S and M_L and independent of them, we shall in general neglect these quantum numbers.

TABLE III. $(d^4vSL[d^3(v'S'L')dSL)$.

d^4	N	d^3 ${}^2P$	${}^4P$	${}^2D$	${}^2D$	${}^2F$	${}^4F$	${}^2G$	${}^2H$
${}^1S$	1	0	0	1	0	0	0	0	0
${}^3S$	1	0	0	0	1	0	0	0	0
${}^2P$	$360^{-\frac{1}{2}}$	$-14^{\frac{1}{2}}$	-8	$135^{\frac{1}{2}}$	$-35^{\frac{1}{2}}$	$-56^{\frac{1}{2}}$	$-56^{\frac{1}{2}}$	0	0
${}^4P$	$90^{-\frac{1}{2}}$	5	$-14^{\frac{1}{2}}$	0	$10^{\frac{1}{2}}$	-5	4	0	0
${}^2D$	$280^{-\frac{1}{2}}$	$-42^{\frac{1}{2}}$	0	$105^{\frac{1}{2}}$	$45^{\frac{1}{2}}$	$28^{\frac{1}{2}}$	0	$-60^{\frac{1}{2}}$	0
${}^4D$	$140^{-\frac{1}{2}}$	$42^{\frac{1}{2}}$	0	0	$20^{\frac{1}{2}}$	$63^{\frac{1}{2}}$	0	$15^{\frac{1}{2}}$	0
${}^2D$	$210^{-\frac{1}{2}}$	$-14^{\frac{1}{2}}$	7	0	$60^{\frac{1}{2}}$	$-21^{\frac{1}{2}}$	$-21^{\frac{1}{2}}$	$45^{\frac{1}{2}}$	0
${}^4D$	$10^{-\frac{1}{2}}$	0	$3^{\frac{1}{2}}$	0	0	0	$7^{\frac{1}{2}}$	0	0
${}^2F$	$560^{-\frac{1}{2}}$	$120^{\frac{1}{2}}$	0	0	$200^{\frac{1}{2}}$	$-105^{\frac{1}{2}}$	0	$-3^{\frac{1}{2}}$	$-132^{\frac{1}{2}}$
${}^4F$	$840^{-\frac{1}{2}}$	4	$-56^{\frac{1}{2}}$	$315^{\frac{1}{2}}$	$15^{\frac{1}{2}}$	$-14^{\frac{1}{2}}$	$224^{\frac{1}{2}}$	$90^{\frac{1}{2}}$	$110^{\frac{1}{2}}$
${}^2F$	$1680^{-\frac{1}{2}}$	$-200^{\frac{1}{2}}$	$-448^{\frac{1}{2}}$	0	$120^{\frac{1}{2}}$	$-175^{\frac{1}{2}}$	$-112^{\frac{1}{2}}$	$-405^{\frac{1}{2}}$	$220^{\frac{1}{2}}$
${}^2G$	$504^{-\frac{1}{2}}$	0	0	$189^{\frac{1}{2}}$	-5	$70^{\frac{1}{2}}$	0	$66^{\frac{1}{2}}$	$-154^{\frac{1}{2}}$
${}^4G$	$1008^{-\frac{1}{2}}$	0	0	0	$88^{\frac{1}{2}}$	$385^{\frac{1}{2}}$	0	$-507^{\frac{1}{2}}$	$-28^{\frac{1}{2}}$
${}^2G$	$1680^{-\frac{1}{2}}$	0	0	0	$200^{\frac{1}{2}}$	$315^{\frac{1}{2}}$	$-560^{\frac{1}{2}}$	$297^{\frac{1}{2}}$	$308^{\frac{1}{2}}$
${}^2H$	$60^{-\frac{1}{2}}$	0	0	0	0	$5^{\frac{1}{2}}$	$20^{\frac{1}{2}}$	-3	$28^{\frac{1}{2}}$
${}^2I$	$10^{-\frac{1}{2}}$	0	0	0	0	0	0	$3^{\frac{1}{2}}$	$7^{\frac{1}{2}}$

$$\psi(p^2({}^1D)p\,{}^2D)=(3/16)^{\frac{1}{2}}\psi(p,\,pp({}^3D),\,{}^2D)-(3/16)^{\frac{1}{2}}\psi(p,\,pp({}^1P),\,{}^2D)-(1/4)\psi(p,\,pp({}^1D),\,{}^2D)+(3/4)\psi(p,\,pp({}^3P),\,{}^2D);$$

since in the development of

$$\Psi(p^3\,{}^2D)=x\psi(p^2({}^3P)p\,{}^2D)+y\psi(p^2({}^1D)p\,{}^2D)$$

the coefficients of

$$\psi(p,\,pp({}^3D),\,{}^2D)\quad\text{and}\quad\psi(p,\,pp({}^1P),\,{}^2D)$$

must vanish, the only possibility, apart from a phase factor, is

$$\Psi(p^3\,{}^2D)=(1/2)^{\frac{1}{2}}\psi(p^2({}^3P)p\,{}^2D)-(1/2)^{\frac{1}{2}}\psi(p^2({}^1D)p\,{}^2D).$$

The same method may also be extended to the configurations l^n, if the fractional parentages of l^{n-1} are known. In this case

$$\Psi(l^n\alpha SL)=\sum_{\alpha'S'L'}\psi(l^{n-1}(\alpha'S'L')lSL)\cdot(l^{n-1}(\alpha'S'L')lSL]\,l^n\alpha SL)$$
$$=\sum_{\alpha'S'L'\alpha''S''L''}\psi(l^{n-2}(\alpha''S''L'')l(S'L')lSL)\cdot(l^{n-2}(\alpha''S''L'')lS'L']\,l^{n-1}\alpha'S'L')\cdot(l^{n-1}(\alpha'S'L')lSL]\,l^n\alpha SL),\quad(10)$$

and the coefficients of fractional parentage $(l^{n-1}(\alpha'S'L')lSL]\,l^n\alpha SL)$ must satisfy the equa-

TABLE IV. $(d^5 v SL[d^4(v'S'L')dSL)$.

		d^4															
d^5	N	^5S	^3S	^3P	^1P	^3D	^1D	^3D	^5D	^3F	^1F	^3F	^3G	^1G	^5G	^3H	^1I
^6S	$5^{-\frac{1}{2}}$	0	0	0	0	0	$-2^{\frac{1}{2}}$	$3^{\frac{1}{2}}$	0	0	0	0	0	0	0	0	0
^8S	1	0	0	0	0	0	0	0	1	0	0	0	0	0	0	0	0
^4P	$150^{-\frac{1}{2}}$	0	0	$14^{\frac{1}{2}}$	5	$30^{\frac{1}{2}}$	$15^{\frac{1}{2}}$	$10^{\frac{1}{2}}$	0	$-15^{\frac{1}{2}}$	-4	-5	0	0	0	0	0
^2P	$300^{-\frac{1}{2}}$	0	0	-8	$14^{\frac{1}{2}}$	0	0	$35^{\frac{1}{2}}$	$-75^{\frac{1}{2}}$	0	$-56^{\frac{1}{2}}$	$56^{\frac{1}{2}}$	0	0	0	0	0
^4D	$50^{-\frac{1}{2}}$	$6^{\frac{1}{2}}$	0	-3	0	$-5^{\frac{1}{2}}$	0	0	0	0	$-21^{\frac{1}{2}}$	0	-3	0	0	0	0
^2D	$350^{-\frac{1}{2}}$	0	$-14^{\frac{1}{2}}$	-7	$-14^{\frac{1}{2}}$	$45^{\frac{1}{2}}$	$-10^{\frac{1}{2}}$	$60^{\frac{1}{2}}$	0	$35^{\frac{1}{2}}$	$21^{\frac{1}{2}}$	$-21^{\frac{1}{2}}$	-5	$-11^{\frac{1}{2}}$	$45^{\frac{1}{2}}$	0	0
^4D	$700^{-\frac{1}{2}}$	0	$-56^{\frac{1}{2}}$	0	$126^{\frac{1}{2}}$	0	$90^{\frac{1}{2}}$	$60^{\frac{1}{2}}$	0	$35^{\frac{1}{2}}$	0	$189^{\frac{1}{2}}$	0	$99^{\frac{1}{2}}$	$45^{\frac{1}{2}}$	0	0
^6D	$700^{-\frac{1}{2}}$	0	0	0	$126^{\frac{1}{2}}$	0	0	$-135^{\frac{1}{2}}$	$-175^{\frac{1}{2}}$	0	0	$-84^{\frac{1}{2}}$	0	0	$180^{\frac{1}{2}}$	0	0
^4F	$2800^{-\frac{1}{2}}$	0	0	$448^{\frac{1}{2}}$	$-200^{\frac{1}{2}}$	$-160^{\frac{1}{2}}$	$180^{\frac{1}{2}}$	$120^{\frac{1}{2}}$	0	$105^{\frac{1}{2}}$	$112^{\frac{1}{2}}$	$-175^{\frac{1}{2}}$	-20	$275^{\frac{1}{2}}$	$-405^{\frac{1}{2}}$	$220^{\frac{1}{2}}$	0
^2F	$2800^{-\frac{1}{2}}$	0	0	0	$360^{\frac{1}{2}}$	0	-10	$600^{\frac{1}{2}}$	0	$-525^{\frac{1}{2}}$	0	$-315^{\frac{1}{2}}$	0	$495^{\frac{1}{2}}$	-3	$-396^{\frac{1}{2}}$	0
^4F	$700^{-\frac{1}{2}}$	0	0	$-56^{\frac{1}{2}}$	-4	0	0	$-15^{\frac{1}{2}}$	$-175^{\frac{1}{2}}$	0	$224^{\frac{1}{2}}$	$14^{\frac{1}{2}}$	0	0	$-90^{\frac{1}{2}}$	$-110^{\frac{1}{2}}$	0
^6G	$8400^{-\frac{1}{2}}$	0	0	0	0	$-800^{\frac{1}{2}}$	-10	$600^{\frac{1}{2}}$	0	$-7^{\frac{1}{2}}$	$1680^{\frac{1}{2}}$	$945^{\frac{1}{2}}$	$880^{\frac{1}{2}}$	$845^{\frac{1}{2}}$	$891^{\frac{1}{2}}$	$924^{\frac{1}{2}}$	$-728^{\frac{1}{2}}$
^4G	$18480^{-\frac{1}{2}}$	0	0	0	0	0	$1452^{\frac{1}{2}}$	$968^{\frac{1}{2}}$	0	$-2541^{\frac{1}{2}}$	0	$4235^{\frac{1}{2}}$	0	$-1215^{\frac{1}{2}}$	$-5577^{\frac{1}{2}}$	$-308^{\frac{1}{2}}$	$-2184^{\frac{1}{2}}$
^4G	$420^{-\frac{1}{2}}$	0	0	0	0	0	0	5	$-105^{\frac{1}{2}}$	0	0	$-70^{\frac{1}{2}}$	0	0	$-66^{\frac{1}{2}}$	$154^{\frac{1}{2}}$	0
^2H	$1100^{-\frac{1}{2}}$	0	0	0	0	0	0	0	0	$33^{\frac{1}{2}}$	$-220^{\frac{1}{2}}$	$55^{\frac{1}{2}}$	$220^{\frac{1}{2}}$	$-5^{\frac{1}{2}}$	$-99^{\frac{1}{2}}$	$286^{\frac{1}{2}}$	$182^{\frac{1}{2}}$
^2I	$550^{-\frac{1}{2}}$	0	0	0	0	0	0	0	0	0	0	0	0	$-45^{\frac{1}{2}}$	$99^{\frac{1}{2}}$	$231^{\frac{1}{2}}$	$-175^{\frac{1}{2}}$

tion system

$$\sum_{\alpha'S'L'} (S''L'', ll(S'''L'''), SL\,|\,S''L''l(S'L')lSL) \cdot (l^{n-2}(\alpha''S''L'')lS'L'][l^{n-1}\alpha'S'L') \cdot (l^{n-1}(\alpha'S'L')lSL][l^n\alpha SL) = 0 \qquad (S'''+L''' \text{ odd}). \quad (11)$$

The systems (9) and (11) do not fix the phases of the eigenfunctions of the different terms, nor the scheme in the case of more terms of the same kind, but give the fractional parentages in any arbitrary orthonormal scheme; the convenience of a particular choice of the scheme will be considered in §6.

The fractional parentages of the terms of p^3, d^3, d^4, and d^5 calculated with this method are given in Tables I–IV. The phases of the eigenfunctions of p^3 and d^3 are in agreement with those of TAS 4^8 $6j$ and 5^8 6 with the exception of $p^3\,{}^2P$; it must however be remarked that these phases differ from those of Ufford[7] for the terms ^4P, ^2F, ^4F, and ^2G of d^3.

The coefficients of fractional parentage considered by Goudsmit and Bacher and by Menzel and Goldberg are n times the squares of our coefficients.

It must be pointed out that the matrix $(l^{n-1}(\alpha'S'L')lSL][l^n\alpha SL)$ is not an ordinary unitary matrix, but only a rectangular matrix which is a part of a unitary one, since its columns do not exhaust all states of $l^{n-1}l$, but only those which are allowed in l^n; the hermitian conjugate

$$(l^n\alpha SL[l^{n-1}(\alpha'S'L')lSL) = [l^{n-1}(\alpha'S'L')lSL][l^n\alpha SL]^* \qquad (12)$$

does therefore satisfy the relation

$$\sum_{\alpha'S'L'} (l^n\alpha SL[l^{n-1}(\alpha'S'L')lSL) \cdot (l^{n-1}(\alpha'S'L')lSL][l^n\alpha''SL) = \delta(\alpha\alpha''); \quad (13)$$

but a matrix multiplication in the opposite order has no sense, if the sum is limited to the antisymmetric states of l^n. In calculations with only symmetrical operators we may however, treat formally the matrix $(l^{n-1}(\alpha'S'L')lSL][l^n\alpha SL)$ as a common unitary matrix without weakening the general laws of matrix calculations, since symmetrical operators do not connect states of different symmetry and, therefore, the sum over the neglected states vanishes.

§4. FRACTIONAL PARENTAGES IN ALMOST CLOSED SHELLS

We shall determine in this section a relation between the fractional parentages of the terms of an almost closed shell l^{4l+2-n} and those of the terms of l^{n+1}. This relation will not only avoid long numerical calculations, but will also give us the eigenfunctions of the terms of l^{4l+2-n} with the phases fixed by the convention of §6 of II.

[7] C. W. Ufford, Phys. Rev. **44**, 732 (1933).

According to §6 of II two terms of l^n and of l^{4l+2-n} will be called conjugated[8] if their eigenfunctions appear multiplied with each other in the relation

$$\Psi(l^{4l+2}\,{}^1S)=\binom{4l+2}{n}^{-\frac{1}{2}}\sum_{\alpha SLM_SM_L}[(2S+1)\cdot(2L+1)]^{\frac{1}{2}}\Psi_{\mathfrak{L}}(l^n\alpha SLM_SM_L)\cdot\Psi_{\mathfrak{R}}(l^{4l+2-n}\alpha SL-M_S-M_L)\cdot(SSM_S-M_S|SS00)\cdot(LLM_L-M_L|LL00),\quad(14)$$

where $\mathfrak{L}$ denotes the group of the first n electrons of the shell and $\mathfrak{R}$ the group of the remaining $4l+2-n$; owing to (16′)II we have

$$\Psi(l^{4l+2}\,{}^1S)=\binom{4l+2}{n}^{-\frac{1}{2}}\sum_{\alpha SLM_SM_L}(-1)^{S+L-M_S-M_L}\Psi_{\mathfrak{L}}(l^n\alpha SLM_SM_L)\cdot\Psi_{\mathfrak{R}}(l^{4l+2-n}\alpha SL-M_S-M_L).\quad(15a)$$

In the same way, if we consider the group $\mathfrak{L}'$ of the first $n+1$ electrons of the shell and the group $\mathfrak{R}'$ of the remaining $4l+1-n$, we may also write

$$\Psi(l^{4l+2}\,{}^1S)=\binom{4l+2}{n+1}^{-\frac{1}{2}}\cdot\sum_{\alpha'S'L'M_S'M_L'}\cdot(-1)^{S'+L'-M_S'-M_L}\cdot\Psi_{\mathfrak{L}'}(l^{n+1}\alpha'S'L'M_S'M_L')\cdot\Psi_{\mathfrak{R}'}(l^{4l+1-n}\alpha'S'L'-M_S'-M_L').\quad(15b)$$

It follows from (10) that

$$\Psi_{\mathfrak{L}'}(l^{n+1}\alpha'S'L'M_S'M_L')=\sum_{\alpha SLM_SM_Lm_sm_l}\Psi_{\mathfrak{L}}(l^n\alpha SLM_SM_L)\cdot\phi_{n+1}(m_sm_l)(S\tfrac{1}{2}M_Sm_s|S\tfrac{1}{2}S'M_S')\cdot(LlM_Lm_l|LlL'M_L')\cdot(l^n(\alpha SL)lS'L'\}l^{n+1}\alpha'S'L'),\quad(16)$$

and

$$\Psi_{\mathfrak{R}}(l^{4l+2-n}\alpha SL-M_S-M_L)=\sum_{\alpha'S'L'M_S'M_L'm_sm_l}\cdot\Psi_{\mathfrak{R}''}(l^{4l+1-n}\alpha'S'L'-M_S'-M_L')\phi_{4l+2}(m_sm_l)\cdot(S'\tfrac{1}{2}-M_S'm_s|S'\tfrac{1}{2}S-M_S)\cdot(L'l-M_L'm_l|L'lL-M_L)\cdot(l^{4l+1-n}(\alpha'S'L')lSL\}l^{4l+2-n}\alpha SL);$$

here $\mathfrak{R}''$ is the group of the electrons $n+1$, $n+2$, $\cdots 4l+1$. Since $\Psi_{\mathfrak{R}}$ is antisymmetric, the substitution of the electron $4l+2$ by the electron $n+1$ and of the group $\mathfrak{R}''$ by the group $\mathfrak{R}'$ multiplies $\Psi_{\mathfrak{R}}$ by $(-1)^{n+1}$, and then

$$\Psi_{\mathfrak{R}}(l^{4l+2-n}\alpha SL-M_S-M_L)=\sum_{\alpha'S'L'M_S'M_L'm_sm_l}(-1)^{n+1}\phi_{n+1}(m_sm_l)\cdot\Psi_{\mathfrak{R}'}(l^{4l+1-n}\alpha'S'L'-M_S'-M_L')\cdot(S'\tfrac{1}{2}-M_S'm_s|S'\tfrac{1}{2}S-M_S)\cdot(L'l-M_L'm_l|L'lL-M_L)\cdot(l^{4l+1-n}(\alpha'S'L')lSL\}l^{4l+2-n}\alpha SL).\quad(17)$$

If we introduce (17) in (15a) and (16) in (15b), we may equate the coefficients of each product $\Psi_{\mathfrak{L}}\phi_{n+1}\Psi_{\mathfrak{R}'}$ separately, since for different quantum numbers these products are orthogonal, and obtain

$$\binom{4l+2}{n}^{-\frac{1}{2}}(-1)^{S+L-M_S-M_L+n+1}\cdot(S'\tfrac{1}{2}-M_S'm_s|S'\tfrac{1}{2}S-M_S)\cdot(L'l-M_L'm_l|L'lL-M_L)\cdot(l^{4l+1-n}(\alpha'S'L')lSL\}l^{4l+2-n}\alpha SL)=\binom{4l+2}{n+1}^{-\frac{1}{2}}(-1)^{S'+L'-M_S'-M_L'}\cdot(S\tfrac{1}{2}M_Sm_s|S\tfrac{1}{2}S'M_S')(LlM_Lm_l|LlL'M_L')\cdot(l^n(\alpha SL)lS'L'\}l^{n+1}\alpha'S'L').\quad(18)$$

Owing to (16′)II and (19a)II, and to the fact that $n+1$ has the same parity as $2(S'+L')$, we get

$$(l^{4l+1-n}(\alpha'S'L')lSL\}l^{4l+2-n}\alpha SL)=(-1)^{S+S'+L+L'-l-\frac{1}{2}}\cdot\left[\frac{(n+1)(2S'+1)(2L'+1)}{(4l+2-n)(2S+1)(2L+1)}\right]^{\frac{1}{2}}\cdot(l^n(\alpha SL)lS'L'\}l^{n+1}\alpha'S'L'),\quad(19)$$

which is the requested relation.

[8] To the correlation defined in §6 of II we shall reserve the word "conjugation," since other types of correlations between terms of different configurations will be found in §6 of this paper.

TABLE V. $(p^2SL\|U^{(2)}\|p^2S'L')$.

	^1S	^3P	^1D
^1S	0	0	$\frac{2}{3}(3)^{\frac{1}{2}}$
^3P	0	-1	0
^1D	$\frac{2}{3}(3)^{\frac{1}{2}}$	0	$\frac{1}{3}(21)^{\frac{1}{2}}$

TABLE VI. $(p^2SL\|U^{(2)}\|p^2SL')$.

	^4S	^2P	^2D
^4S	0	0	0
^2P	0	0	$-(3)^{\frac{1}{2}}$
^2D	0	$(3)^{\frac{1}{2}}$	0

From (19) and (13) we obtain also

$$\sum_{\alpha SL}(2S+1)(2L+1)(l^{n-1}(\alpha'S'L')lSL\|l^n\alpha SL)\cdot(l^n\alpha SL\|l^{n-1}(\alpha''S'L')lSL)=[(4l+3-n)/n](2S'+1)(2L'+1)\delta(\alpha'\alpha''). \quad (20)$$

For the determination of the fractional parentages of the terms of l^{2l+2} it must, however, be observed that (19) gives the parentages of $\Psi_{\mathfrak{N}}(l^{2l+2})$ with respect to $\Psi_{\mathfrak{N}}(l^{2l+1})$, and that the eigenfunctions of l^{2l+1} determined by the methods of the preceding section are $\Psi_{\mathfrak{L}}(l^{2l+1})$; since it was shown in §6 of II that the terms of l^{2l+1} split in two classes, according to the two possibilities of (76)II, we must change the sign in the relation (19) if $\Psi_{\mathfrak{N}}(l^{2l+1}\alpha'S'L')$ belongs to the class for which the minus sign holds in (76)II. The classification of the terms from this point of view will be considered in subsection (5) of §6.

§5. MATRIX COMPONENTS OF SYMMETRIC OPERATORS

We are at first interested in the matrix components $(\lambda^{\mathrm{I}}|F|\lambda^{\mathrm{II}})$ of the quantity

$$F=\sum_1^n f_i, \quad (21)$$

where f_i is an operator which operates on the

TABLE VII. $(d^3vSL\|35U^{(2)}\|d^3v'S'L')$.

	^2P	^4P	^2D	^2D	^2F	^4F	^2G	^2H
^2P	$-2(21)^{\frac{1}{2}}$	0	$-2\frac{1}{2}(10)^{\frac{1}{2}}$	$\frac{1}{2}(210)^{\frac{1}{2}}$	$-4(21)^{\frac{1}{2}}$	0	0	0
^4P	0	$7(21)^{\frac{1}{2}}$	0	0	0	$-14(6)^{\frac{1}{2}}$	0	0
^2D	$2\frac{1}{2}(10)^{\frac{1}{2}}$	0	$3\frac{5}{2}$	$1\frac{5}{2}(21)^{\frac{1}{2}}$	$-7(15)^{\frac{1}{2}}$	0	$-15(7)^{\frac{1}{2}}$	0
^2D	$-\frac{1}{2}(210)^{\frac{1}{2}}$	0	$1\frac{5}{2}(21)^{\frac{1}{2}}$	$1\frac{5}{2}$	$-9(35)^{\frac{1}{2}}$	0	$-5(3)^{\frac{1}{2}}$	0
^2F	$-4(21)^{\frac{1}{2}}$	0	$7(15)^{\frac{1}{2}}$	$9(35)^{\frac{1}{2}}$	$7(6)^{\frac{1}{2}}$	0	$2(210)^{\frac{1}{2}}$	$-(2310)^{\frac{1}{2}}$
^4F	0	$-14(6)^{\frac{1}{2}}$	0	0	0	$-7(6)^{\frac{1}{2}}$	0	0
^2G	0	0	$-15(7)^{\frac{1}{2}}$	$-5(3)^{\frac{1}{2}}$	$-2(210)^{\frac{1}{2}}$	0	$3(22)^{\frac{1}{2}}$	$-(462)^{\frac{1}{2}}$
^2H	0	0	0	0	$-(2310)^{\frac{1}{2}}$	0	$(462)^{\frac{1}{2}}$	$(3003)^{\frac{1}{2}}$

TABLE VIIIa. $(d^4\,{}_v{}^1L\|35U^{(2)}\|d^4\,{}_v{}^1L')$.

	${}_0{}^1S$	${}_4{}^1S$	${}_2{}^1D$	${}_4{}^1D$	${}_4{}^1F$	${}_2{}^1G$	${}_4{}^1G$	${}_4{}^1I$
${}_0{}^1S$	0	0	$7(30)^{\frac{1}{2}}$	0	0	0	0	0
${}_4{}^1S$	0	0	$3(70)^{\frac{1}{2}}$	$4(35)^{\frac{1}{2}}$	0	0	0	0
${}_2{}^1D$	$7(30)^{\frac{1}{2}}$	$3(70)^{\frac{1}{2}}$	-5	$-30(2)^{\frac{1}{2}}$	0	$4(5)^{\frac{1}{2}}$	$8(55)^{\frac{1}{2}}$	0
${}_4{}^1D$	0	$4(35)^{\frac{1}{2}}$	$-30(2)^{\frac{1}{2}}$	-15	$10(14)^{\frac{1}{2}}$	$10(10)^{\frac{1}{2}}$	$2(110)^{\frac{1}{2}}$	0
${}_4{}^1F$	0	0	0	$-10(14)^{\frac{1}{2}}$	$3\frac{5}{2}(6)^{\frac{1}{2}}$	$-7(70)^{\frac{1}{2}}$	$-\frac{1}{2}(770)^{\frac{1}{2}}$	0
${}_2{}^1G$	0	0	$4(5)^{\frac{1}{2}}$	$10(10)^{\frac{1}{2}}$	$7(70)^{\frac{1}{2}}$	$5(22)^{\frac{1}{2}}$	$5(2)^{\frac{1}{2}}$	$-2(455)^{\frac{1}{2}}$
${}_4{}^1G$	0	0	$8(55)^{\frac{1}{2}}$	$2(110)^{\frac{1}{2}}$	$1\frac{1}{2}(770)^{\frac{1}{2}}$	$5(2)^{\frac{1}{2}}$	$-12\frac{5}{22}(22)^{\frac{1}{2}}$	$-\frac{8}{11}(5005)^{\frac{1}{2}}$
${}_4{}^1I$	0	0	0	0	0	$-2(455)^{\frac{1}{2}}$	$-\frac{8}{11}(5005)^{\frac{1}{2}}$	$3\frac{5}{11}(143)^{\frac{1}{2}}$

TABLE VIIIb. $(d^4vSL\|35U^{(2)}\|d^4v'S'L')$ for $S=1, 2$.

	^2P	^4P	^2D	^2D	^2F	^4F	^2G	^2H
${}_2{}^3P$	$-\frac{7}{3}(21)^{\frac{1}{2}}$	$1\frac{4}{3}(6)^{\frac{1}{2}}$	$-2\frac{8}{3}(15)^{\frac{1}{2}}$	0	$1\frac{4}{3}(6)^{\frac{1}{2}}$	$2\frac{8}{3}(6)^{\frac{1}{2}}$	0	0
${}_4{}^3P$	$1\frac{4}{3}(6)^{\frac{1}{2}}$	$1\frac{9}{3}(21)^{\frac{1}{2}}$	$-\frac{4}{3}(210)^{\frac{1}{2}}$	0	$2\frac{2}{3}(21)^{\frac{1}{2}}$	$\frac{8}{3}(21)^{\frac{1}{2}}$	0	0
${}_4{}^3D$	$2\frac{8}{3}(15)^{\frac{1}{2}}$	$\frac{4}{3}(210)^{\frac{1}{2}}$	5	0	$-4(35)^{\frac{1}{2}}$	$4(35)^{\frac{1}{2}}$	$20(3)^{\frac{1}{2}}$	0
${}_4{}^5D$	0	0	0	-35	0	0	0	0
${}_2{}^3F$	$1\frac{4}{3}(6)^{\frac{1}{2}}$	$2\frac{2}{3}(21)^{\frac{1}{2}}$	$4(35)^{\frac{1}{2}}$	0	$\frac{7}{3}(6)^{\frac{1}{2}}$	$4\frac{9}{3}(6)^{\frac{1}{2}}$	$-3(210)^{\frac{1}{2}}$	$\frac{2}{3}(2310)^{\frac{1}{2}}$
${}_4{}^3F$	$2\frac{8}{3}(6)^{\frac{1}{2}}$	$\frac{8}{3}(21)^{\frac{1}{2}}$	$-4(35)^{\frac{1}{2}}$	0	$4\frac{9}{3}(6)^{\frac{1}{2}}$	$7\frac{7}{6}(6)^{\frac{1}{2}}$	$-\frac{1}{2}(210)^{\frac{1}{2}}$	$\frac{2}{3}(2310)^{\frac{1}{2}}$
${}_4{}^3G$	0	0	$20(3)^{\frac{1}{2}}$	0	$3(210)^{\frac{1}{2}}$	$\frac{1}{2}(210)^{\frac{1}{2}}$	$-3\frac{1}{2}(22)^{\frac{1}{2}}$	$-2(462)^{\frac{1}{2}}$
${}_4{}^3H$	0	0	0	0	$\frac{2}{3}(2310)^{\frac{1}{2}}$	$\frac{2}{3}(2310)^{\frac{1}{2}}$	$2(462)^{\frac{1}{2}}$	$\frac{1}{3}(3003)^{\frac{1}{2}}$

TABLE IXa. $(d^5\ {}^3L\|35U^{(2)}\|d^5\ {}^3L')$.

	^3S	^3P	^3D	^3D	^3D	^3F	^3F	^3G	^3G	^3H	^3I
^3S	0	0	0	$4(70)^{\frac{1}{2}}$	0	0	0	0	0	0	0
^3P	0	0	$-7(30)^{\frac{1}{2}}$	0	$5(105)^{\frac{1}{2}}$	0	$4(105)^{\frac{1}{2}}$	0	0	0	0
^3D	0	$7(30)^{\frac{1}{2}}$	0	$15(7)^{\frac{1}{2}}$	0	$-14(5)^{\frac{1}{2}}$	0	$-10(21)^{\frac{1}{2}}$	0	0	0
^3D	$4(70)^{\frac{1}{2}}$	0	$15(7)^{\frac{1}{2}}$	0	$5(2)^{\frac{1}{2}}$	0	$10(7)^{\frac{1}{2}}$	0	$-6(55)^{\frac{1}{2}}$	0	0
^3D	0	$-5(105)^{\frac{1}{2}}$	0	$5(2)^{\frac{1}{2}}$	0	0	0	$20(6)^{\frac{1}{2}}$	0	0	0
^3F	0	0	$14(5)^{\frac{1}{2}}$	0	0	0	$-7(30)^{\frac{1}{2}}$	0	0	0	0
^3F	0	$4(105)^{\frac{1}{2}}$	0	$-10(7)^{\frac{1}{2}}$	0	$-7(30)^{\frac{1}{2}}$	0	$4(42)^{\frac{1}{2}}$	0	$-2(462)^{\frac{1}{2}}$	0
^3G	0	0	$-10(21)^{\frac{1}{2}}$	0	$20(6)^{\frac{1}{2}}$	0	$-4(42)^{\frac{1}{2}}$	0	$9(30)^{\frac{1}{2}}$	0	$4(273)^{\frac{1}{2}}$
^3G	0	0	0	$-6(55)^{\frac{1}{2}}$	0	0	0	$9(30)^{\frac{1}{2}}$	0	$6(70)^{\frac{1}{2}}$	0
^3H	0	0	0	0	0	0	$-2(462)^{\frac{1}{2}}$	0	$-6(70)^{\frac{1}{2}}$	0	$7(13)^{\frac{1}{2}}$
^3I	0	0	0	0	0	0	0	$4(273)^{\frac{1}{2}}$	0	$-7(13)^{\frac{1}{2}}$	0

TABLE IXb. $(d^5\ {}^4L\|35U^{(2)}\|d^5\ {}^4L')$.

	^4P	^4D	^4F	^4G
^4P	0	$7(15)^{\frac{1}{2}}$	0	0
^4D	$-7(15)^{\frac{1}{2}}$	0	$8(35)^{\frac{1}{2}}$	0
^4F	0	$-8(35)^{\frac{1}{2}}$	0	$15(14)^{\frac{1}{2}}$
^4G	0	0	$-15(14)^{\frac{1}{2}}$	0

TABLE X. $(p^2SL\|6^{\frac{1}{2}}V^{(11)}\|p^2S'L')$.

	^1S	^3P	^1D
^1S	0	$-\frac{1}{2}(30)^{\frac{1}{2}}$	0
^3P	$-\frac{1}{2}(30)^{\frac{1}{2}}$	3	$(6)^{\frac{1}{2}}$
^1D	0	$(6)^{\frac{1}{2}}$	0

TABLE XI. $(p^2SL\|6^{\frac{1}{2}}V^{(11)}\|p^2S'L')$.

	^4S	^2P	^2D
^4S	0	$2(3)^{\frac{1}{2}}$	0
^2P	$2(3)^{\frac{1}{2}}$	0	$(15)^{\frac{1}{2}}$
^2D	0	$-(15)^{\frac{1}{2}}$	0

electron i, and λ^{I} and λ^{II} are states of the configurations I and II; owing to the antisymmetry of $\Psi(\lambda^{\mathrm{I}})$ and $\Psi(\lambda^{\mathrm{II}})$ we have

$$(\lambda^{\mathrm{I}}|F|\lambda^{\mathrm{II}}) = \sum_1^n{}_i \int \bar{\Psi}(\lambda^{\mathrm{I}}) f_i \Psi(\lambda^{\mathrm{II}}) d\tau = n\int \bar{\Psi}(\lambda^{\mathrm{I}}) f_i \Psi(\lambda^{\mathrm{II}}) d\tau. \quad (22)$$

If $\mathrm{I}=\mathrm{II}=l^n$, putting $i=n$ and assuming for Ψ the expression (10), we obtain

$$(l^n\alpha SLM_SM_L|F|l^n\alpha'S'L'M_S'M_L') = n\sum_{\alpha_1S_1L_1}(l^n\alpha SL[l^{n-1}(\alpha_1S_1L_1)lSL) \cdot (S_1L_1l_nSLM_SM_L|f_n|S_1L_1l_nS'L'M_S'M_L') \cdot (l^{n-1}(\alpha_1S_1L_1)lS'L']l^n\alpha'S'L'), \quad (23)$$

where $(S_1L_1l_nSLM_SM_L|f_n|S_1L_1l_nS'L'M_S'M_L')$ may now be calculated with the ordinary matrix methods of Chapter III of TAS and of II.

As application of this formula we calculated the matrix components of the tensors $U^{(2)}$ and $V^{(11)}$, defined by (102)II, for the configurations p^2, p^3, d^3, d^4, and d^5; the results are given in Tables V–XIV. For d^2 the matrices were already given by (103)II; it must, however, be noted that an error occurred in the final form of the manuscript, and all the elements of (103c)II and (103d)II must be multiplied by $(3/2)^{\frac{1}{2}}$.

From the elements of $V^{(11)}$ the matrix components of the spin-orbit interaction may easily be obtained: it follows in effect from the relation

$$l=[l(l+1)(2l+1)]^{\frac{1}{2}}u^{(1)} \quad (24)$$

and from (38)II and (102)II that

$$(l^n\alpha SLJM|\textstyle\sum_i(\boldsymbol{s}_i\cdot\boldsymbol{l}_i)|l^n\alpha'S'L'JM) = (-1)^{S+L'-J}[l(l+1)(2l+1)]^{\frac{1}{2}} \cdot (l^n\alpha SL\|V^{(11)}\|l^n\alpha'S'L')W(SLS'L';J1). \quad (25)$$

If in (22) $\mathrm{I}=l^n$ and $\mathrm{II}=l^{n-1}l'$, the terms of II are characterized by S and L and by the quantum numbers of the parent ion l^{n-1}; $\Psi(\lambda^{\mathrm{II}})$ has in this case the expression

$$\Psi(l^{n-1}(\alpha_1S_1L_1)l'S'L'M_S'M_L') = (1/n)^{\frac{1}{2}}\sum_1^n{}_i(-1)^{P_i} \cdot\psi(l^{n-1}(\alpha_1S_1L_1)l_i'S'L'M_S'M_L'), \quad (26)$$

where in the right side we consider the group l^{n-1} as composed by the electrons 1, 2, $\cdots$, $i-1$, $i+1$, $\cdots$, n, and P_i is the parity of the permutation which exchanges i with n. Introducing

TABLE XII. $(d^2vSL\|30^{\frac{1}{2}}V^{(11)}\|d^2v'S'L')$.

	s^2P	s^4P	s^2D	s^4D	s^2F	s^4F	s^2G	s^2H
s^2P	2	$-2(14)^{\frac{1}{2}}$	$-\frac{1}{2}(42)^{\frac{1}{2}}$	$\frac{9}{2}(2)^{\frac{1}{2}}$	0	0	0	0
s^4P	$2(14)^{\frac{1}{2}}$	$(10)^{\frac{1}{2}}$	$-4(3)^{\frac{1}{2}}$	0	0	0	0	0
s^2D	$\frac{1}{2}(42)^{\frac{1}{2}}$	$-4(3)^{\frac{1}{2}}$	$\frac{3}{2}(5)^{\frac{1}{2}}$	$-\frac{1}{2}(105)^{\frac{1}{2}}$	$(42)^{\frac{1}{2}}$	$-(42)^{\frac{1}{2}}$	0	0
s^4D	$-\frac{9}{2}(2)^{\frac{1}{2}}$	0	$-\frac{1}{2}(105)^{\frac{1}{2}}$	$-\frac{1}{2}(5)^{\frac{1}{2}}$	$(2)^{\frac{1}{2}}$	$5(2)^{\frac{1}{2}}$	0	0
s^2F	0	0	$-(42)^{\frac{1}{2}}$	$-(2)^{\frac{1}{2}}$	$-\frac{1}{2}(14)^{\frac{1}{2}}$	$-(14)^{\frac{1}{2}}$	$\frac{3}{2}-(10)^{\frac{1}{2}}$	0
s^4F	0	0	$-(42)^{\frac{1}{2}}$	$5(2)^{\frac{1}{2}}$	$(14)^{\frac{1}{2}}$	$2(35)^{\frac{1}{2}}$	$-3(10)^{\frac{1}{2}}$	0
s^2G	0	0	0	0	$\frac{3}{2}(10)^{\frac{1}{2}}$	$-3(10)^{\frac{1}{2}}$	$\frac{9}{10}(30)^{\frac{1}{2}}$	$\frac{6}{5}(55)^{\frac{1}{2}}$
s^2H	0	0	0	0	0	0	$-\frac{6}{5}(55)^{\frac{1}{2}}$	$\frac{3}{5}(55)^{\frac{1}{2}}$

TABLE XIII. $(d^3vSL\|30^{\frac{1}{2}}V^{(11)}\|d^3v'S'L')$.

	o^1S	o^3S	s^2P	s^4P	s^2D	s^4D	s^2D	s^4D	s^2F	s^4F	s^2G	s^4G	s^2G	s^2H	s^2I
o^1S	0	0	$3(3)^{\frac{1}{2}}$	0	0	0	0	0	0	0	0	0	0	0	0
o^3S	0	0	$-(7)^{\frac{1}{2}}$	$2(2)^{\frac{1}{2}}$	0	0	0	0	0	0	0	0	0	0	0
s^2P	$3(3)^{\frac{1}{2}}$	$-(7)^{\frac{1}{2}}$	1	$-2(14)^{\frac{1}{2}}$	$-\frac{1}{2}(14)^{\frac{1}{2}}$	$2(7)^{\frac{1}{2}}$	0	$-4(5)^{\frac{1}{2}}$	0	0	0	0	0	0	0
s^4P	0	$2(2)^{\frac{1}{2}}$	$-2(14)^{\frac{1}{2}}$	2	2	$\frac{1}{2}(2)^{\frac{1}{2}}$	$\frac{9}{2}(2)^{\frac{1}{2}}$	$\frac{1}{2}(70)^{\frac{1}{2}}$	0	0	0	0	0	0	0
s^2D	0	0	$-\frac{1}{2}(14)^{\frac{1}{2}}$	2	0	0	$2(10)^{\frac{1}{2}}$	0	0	2	4	0	0	0	0
s^4D	0	0	$2(7)^{\frac{1}{2}}$	$\frac{1}{2}(2)^{\frac{1}{2}}$	0	0	$-(5)^{\frac{1}{2}}$	0	0	$(2)^{\frac{1}{2}}$	$-4(2)^{\frac{1}{2}}$	0	0	0	0
s^2D	0	0	0	$-\frac{9}{2}(2)^{\frac{1}{2}}$	$-2(10)^{\frac{1}{2}}$	$(5)^{\frac{1}{2}}$	$-\frac{1}{2}(5)^{\frac{1}{2}}$	$\frac{5}{2}(7)^{\frac{1}{2}}$	$-2(5)^{\frac{1}{2}}$	$5(2)^{\frac{1}{2}}$	$(2)^{\frac{1}{2}}$	0	0	0	0
s^4D	0	0	$-4(5)^{\frac{1}{2}}$	$\frac{1}{2}(70)^{\frac{1}{2}}$	0	0	$-\frac{5}{2}(7)^{\frac{1}{2}}$	$1\frac{5}{2}$	0	$-(70)^{\frac{1}{2}}$	$(70)^{\frac{1}{2}}$	0	0	0	0
s^1F	0	0	0	0	0	0	$-2(5)^{\frac{1}{2}}$	0	0	$(35)^{\frac{1}{2}}$	$\frac{1}{2}(35)^{\frac{1}{2}}$	0	0	$-\frac{9}{2}$	0	0
s^3F	0	0	0	0	2	$(2)^{\frac{1}{2}}$	$-5(2)^{\frac{1}{2}}$	$-(70)^{\frac{1}{2}}$	$-(35)^{\frac{1}{2}}$	$(14)^{\frac{1}{2}}$	$-(14)^{\frac{1}{2}}$	$-(3)^{\frac{1}{2}}$	$(33)^{\frac{1}{2}}$	$3(10)^{\frac{1}{2}}$	0	0
s^3F	0	0	0	0	4	$-4(2)^{\frac{1}{2}}$	$-(2)^{\frac{1}{2}}$	$(70)^{\frac{1}{2}}$	$-\frac{1}{2}(35)^{\frac{1}{2}}$	$-(14)^{\frac{1}{2}}$	$-\frac{1}{2}(14)^{\frac{1}{2}}$	$5(3)^{\frac{1}{2}}$	$-\frac{1}{2}(33)^{\frac{1}{2}}$	$-\frac{3}{2}(10)^{\frac{1}{2}}$	0	0
s^1G	0	0	0	0	0	0	0	0	0	$-(3)^{\frac{1}{2}}$	$5(3)^{\frac{1}{2}}$	0	0	3	$-(66)^{\frac{1}{2}}$	0
s^3G	0	0	0	0	0	0	0	0	0	$(33)^{\frac{1}{2}}$	$-\frac{1}{2}(33)^{\frac{1}{2}}$	0	0	$3\frac{1}{2}(11)^{\frac{1}{2}}$	$2(6)^{\frac{1}{2}}$	0
s^3G	0	0	0	0	0	0	0	0	$-9\frac{1}{2}$	$-3(10)^{\frac{1}{2}}$	$\frac{9}{2}(10)^{\frac{1}{2}}$	-3	$-3\frac{1}{2}(11)^{\frac{1}{2}}$	$3\frac{1}{10}(30)^{\frac{1}{2}}$	$^6/_{11}(55)^{\frac{1}{2}}$	0
s^3H	0	0	0	0	0	0	0	0	0	0	0	$-(66)^{\frac{1}{2}}$	$2(6)^{\frac{1}{2}}$	$-^6/_{11}(55)^{\frac{1}{2}}$	$^3/_{11}(55)^{\frac{1}{2}}$	$-3\frac{1}{2}(26)$
s^1I	0	0	0	0	0	0	0	0	0	0	0	0	0	0	$-3\frac{1}{2}(26)^{\frac{1}{2}}$	0

(10) and (26) in (22) and putting $i=n$, we have

$$(l^n\alpha SLM_SM_L|F|l^{n-1}(\alpha_1S_1L_1)l'S'L'M_S'M_L') = n^{\frac{1}{2}}(l^n\alpha SL\|l^{n-1}(\alpha_1S_1L_1)lSL) \cdot (S_1L_1l_nSLM_SM_L|f_n|S_1L_1l_n'S'L'M_S'M_L'). \quad (27)$$

This formula, which is the extension of TAS 6[8]17, gives a rigorous demonstration to the method of Menzel and Goldberg[9] and also fixes for such transitions the phases of the matrix components, which are necessary for transformations to other types of vector coupling (TAS, p. 252).

If in (22) $\mathrm{I}=l^{n-p}l'^p$ and $\mathrm{II}=l^{n-p-1}l'^{p+1}$, the terms of each configuration are characterized by S and L and by the quantum numbers of the groups of equivalent electrons; in the same way as for the precedent case we obtain

$$(l^{n-p}(\alpha_1S_1L_1),\ l'^p(\alpha_2S_2L_2),\ SLM_SM_L|F|l^{n-p-1}(\alpha_1'S_1'L_1'),\ l'^{p+1}(\alpha_2'S_2'L_2'),\ S'L'M_S'M_L') = [(n-p)(p+1)]^{\frac{1}{2}}\sum_{S_3L_3} (l^{n-p}\alpha_1S_1L_1\cdot\|l^{n-p-1}(\alpha_1'S_1'L_1')lS_1L_1) \cdot (S_1'L_1'l_{n-p}(S_1L_1),\ S_2L_2,\ SLM_SM_L|f_{n-p}|S_1'L_1'l_{n-p}'(S_3L_3),\ S_2L_2,\ S'L'M_S'M_L') \cdot (S_1'L_1'l'(S_3L_3),\ S_2L_2,\ S'L'|S_1'L_1',\ l'S_2L_2(S_2'L_2'),\ S'L') \cdot (l',\ l'^p(\alpha_2S_2I_2),\ S_2'L_2'\|l'^{p+1}\alpha_2'S_2'L_2'). \quad (28)$$

In connection with this result it must be observed that $(l,\ l^{n-1}(\alpha'S'L'),\ SL\|l^n\alpha SL)$ is not $(l^{n-1}(\alpha'S'L')lSL\|l^n\alpha SL)$, but it is easy to see that the two coefficients are connected by the relation

$$(l,\ l^{n-1}(\alpha'S'L'),\ SL\|l^n\alpha SL) = (-)^{S+L+S'+L'-l-\frac{1}{2}} \cdot (l^{n-1}(\alpha'S'L')lSL\|l^n\alpha SL). \quad (29)$$

It is unnecessary to consider the matrix elements of F for transitions between more com-

[9] D. H. Menzel and L. Goldberg, Phys. Rev. **47**, 424 (1935) and reference 5.

TABLE XIV. $(d^{1/2}SL\|30^{1/2}V^{(11)}\|d^{1/2}S'L')$.

	^2S	^4S	^2P	^4P	^2D	^4D	^2D	^4D	^2F	^4P	^4F	^2G	^2G	^4G	^2H	^2I
^2S	0	0	−4	$(14)^{1/2}$	0	0	0	0	0	0	0	0	0	0	0	0
^4S	0	0	0	$3(10)^{1/2}$	0	0	0	0	0	0	0	0	0	0	0	0
^2P	4	0	0	0	$-(14)^{1/2}$	0	1	$2(2)^{1/2}$	0	0	0	0	0	0	0	0
^4P	$(14)^{1/2}$	$3(10)^{1/2}$	0	0	−8	0	$-2(14)^{1/2}$	$-(70)^{1/2}$	0	0	0	0	0	0	0	0
^2D	0	0	$(14)^{1/2}$	−8	0	$-(35)^{1/2}$	0	0	$2(14)^{1/2}$	0	$-2(14)^{1/2}$	0	0	0	0	0
^4D	0	0	0	0	$-(35)^{1/2}$	0	$(10)^{1/2}$	$-4(5)^{1/2}$	0	$-2(10)^{1/2}$	0	0	0	0	0	0
^2D	0	0	−1	$-2(14)^{1/2}$	0	$(10)^{1/2}$	0	0	8	0	−2	0	0	0	0	0
^4D	0	0	$2(2)^{1/2}$	$(70)^{1/2}$	0	$4(5)^{1/2}$	0	0	$4(2)^{1/2}$	0	$-4(5)^{1/2}$	0	0	0	0	0
^2F	0	0	0	0	$-2(14)^{1/2}$	0	−8	$4(2)^{1/2}$	0	$-\frac{1}{2}(70)^{1/2}$	0	0	$-\frac{1}{2}(66)^{1/2}$	$5(6)^{1/2}$	0	0
^4P	0	0	0	0	0	$2(10)^{1/2}$	0	0	$-\frac{1}{2}(70)^{1/2}$	0	$-(70)^{1/2}$	$9\frac{1}{2}(2)^{1/2}$	0	0	0	0
^4F	0	0	0	0	$-2(14)^{1/2}$	0	−2	$4(5)^{1/2}$	0	$(70)^{1/2}$	0	0	$-(66)^{1/2}$	$(15)^{1/2}$	0	0
^2G	0	0	0	0	0	0	0	0	0	$-3\frac{1}{2}(2)^{1/2}$	0	0	$-3\frac{1}{2}(22)^{1/2}$	$-3(2)^{1/2}$	0	0
^2G	0	0	0	0	0	0	0	0	$3\frac{1}{2}(66)^{1/2}$	0	$-(66)^{1/2}$	$-3\frac{1}{2}(22)^{1/2}$	0	0	$-4(3)^{1/2}$	0
^4G	0	0	0	0	0	0	0	0	$5(6)^{1/2}$	0	$2(15)^{1/2}$	$3(2)^{1/2}$	0	0	$-2(33)^{1/2}$	0
^2H	0	0	0	0	0	0	0	0	0	0	0	0	$4(3)^{1/2}$	$-2(33)^{1/2}$	0	$-3(13)^{1/2}$
^2I	0	0	0	0	0	0	0	0	0	0	0	0	0	0	$3(13)^{1/2}$	0

plicated configurations, since all other cases may be reduced to these three by means of TAS I[8]16.

The calculation by the same method of the matrix components of the scalar operator

$$G=\sum_{i<j} g_{ij} \tag{30}$$

needs in some cases the knowledge of $\Psi(l^n\alpha SL)$ as linear combination of the eigenfunctions of $l^{n-2}l^2$:

$$\Psi(l^n\alpha SL)=\sum_{\alpha_1S_1L_1S_2L_2}\psi(l^{n-2}(\alpha_1S_1L_1),\, l^2(S_2L_2),\, SL)(l^{n-2}(\alpha_1S_1L_1),\, l^2(S_2L_2),\, SL]l^n\alpha SL); \tag{31}$$

the coefficients of this expression are given by the formula

$$(l^{n-2}(\alpha_1S_1L_1),\, l^2(S_2L_2),\, SL]l^nSL)=\sum_{\alpha'S'L'}(S_1L_1,\, l^2(S_2L_2),\, SL]S_1L_1l(S'L')lSL)\cdot(l^{n-2}(\alpha_1S_1L_1)lS'L']l^{n-1}\alpha'S'L')\cdot(l^{n-1}(\alpha'S'L')lSL]l^n\alpha SL). \tag{32}$$

The following results are easily derived:

$$(l^n\alpha SL|G|l^n\alpha'SL)=\tfrac{1}{2}n(n-1)\sum_{\alpha_1S_1L_1S_2L_2}(l^n\alpha SL[l^{n-2}(\alpha_1S_1L_1),\, l^2(S_2L_2),\, SL)(l^2S_2L_2|g|l^2S_2L_2)\cdot(l^{n-2}(\alpha_1S_1L_1),\, l^2(S_2L_2),\, SL]l^n\alpha'SL), \tag{33a}$$

$$(l^n\alpha SL|G|l^{n-1}(\alpha'S'L')l'SL)=(n-1)n^{1/2}\sum_{\alpha_1S_1L_1S_2L_2}(l^n\alpha SL[l^{n-2}(\alpha_1S_1L_1),\, l^2(S_2L_2),\, SL)(l_il_jS_2L_2|g_{ij}|l_il_j'S_2L_2)\cdot(S_1L_1,\, ll'(S_2L_2),\, SL|S_1L_1l(S'L')l'SL)\cdot(l^{n-2}(\alpha_1S_1L_1)lS'L']l^{n-1}\alpha'S'L'), \tag{33b}$$

$$(l^n\alpha SL|G|l^{n-2}(\alpha_1S_1L_1),\, l'^2(S_2L_2),\, SL)=[n(n-1)/2]^{1/2}(l^n\alpha SL[l^{n-2}(\alpha_1S_1L_1),\, l^2(S_2L_2),\, SL)(l^2S_2L_2|g|l'^2S_2L_2). \tag{33c}$$

Since the actual application of (32) needs generally very long calculations, the formulas (33) are of practical use only in a few particular cases; in other cases it is simpler to express g_{ij} as a sum of scalar products of tensors and to reduce the problem to the calculation of tensors of the type F. Applications of both methods will be shown in the next sections.

§6. THE STRUCTURE OF THE CONFIGUATIONS l^n

In this section we shall classify the terms of the configuration l^n according to the eigenvalues of

$$Q=\sum_{i<j} q_{ij}, \tag{34}$$

where q_{ij} is a scalar operator which operates on the two equivalent electrons i and j and is defined by the relation

$$(l^2LM|q_{ij}|l^2LM)=(2l+1)\delta(L,0). \tag{35}$$

It will be shown that to every term of l^n with non-vanishing Q a term of the same kind corresponds in l^{n-2}, and this fact will allow us to assign to each term a "seniority number" according to the value of n for which the term appeared for the first time. Some useful relation between the fractional parentages of corresponding terms will be obtained and it will also be shown that the classification of the terms of l^{2l+1} according to the two possibilities of (76)II depends only on the seniority of the term.

(1) The Eigenvalues of Q

It follows from (42)II and (40a)II that

$$\sum_0^{2l}{}_r (2r+1)W(llll;0r)W(llll;Lr)=\delta(L,0); \quad (36)$$

expressing $W(llll;0r)$ by (36′)II and using also (38)II and (58)II we get for q_{ij} the expression

$$q_{ij}=\sum_0^{2l}{}_r (-1)^r(2r+1)(\boldsymbol{u}_i^{(r)}\cdot\boldsymbol{u}_j^{(r)}). \quad (37)$$

Since $\boldsymbol{u}^{(0)}$ is a scalar and, owing to (33)II,

$$\boldsymbol{u}^{(r)2}=(2l+1)^{-1}, \quad (38)$$

we have also

$$q_{ij}=(2l+1)^{-1}+\sum_1^{2l}{}_r (-1)^r(2r+1)(\boldsymbol{u}_i^{(r)}\cdot\boldsymbol{u}_j^{(r)}) \quad (37')$$

and

$$Q=\tfrac{1}{2}n(n-2l-1)(2l+1)^{-1}+\tfrac{1}{2}\sum_1^{2l}{}_r (-1)^r(2r+1)\boldsymbol{U}^{(r)2}. \quad (39)$$

We shall henceforth consider only schemes for which also Q is diagonal, i.e., schemes for which

$$(l^n\alpha SL|Q|l^n\alpha' SL)=Q(l^n\alpha SL)\delta(\alpha\alpha'). \quad (40)$$

It follows from (39) and (74)II that if Q is diagonal in a given scheme of l^n, it is also diagonal in the conjugate scheme of l^{4l+2-n}, and that

$$Q(l^{4l+2-n}\alpha SL)=Q(l^n\alpha SL)+2l+1-n. \quad (41)$$

In order to calculate the possible values of $Q(l^n\alpha SL)$, we express it by means of (33a) and (35):

$$Q(l^n\alpha SL)\delta(\alpha\alpha')=\tfrac{1}{2}n(n-1)(2l+1)\cdot\sum_{\beta'}(l^n\alpha SL[l^{n-2}(\beta' SL),l^2(^1S),SL)\cdot(l^{n-2}(\beta' SL),l^2(^1S),SL]l^n\alpha' SL). \quad (42)$$

Multiplying the two sides by

$$(l^n\alpha' SL[l^{n-2}(\beta SL),l^2(^1S),SL)$$

and adding with respect to α' we have

$$Q(l^n\alpha SL)(l^n\alpha SL[l^{n-2}(\beta SL),l^2(^1S),SL)=\sum_{\alpha'\beta'}(l^n\alpha SL[l^{n-2}(\beta' SL),l^2(^1S),SL)\cdot(l^{n-2}(\beta' SL),l^2(^1S),SL]l^n\alpha' SL)\cdot(l^n\alpha' SL[l^{n-2}(\beta SL),l^2(^1S),SL);$$

the summation with respect to α' may be made by means of (42) after transforming the last two factors by the relation

$$(l^{n-2}(\beta SL),l^2(^1S),SL]l^n\alpha SL)=\left[\frac{(4l+3-n)(4l+4-n)}{n(n-1)}\right]^{\frac{1}{2}}\cdot(l^{4l+2-n}(\alpha SL),l^2(^1S),SL]l^{4l+4-n}\beta SL), \quad (43)$$

which is analogous to (19) and may be obtained in the same way; we get

$$Q(l^n\alpha SL)(l^n\alpha SL[L^{n-2}(\beta SL),l^2(^1S),SL)=(l^n\alpha SL[l^{n-2}(\beta SL),l^2(^1S),SL)Q(l^{4l+4-n}\beta SL). \quad (44)$$

Owing to (41) $(l^n\alpha SL[l^{n-2}(\beta SL),l^2(^1S),SL)$ may be different from zero only if

$$Q(l^n\alpha SL)=Q(l^{n-2}\beta SL)+2l+3-n, \quad (45)$$

and according to (42) the only non-vanishing values of $Q(l^n\alpha SL)$ are those which are connected to a $Q(l^{n-2}\beta SL)$ by (45).

(2) The "Seniority Number"

Putting for $Q\neq 0$

$$v_{\alpha\beta}(QSL)=(l^n\alpha SL[l^{n-2}(\beta SL),l^2(^1S),SL), \quad (46)$$

where α may assume all values for which $Q(l^n\alpha SL)=Q$, and β all values which satisfy (45), we have from (42) that

$$\tfrac{1}{2}n(n-1)(2l+1)\cdot\sum_\beta v_{\alpha\beta}(QSL)\overset{\dagger}{v}_{\beta\alpha'}(QSL)=Q\delta(\alpha\alpha'), \quad (47)$$

and also from (43) and again (42) that

$$\tfrac{1}{2}n(n-1)(2l+1)\cdot\sum_\alpha \overset{\dagger}{v}_{\beta\alpha}(QSL)v_{\alpha\beta'}(QSL)=Q\delta(\beta\beta'); \quad (47')$$

it follows that for two given values of Q which are connected by (45) the number of independent states of given S and L is the same in l^n and l^{n-2}, and that the matrix

$$u_{\alpha\beta}(QSL)=[\tfrac{1}{2}n(n-1)(2l+1)/Q]^{\frac{1}{2}}v_{\alpha\beta}(QSL) \quad (48)$$

is a unitary one. If we apply to the eigenfunctions of l^n the transformation u, and consider the states with eigenfunctions

$$\Psi(l^n\beta SL)=\textstyle\sum_\alpha \Psi(l^n\alpha SL)u_{\alpha\beta},$$

we obtain

$$(l^{n-2}(\beta' SL), l^2(^1S), SL]l^n\beta SL)$$
$$=[Q(l^n\beta SL)]^{\frac{1}{2}}[\tfrac{1}{2}n(n-1)(2l+1)]^{-\frac{1}{2}}\delta(\beta\beta'); \quad (49)$$

i.e., it is possible to find a scheme of l^n in which not only Q is diagonal, but also each term of l^n with $Q\neq 0$ corresponds to a well-defined term of l^{n-2} whose Q is connected to $Q(l^n\beta SL)$ by (45). If also $Q(l^{n-2}\beta SL)\neq 0$, this term corresponds to a term of l^{n-4} and so forth; each chain of corresponding terms begins with a term $l^v\beta SL$ which has $Q=0$.

We may thus assign to each term in the QSL scheme a "seniority number" v, which indicates the number of electrons of the first member of its chain; it follows immediately from (45) that Q depends only on n and v and that its values are given by

$$Q(n,v)=\tfrac{1}{4}(n-v)(4l+4-n-v). \quad (50)$$

Confronting (41) and (50) we see that conjugate terms have the same seniority.

The seniority number suffices for distinguishing the different terms of the same kind in the configurations d^n but not in f^n, since there are in f^n terms of the same kind which have also the same seniority. For such configurations an unspecified parameter α must be maintained besides v; terms corresponding according to (49) will have the same values of v and of α.

With this convention Eq. (49) which defines the correspondence between terms of the same chain becomes

$$(l^{n-2}(\alpha' v' SL), l^2(^1S), SL]l^n\alpha vSL)$$
$$=[Q(n,v)]^{\frac{1}{2}}[\tfrac{1}{2}n(n-1)$$
$$\cdot(2l+1)]^{-\frac{1}{2}}\delta(vv')\delta(\alpha\alpha'). \quad (49')$$

In this paper all tables of matrix elements are given in the QSL scheme and the seniority number is indicated by a prefix under the multiplicity number of each term: for instance the two ^2D terms of d^3, which were indicated in TAS (p. 228) by a^2D and b^2D, are therefore, respectively, denoted by ${}_1{}^2D$ and ${}_3{}^2D$.

(3) The High Degeneracies

Majorana's operator of position exchange may be defined for equivalent electrons by the relation

$$(l^2LM\,|\,M_{ij}\,|\,l^2LM)=(-1)^L \quad (51)$$

and may also be expressed, according to Dirac's vector model, by

$$M_{ij}=-[\tfrac{1}{2}+2(\boldsymbol{s}_i\cdot\boldsymbol{s}_j)]. \quad (52)$$

From (43)II we have

$$\sum_0^{2l}{}_r\,(-1)^r(2r+1)W(llll;0r)W(llll;Lr)$$
$$=(-1)^LW(llll;L0); \quad (53)$$

expressing $W(llll;0r)$ and $W(llll;L0)$ by (36)II and using also (38)II and (58)II we get for M_{ij} the expression

$$M_{ij}=\sum_0^{2l}{}_r\,(2r+1)(\boldsymbol{u}_i^{(r)}\cdot\boldsymbol{u}_j^{(r)}). \quad (54)$$

Adding this equation to (37) and introducing (52) we have

$$2\sum_0^{l}{}_t\,(4t+1)(\boldsymbol{u}_i^{(2t)}\cdot\boldsymbol{u}_j^{(2t)})$$
$$=q_{ij}-[\tfrac{1}{2}+2(\boldsymbol{s}_i\cdot\boldsymbol{s}_j)]. \quad (55)$$

It follows therefore from §4 of II and particularly from (51)II that if Slater's integrals F^k are proportional to $(2k+1)/C_{llk}$, the electrostatic interaction between two equivalent electrons is proportional to (55) and then the electrostatic-energy matrix is diagonal in the QSL scheme and its eigenvalues are only functions of n, v, and S. This fact explains the high degeneracies observed by Laporte and Platt[10] for these particular ratios of the parameters; unfortunately these ratios are only hypothetical, since they are excluded by the property of F^k of being a decreasing function of k (TAS, p. 177).

[10] O. Laporte and J. R. Platt, Phys. Rev. 61, 305 (1942).

(4) Relations Between Parentages of Corresponding Terms

If we express $\Psi(l^n)$ as linear combination of $\psi(l^{n-1}l)$ with $\Psi(l^{n-1})$ as linear combination of $\psi(l^{n-3}l^2)$, express on the other hand $\Psi(l^n)$ as combination of $\psi(l^{n-2}l^2)$ with $\Psi(l^{n-2})$ as combination of $\psi(l^{n-3}l)$, and compare the two developments, we obtain

$$\sum_{\alpha''v''}(l^{n-3}(\alpha'v'S'L'),l^2(^1S),S'L'][l^{n-1}\alpha''v''S'L')\cdot(l^{n-1}(\alpha''v''S'L')lSL][l^n\alpha vSL)=\sum_{\alpha'''v'''}(l^{n-3}(\alpha'v'S'L')lSL][l^{n-2}\alpha'''v'''SL)\cdot(l^{n-2}(\alpha'''v'''SL),l^2(^1S),SL][l^n\alpha vSL),\quad(56)$$

and owing to (49′) and (50)

$$[(n-v'-1)(4l+5-n-v')/(n-2)]^{\frac{1}{2}}\cdot(l^{n-1}(\alpha'v'S'L')lSL][l^n\alpha vSL)=(l^{n-3}(\alpha'v'S'L')lSL][l^{n-2}\alpha vSL)\cdot[(n-v)(4l+4-n-v)/n]^{\frac{1}{2}}.\quad(57)$$

It is easy to deduce from this recursion formula that

$$(l^{n-1}(\alpha'v'S'L')lSL][l^n\alpha vSL)=0\qquad(v'\neq v\pm1),\quad(58a)$$

$$(l^{n-1}(\alpha'v-1S'L')lSL][l^n\alpha vSL)=[(4l+4-n-v)v/2n(2l+2-v)]^{\frac{1}{2}}\cdot(l^{v-1}(\alpha'v-1S'L')lSL][l^v\alpha vSL),\quad(58b)$$

$$(l^{n-1}(\alpha'v+1S'L')lSL][l^n\alpha vSL)=[(n-v)(v+2)/2n]^{\frac{1}{2}}\cdot(l^{v+1}(\alpha'v+1S'L')lSL][l^{v+2}\alpha vSL).\quad(58c)$$

Comparing (58b) with (13) we obtain the more accurate orthogonality relations

$$\sum_{\alpha'S'L'}(l^n\alpha vSL[l^{n-1}(\alpha'v-1S'L')lSL)\cdot(l^{n-1}(\alpha'v-1S'L')lSL][l^n\alpha''vSL)=[(4l+4-n-v)v/2n(2l+2-v)]\delta(\alpha\alpha'')\quad(59a)$$

and

$$\sum_{\alpha'S'L'}(l^n\alpha vSL[l^{n-1}(\alpha'v+1S'L')lSL)\cdot(l^{n-1}(\alpha'v+1S'L')lSL][l^n\alpha''vSL)=[(n-v)(4l+4-v)/2n(2l+2-v)]\delta(\alpha\alpha'');\quad(59b)$$

comparing (58c) with (20) we obtain also

$$\sum_{\alpha SL}(2S+1)(2L+1)\cdot(l^{n-1}(\alpha'v+1S'L')lSL][l^n\alpha vSL)\cdot(l^n\alpha vSL[l^{n-1}(\alpha''v+1S'L')lSL)=(2S'+1)(2L'+1)\cdot[(n-v)(v+1)/2n(2l+1-v)]\delta(\alpha'\alpha'')\quad(60a)$$

and

$$\sum_{\alpha SL}(2S+1)(2L+1)\cdot(l^{n-1}(\alpha'v-1S'L')lSL][l^n\alpha vSL)\cdot(l^n\alpha vSL[l^{n-1}(\alpha''v-1S'L')lSL)=(2S'+1)(2L'+1)[(4l+4-n-v)\cdot(4l+5-v)/2n(2l+3-v)]\delta(\alpha'\alpha'').\quad(60b)$$

Another useful relation is the following:

$$(l^{v+1}(\alpha'v+1S'L')lSL][l^{v+2}\alpha vSL)=(-1)^{S+L+l+\frac{1}{2}-S'-L'}\cdot\left[\frac{(2S'+1)(2L'+1)(v+1)}{(2S+1)(2L+1)(v+2)(2l+1-v)}\right]^{\frac{1}{2}}\cdot(l^v(\alpha vSL)lS'L'][l^{v+1}\alpha'v+1S'L');\quad(61)$$

since this relation is verified for $v=0$ ($S=L=0$, $S'=\frac{1}{2}$, $L'=l$), it suffices to prove that if it holds for $v=v'-1$ it holds also for $v=v'$.

We use for this purpose the expressions (32) and (49′) of $(l^{v'}(\alpha v'SL),\ l^2(^1S),\ SL][l^{v'+2}\alpha v'SL)$: owing to (6), (58), and (50) we have

$$\sum_{\alpha_1S_1L_1}(-1)^{S+L+l+\frac{1}{2}-S_1-L_1}\cdot\left[\frac{(2S_1+1)(2L_1+1)}{2(2l+1)(2S+1)(2L+1)}\right]^{\frac{1}{2}}\cdot(l^{v'}(\alpha v'SL)lS_1L_1][l^{v'+1}\alpha_1v'-1S_1L_1)\cdot\left[\frac{(2l+1-v')v'}{(v'+2)(2l+2-v')}\right]^{\frac{1}{2}}\cdot(l^{v'-1}(\alpha_1v'-1S_1L_1)lSL][l^{v'}\alpha v'SL)+\sum_{\alpha_2S_2L_2}(-1)^{S+L+l+\frac{1}{2}-S_2-L_2}\cdot\left[\frac{(2S_2+1)(2L_2+1)}{2(2l+1)(2S+1)(2L+1)}\right]^{\frac{1}{2}}\cdot(l^{v'}(\alpha v'SL)lS_2L_2][l^{v'+1}\alpha_2v'+1S_2L_2)\cdot(l^{v'+1}(\alpha_2v'+1S_2L_2)lSL][l^{v'+2}\alpha v'SL)=\left[\frac{2(2l+1-v')}{(v'+1)(v'+2)(2l+1)}\right]^{\frac{1}{2}}.\quad(62)$$

If (61) holds for $v=v'-1$ we may calculate the first sum with the aid of (59a) and obtain

$$-\frac{v'}{2l+2-v'}\left[\frac{2l+1-v'}{2(v'+1)(v'+2)(2l+1)}\right]^{\frac{1}{2}};$$

the second sum must then have the value

$$\frac{4l+4-v'}{2l+2-v'}\left[\frac{2l+1-v'}{2(v'+1)(v'+2)(2l+1)}\right]^{\frac{1}{2}},$$

and owing to (59b), to (60b) and to the well-known corollary of Schwarz's inequality, this fact is possible only if (61) holds also for $v=v'$.

By the use of the formulas (58) and (61) the calculation of the fractional parentages is considerably simplified: Only the parentages of the "new" terms ($v=n$) must really be calculated by the methods of §3; all others may be quickly deduced from them.

(5) Relations Between Correspondence and Conjugation

It follows from (43) that if two eigenfunctions $\Psi_{\mathfrak{L}}(l^n\alpha vSL)$ and $\Psi_{\mathfrak{L}}(l^{n+2}\alpha vSL)$ correspond according to (49′), also the eigenfunctions of their conjugate states $\Psi_{\mathfrak{R}}(l^{4l+2-n}\alpha vSL)$ and $\Psi_{\mathfrak{R}}(l^{4l-n}\alpha vSL)$ correspond in the same way. But if, in order to make full use of (74)II, we assume as standard scheme the scheme of the $\Psi_{\mathfrak{L}}$ for $n\leqslant 2l+1$ and that of the $\Psi_{\mathfrak{R}}$ for $n\geqslant 2l+2$, we cannot use (49′) for the determination of $(l^{2l}(\alpha' vSL),\ l^2(^1S),\ SL]l^{2l+2}\alpha vSL)$, nor can we use (19) for $n=2l$ without knowing which of the two possibilities of (76)II holds for each term of l^{2l+1}.

In order to solve these questions we consider provisorily the system of functions $\Psi_{\mathfrak{L}}(l^{2l+2}\alpha vSL)$ defined by means of (49′) and the system of functions $\Psi_{\mathfrak{R}}(l^{2l+1}\alpha' v'S'L')$ defined by means of (14), and seek the relation between the parentages of $\Psi_{\mathfrak{L}}(l^{2l+2}\alpha vSL)$ with respect to $\Psi_{\mathfrak{L}}(l^{2l+1}\alpha' v'S'L')$ and the parentages of $\Psi_{\mathfrak{R}}(l^{2l+2}\alpha vSL)$ with respect to $\Psi_{\mathfrak{R}}(l^{2l+1}\alpha' v'S'L')$. Using (19), (58), and (61), and owing to the fact that $2S$ is even and $2S'$ is odd, we get

$$(l^{2l+1}(\alpha' v+1S'L')lSL]l^{2l+2}\alpha vSL)_{\mathfrak{R}} = (l^{2l+1}(\alpha' v+1S'L')lSL]l^{2l+2}\alpha vSL)_{\mathfrak{L}} \quad (63a)$$

and

$$(l^{2l+1}(\alpha' v-1S'L')lSL]l^{2l+2}\alpha vSL)_{\mathfrak{R}} = -(l^{2l+1}(\alpha' v-1S'L')lSL]l^{2l+2}\alpha vSL). \quad (63b)$$

If we assume

$$\Psi_{\mathfrak{R}}(l^{2l+1}\,{}_1{}^2L) = \Psi_{\mathfrak{L}}(l^{2l+1}\,{}_1{}^2L), \quad (64)$$

it follows by the alternate use of (63a) and (63b) that

$$\begin{aligned}\Psi_{\mathfrak{R}}(l^{2l+1}\alpha vSL) &= (-1)^{v-1/2}\Psi_{\mathfrak{L}}(l^{2l+1}\alpha vSL),\\ \Psi_{\mathfrak{R}}(l^{2l+2}\alpha vSL) &= (-1)^{v/2}\Psi_{\mathfrak{L}}(l^{2l+2}\alpha vSL).\end{aligned} \quad (65)$$

If we had assumed a minus sign in (64), the relations (65) would have also the opposite sign; the choice between these two possibilities depends on the phase of $\Psi(l^{4l+2}\,{}_1{}^1{}_0S)$, and it may be shown that (64) is in agreement with the convention of §5 of TAS for the eigenfunctions of closed shells.

The relations (65) must be taken in account if we use (19) for $n=21$ or (49′) for $n=2l+2$ and $n=2l+3$, and also if we calculate the coefficients of fractional parentage for $n\geqslant 2l+2$ by means of (58) instead of (19).

(6) Relations Between Matrix Components of Tensors

It follows immediately from (23) and (58) that the matrix components of every operator F between two states of l^n may be different from zero only if

$$\Delta v=0,\quad \pm 2, \quad (66)$$

and that

$$\begin{aligned}&(l^n\alpha vSLM_SM_L|F|l^n\alpha' v-2S'L'M_S'M_L')\\ &=\tfrac{1}{2}[(n+2-v)(4l+4-n-v)/(2l+2-v)]^{\frac{1}{2}}\\ &\cdot(l^v\alpha vSLM_SM_L|F|l^v\alpha' v-2S'L'M_S'M_L');\end{aligned} \quad (67)$$

owing to (65) a minus sign, however, must be introduced in this formula for $n\geqslant 2l+2$.

If $\Delta v=0$ the sum (23) splits in two sums according to the two possibilities $v-1$ and $v+1$ of the seniority numbers of l^{n-1}, but only the first sum may be immediately expressed as in the preceding case by means of the matrix components for l^v; the second sum is to be expressed by means of the matrix components for l^v and those for another arbitrary configuration $l^{n'}$. If

we assume $n'=4l+2-v$, the final result is found to be

$$(l^n\alpha vSLM_SM_L|F|l^n\alpha'vS'L'M_S'M_L')$$
$$=[(4l+2-n-v)/2(2l+1-v)]$$
$$\cdot(l^v\alpha vSLM_SM_L|F|l^v\alpha'vS'L'M_S'M_L')$$
$$+[(n-v)/2(2l+1-v)]$$
$$\cdot(l^{4l+2-v}\alpha vSLM_SM_L|F|l^{4l+2-v}$$
$$\cdot\alpha'vS'L'M_S'M_L'). \quad (68)$$

If F is an irreducible tensor, it follows from (68) and (74)II that

$$(l^n\alpha vSL\|T^{(\kappa k)}\|l^n\alpha'vS'L')$$
$$=(l^v\alpha vSL\|T^{(\kappa k)}\|l^v\alpha'vS'L') \quad (\kappa+k \text{ odd}), \quad (69a)$$
$$(l^n\alpha vSL\|T^{(\kappa k)}\|l^n\alpha'vS'L')$$
$$=\frac{2l+1-n}{2l+1-v}(l^v\alpha vSL\|T^{(\kappa k)}\|l^v\alpha'vS'L')$$
$$(\kappa+k \text{ even}). \quad (69b)$$

From (67), (65), and (74)II we get also

$$(l^n\alpha vSL\|T^{(\kappa k)}\|l^n\alpha'v-2S'L')=0$$
$$(\kappa+k \text{ odd}). \quad (70)$$

The remarkable result that a tensor of odd degree is diagonal with respect to v and that its submatrices are independent of n may be obtained also in a more direct way. It follows from the triangular conditions and from the fact that in l^2 only states with even $S+L$ are allowed, that for $\kappa+k$ odd

$$(l^2\ {}^1S|t_1^{(\kappa k)}+t_2^{(\kappa k)}|l^2SLM_SM_L)$$
$$=(l^2SLM_SM_L|t_1^{(\kappa k)}+t_2^{(\kappa k)}|l^2\ {}^1S)=0$$

TABLE XV. $(p^2SL\|2V^{(12)}\|p^2S'L')$.

	^1S	^3P	^1D
^1S	0	0	0
^3P	0	$-(6)^{\frac{1}{2}}$	-3
^1D	0	-3	0

TABLE XVI. $(p^3SL\|2V^{(12)}\|p^3S'L')$.

	^4S	^2P	^2D
^4S	0	0	$-2(2)^{\frac{1}{2}}$
^2P	0	$(6)^{\frac{1}{2}}$	0
^2D	$2(2)^{\frac{1}{2}}$	0	$-(14)^{\frac{1}{2}}$

and, therefore,

$$q_{ij}(t_i^{(\kappa k)}+t_j^{(\kappa k)})=(t_i^{(\kappa k)}+t_j^{(\kappa k)})q_{ij}=0$$
$$(\kappa+k \text{ odd}); \quad (71)$$

since all other $t_h^{(\kappa k)}$ commute with q_{ij}, $T^{(\kappa k)}$ commutes with q_{ij} and also with Q, and is therefore diagonal with respect to v. From (71) we have also

$$QT=TQ=\sum_{\substack{i<j\\ i\neq h\neq j}} t_hq_{ij};$$

calculating the matrix of this operator with the methods of §5 and owing to (49′) we obtain

$$(l^n\alpha vSL\|T^{(\kappa k)}\|l^n\alpha'vS'L')$$
$$=(l^{n-2}\alpha vSL\|T^{(\kappa k)}\|l^{n-2}\alpha'vS'L'),$$

which is equivalent to (69a).

The matrices of the tensor $V^{(12)}$ defined by (102)II were calculated for the configurations p^2, p^3, d^3, d^4 and d^5 using also (69a); the results are given in Tables XV–XIX. The matrices given in Tables V and XIX are sufficient for the calculation of the spectra of the configurations p^nl and d^np with the methods of §8 of II.

§7. THE ELECTROSTATIC INTERACTION BETWEEN d^n, $d^{n-1}s$ AND $d^{n-2}s^2$

The electrostatic interaction between $d^2\ {}^1S$ and $s^2\ {}^1S$ is given by

$$(d^2\ {}^1S|e^2/r|s^2\ {}^1S)$$
$$=R^2(dd, ss)(d^2\ {}^1S|P_2(\cos\omega)|s^2\ {}^1S), \quad (72)$$

where R^2 is defined by TAS 8°8 and ω is the angle between the radii vectors of the two electrons. From (51)II we have

$$(2\|C^{(2)}\|0)=1, \quad (73)$$

and hence from (45)II and (38)II we get

$$(d^2\ {}^1S|P_2(\cos\omega)|s^2\ {}^1S)=1/5^{\frac{1}{2}};$$

since

$$R^2(dd, ss)=R^2(ds, sd)=G^2(ds)=5G_2(ds),$$

(72) becomes

$$(d^2\ {}^1S|e^2/r|s^2\ {}^1S)=5^{\frac{1}{2}}G_2. \quad (74)$$

Introducing this result in (33c) and owing to

TABLE XVII. $(d^3vSL\|70V^{(12)}\|d^3v'S'L')$.

	^3P	^4P	^1D	^3D	^3F	^4F	^3G	^3H
^3P	$-19(14)^{\frac{1}{2}}$	-28	0	$8(35)^{\frac{1}{2}}$	$-8(14)^{\frac{1}{2}}$	$-22(14)^{\frac{1}{2}}$	0	0
^4P	28	$14(35)^{\frac{1}{2}}$	0	$-28(10)^{\frac{1}{2}}$	56	$-28(10)^{\frac{1}{2}}$	0	0
^1D	0	0	$35(6)^{\frac{1}{2}}$	0	0	0	0	0
^3D	$-8(35)^{\frac{1}{2}}$	$-28(10)^{\frac{1}{2}}$	0	$-5(6)^{\frac{1}{2}}$	$-4(210)^{\frac{1}{2}}$	$4(210)^{\frac{1}{2}}$	$-60(2)^{\frac{1}{2}}$	0
^3F	$-8(14)^{\frac{1}{2}}$	-56	0	$4(210)^{\frac{1}{2}}$	-77	-98	$3(35)^{\frac{1}{2}}$	$-4(385)^{\frac{1}{2}}$
^4F	$22(14)^{\frac{1}{2}}$	$-28(10)^{\frac{1}{2}}$	0	$4(210)^{\frac{1}{2}}$	98	$-14(10)^{\frac{1}{2}}$	$-18(35)^{\frac{1}{2}}$	$4(385)^{\frac{1}{2}}$
^3G	0	0	0	$-60(2)^{\frac{1}{2}}$	$-3(35)^{\frac{1}{2}}$	$-18(35)^{\frac{1}{2}}$	$3(33)^{\frac{1}{2}}$	$12(77)^{\frac{1}{2}}$
^3H	0	0	0	0	$-4(385)^{\frac{1}{2}}$	$-4(385)^{\frac{1}{2}}$	$-12(77)^{\frac{1}{2}}$	$-(2002)^{\frac{1}{2}}$

TABLE XVIII. $(d^4vSL\|70V^{(12)}\|d^4vS'L')$.

	^1S	^3P	^1D	^3D	^5D	^1F	^3F	^1G	^3G	^3H	^1I
^1S	0	0	0	$4(210)^{\frac{1}{2}}$	0	0	0	0	0	0	0
^3P	0	$6(14)^{\frac{1}{2}}$	$-15(35)^{\frac{1}{2}}$	$-3(35)^{\frac{1}{2}}$	-105	$-12(35)^{\frac{1}{2}}$	$12(14)^{\frac{1}{2}}$	0	0	0	0
^1D	0	$-15(35)^{\frac{1}{2}}$	0	$5(6)^{\frac{1}{2}}$	0	0	0	0	$60(2)^{\frac{1}{2}}$	0	0
^3D	$-4(210)^{\frac{1}{2}}$	$3(35)^{\frac{1}{2}}$	$-5(6)^{\frac{1}{2}}$	$-1\frac{5}{7}(6)^{\frac{1}{2}}$	$1\frac{5}{7}(210)^{\frac{1}{2}}$	$-10(21)^{\frac{1}{2}}$	$9(210)^{\frac{1}{2}}$	$6(165)^{\frac{1}{2}}$	$15(2)^{\frac{1}{2}}$	0	0
^5D	0	-105	0	$-1\frac{5}{7}(210)^{\frac{1}{2}}$	$-3\frac{5}{7}(30)^{\frac{1}{2}}$	0	$35(6)^{\frac{1}{2}}$	0	$15(70)^{\frac{1}{2}}$	0	0
^1F	0	$12(35)^{\frac{1}{2}}$	0	$-10(21)^{\frac{1}{2}}$	0	0	$-21(10)^{\frac{1}{2}}$	0	$12(14)^{\frac{1}{2}}$	$-6(154)^{\frac{1}{2}}$	0
^3F	0	$12(14)^{\frac{1}{2}}$	0	$-9(210)^{\frac{1}{2}}$	$35(6)^{\frac{1}{2}}$	$21(10)^{\frac{1}{2}}$	-42	0	$-12(35)^{\frac{1}{2}}$	$6(385)^{\frac{1}{2}}$	0
^1G	0	0	0	$-6(165)^{\frac{1}{2}}$	0	0	0	0	$27(10)^{\frac{1}{2}}$	$6(210)^{\frac{1}{2}}$	0
^3G	0	0	$-60(2)^{\frac{1}{2}}$	$15(2)^{\frac{1}{2}}$	$-15(70)^{\frac{1}{2}}$	$12(14)^{\frac{1}{2}}$	$12(35)^{\frac{1}{2}}$	$-27(10)^{\frac{1}{2}}$	$-6(33)^{\frac{1}{2}}$	$-6(77)^{\frac{1}{2}}$	$-12(91)^{\frac{1}{2}}$
^3H	0	0	0	0	0	$6(154)^{\frac{1}{2}}$	$6(385)^{\frac{1}{2}}$	$6(210)^{\frac{1}{2}}$	$6(77)^{\frac{1}{2}}$	$-3(2002)^{\frac{1}{2}}$	$-7(39)^{\frac{1}{2}}$
^1I	0	0	0	0	0	0	0	0	$12(91)^{\frac{1}{2}}$	$-7(39)^{\frac{1}{2}}$	0

TABLE XIX. $(d^5vSL\|70V^{(12)}\|d^5vS'L')$.

	^2S	^6S	^2D	^4D	^2F	^2G	^4G	^2I
^2S	0	0	$-4(210)^{\frac{1}{2}}$	$-6(105)^{\frac{1}{2}}$	0	0	0	0
^6S	0	0	0	$70(3)^{\frac{1}{2}}$	0	0		0
^2D	$-4(210)^{\frac{1}{2}}$	0	$15(6)^{\frac{1}{2}}$	$60(3)^{\frac{1}{2}}$	$-20(21)^{\frac{1}{2}}$	-4	$-20(15)^{\frac{1}{2}}$	0
^4D	$6(105)^{\frac{1}{2}}$	$-70(3)^{\frac{1}{2}}$	$-60(3)^{\frac{1}{2}}$	$10(15)^{\frac{1}{2}}$	0	$8(330)^{\frac{1}{2}}$	$-40(3)^{\frac{1}{2}}$	0
^2F	0	0	$20(21)^{\frac{1}{2}}$	0	-105	$(1155)^{\frac{1}{2}}$	$14(105)^{\frac{1}{2}}$	0
^2G	0	0	$-4(165)^{\frac{1}{2}}$	$-8(330)^{\frac{1}{2}}$	$-(1155)^{\frac{1}{2}}$	$12\frac{5}{11}(33)^{\frac{1}{2}}$	$-10(3)^{\frac{1}{2}}$	$\frac{5}{11}(30030)^{\frac{1}{2}}$
^4G	0	0	$20(15)^{\frac{1}{2}}$	$-40(3)^{\frac{1}{2}}$	$14(105)^{\frac{1}{2}}$	$10(3)^{\frac{1}{2}}$	$-10(330)^{\frac{1}{2}}$	$-2(2730)^{\frac{1}{2}}$
^2I	0	0	0	0	0	$\frac{5}{11}(30030)^{\frac{1}{2}}$	$2(2730)^{\frac{1}{2}}$	$-3\frac{5}{11}(858)^{\frac{1}{2}}$

(49′) we obtain

$$(d^nvSL|\sum e^2/r_{ij}|d^{n-2}s^2v'SL) = [Q(n,v)]^{\frac{1}{2}}\delta(vv')G_2; \quad (75)$$

owing to the conventions of subsection (5) of §6, a minus sign must be introduced for $n=6$, $v=2$ and for $n=7$, $v=3$.

The calculation of the interaction between the configurations d^n and $d^{n-1}s$ by means of (33b) is easy only for $n=3$, since in this case

$$(d, d^2(^1D), SL]d^3vSL)$$

may be obtained from Table II by means of (29); but, as it was already mentioned at the end of §5, the calculations for $n \geqslant 4$ become very long, and it appears more convenient to use the following method.

The interaction in question is given by

$$(d^nvSL|\sum e^2/r_{ij}|d^{n-1}(v'S'L)sSL) = R^2(dd, ds) \cdot (d^nvSL|\sum P_2(\cos\omega_{ij})|d^{n-1}(v'S'L)sSL); \quad (76)$$

owing to (45)II and to the fact that $\sum_i C_i^{(2)2}$ is a scalar and its non-diagonal matrix components vanish, we have

$$(d^nvSL|\sum_{i<j} P_2(\cos\omega_{ij})|d^{n-1}(v'S'L)sSL) = \tfrac{1}{2}(d^nvSL|[\textstyle\sum_i C_i^{(2)}]^2|d^{n-1}(v'S'L)sSL), \quad (77)$$

TABLE XX. $(d^3vSL|\Sigma e^2/r_{ij}|d^2(v'S'L')sSL)$.

d^3	d^2s	H_2
^2P	$(^3P)^2P$	$3(35)^{\frac{1}{2}}$
^4P	$(^3P)^4P$	0
^2D	$(^1D)^2D$	$-1\frac{1}{2}(70)^{\frac{1}{2}}$
^2D	$(^3D)^2D$	$3\frac{1}{2}(30)^{\frac{1}{2}}$
^2F	$(^3F)^2F$	$-3(10)^{\frac{1}{2}}$
^4F	$(^3F)^4F$	0
^2G	$(^1G)^2G$	$-5(2)^{\frac{1}{2}}$

and using (33)II we obtain

$$2(2L+1)(d^nvSL|\sum_{i<j} P_2(\cos\omega_{ij})|d^{n-1}(v'S'L)sSL)$$
$$=\sum_{v''L''}(-1)^{L-L''}\cdot(d^nvSL\|\textstyle\sum_i C_i^{(2)}\|d^nv''SL'')\cdot(d^nv''SL''\|\sum_i C_i^{(2)}\|d^{n-1}(v'S'L)sSL)$$
$$+\sum_{v''L''}(-1)^{L-L''}\cdot(d^nvSL\|\textstyle\sum_i C_i^{(2)}\|d^{n-1}(v''S'L'')sSL'')$$
$$\cdot(d^{n-1}(v''S'L'')sSL''\|\textstyle\sum_i C_i^{(2)}\|d^{n-1}(v'S'L)sSL). \quad (78)$$

From (27), (44)II, (80)II, and (73) we obtain finally

$$(d^nvSL|\textstyle\sum e^2/r_{ij}|d^{n-1}(v'S'L)sSL)$$
$$=(n/14)^{\frac{1}{2}}[\sum_{v''L''}(-1)^{L-L''}\cdot(d^nvSL\|U^{(2)}\|d^nv''SL'')\cdot(d^nv''SL''\|d^{n-1}(v'S'L)dSL)\cdot(2L''+1)^{\frac{1}{2}}/(2L+1)+\sum_{v''L''}(-1)^{L-L''}\cdot(d^nvSL\|d^{n-1}(v''S'L'')dSL)\cdot(d^{n-1}v''S'L''\|U^{(2)}\|d^{n-1}v'S'L)/(2L+1)^{\frac{1}{2}}]R^2(dd,ds). \quad (79)$$

By means of this formula the interaction between the configurations d^n and $d^{n-1}s$ was calculated for $n=3$, 4, 5; the results are different from zero only if $v'=v\pm1$ and are given in Tables XX–XXII, where the quantity

$$H_2=R^2(dd,ds)/35 \quad (80)$$

was assumed as parameter. For $n=3$ our results agree with those given by Marvin.[11]

The interaction between the configurations $d^{n-1}s$ and $d^{n-2}s^2$ may be calculated in the same way; the result is

$$(d^{n-1}(v'S'L)sSL|\textstyle\sum e^2/r_{ij}|d^{n-2}s^2vSL)$$
$$=(-1)^{S+\frac{1}{2}-S'}\left[\frac{2S'+1}{2S+1}\right]^{\frac{1}{2}}\cdot(d^{n-1}v'S'L|\textstyle\sum e^2/r_{ij}|d^{n-2}(vSL)sS'L). \quad (81)$$

TABLE XXI. $(d^4vSL|\Sigma e^2/r_{ij}|d^3(v'S'L')sSL)$.

d^4	d^3s	H_2	d^4	d^3s	H_2
^2P	$(^2P)^2P$	$(70)^{\frac{1}{2}}$	^1F	$(^2F)^1F$	-15
^2P	$(^4P)^2P$	0	^3F	$(^2F)^3F$	$-2(5)^{\frac{1}{2}}$
^4P	$(^2P)^4P$	$-2(5)^{\frac{1}{2}}$	^3F	$(^4F)^3F$	0
^4P	$(^4P)^4P$	$2(70)^{\frac{1}{2}}$	^3F	$(^2F)^3F$	$3(5)^{\frac{1}{2}}$
^1D	$(^3D)^1D$	$-(105)^{\frac{1}{2}}$	^3F	$(^4F)^3F$	$-4(5)^{\frac{1}{2}}$
^1D	$(^2D)^1D$	$-3(5)^{\frac{1}{2}}$	^1G	$(^2G)^1G$	$10\frac{1}{2}(3)^{\frac{1}{2}}$
^1D	$(^3D)^1D$	$6(10)^{\frac{1}{2}}$	^1G	$(^2G)^1G$	$5\frac{1}{2}(33)^{\frac{1}{2}}$
^3D	$(^2D)^3D$	$-4(5)^{\frac{1}{2}}$	^3G	$(^2G)^3G$	$3(5)^{\frac{1}{2}}$
			^3H	$(^2H)^3H$	$-2(5)^{\frac{1}{2}}$

TABLE XXII. $(d^5vSL|\Sigma e^2/r_{ij}|d^4(v'S'L')sSL)$.

d^5	d^4s	H_2	d^5	d^4s	H_2
^2S	$(^1S)^2S$	$8(5)^{\frac{1}{2}}$	^2F	$(^2F)^2F$	$-2(15)^{\frac{1}{2}}$
^2P	$(^2P)^2P$	$(210)^{\frac{1}{2}}$	^2F	$(^3F)^2F$	$-3\frac{1}{2}(15)^{\frac{1}{2}}$
^2P	$(^3P)^2P$	$(15)^{\frac{1}{2}}$	^2F	$(^1F)^2F$	$7\frac{1}{2}(5)^{\frac{1}{2}}$
^4P	$(^2P)^4P$	0	^2F	$(^3F)^2F$	$15\frac{1}{2}(3)^{\frac{1}{2}}$
^4P	$(^3P)^4P$	$(105)^{\frac{1}{2}}$	^4F	$(^2F)^4F$	0
^2D	$(^2D)^2D$	$-(35)^{\frac{1}{2}}$	^4F	$(^3F)^4F$	$-(30)^{\frac{1}{2}}$
^2D	$(^2D)^2D$	$3(5)^{\frac{1}{2}}$	^2G	$(^2G)^2G$	$-10\frac{1}{2}(3)^{\frac{1}{2}}$
^2D	$(^1D)^2D$	$3(10)^{\frac{1}{2}}$	^2G	$(^1G)^2G$	$5\frac{1}{2}(33)^{\frac{1}{2}}$
^2D	$(^3D)^2D$	$2(15)^{\frac{1}{2}}$	^2G	$(^3G)^2G$	$-3\frac{1}{2}(15)^{\frac{1}{2}}$
^2D	$(^1D)^2D$	$-(5)^{\frac{1}{2}}$	^2G	$(^1G)^2G$	$-9\frac{1}{2}(5)^{\frac{1}{2}}$
^2D	$(^3D)^2D$	$-3(30)^{\frac{1}{2}}$	^2G	$(^3G)^2G$	$-5\frac{1}{2}(11)^{\frac{1}{2}}$
^4D	$(^3D)^4D$	$-3\frac{1}{2}(30)^{\frac{1}{2}}$	^4G	$(^3G)^4G$	$5(2)^{\frac{1}{2}}$
^4D	$(^5D)^4D$	$-5\frac{1}{2}(14)^{\frac{1}{2}}$	^2H	$(^3H)^2H$	$(15)^{\frac{1}{2}}$
^2F	$(^1F)^2F$	$-15\frac{1}{2}$	^2I	$(^1I)^2I$	$(5)^{\frac{1}{2}}$

[11] H. H. Marvin, Phys. Rev. **47**, 521 (1935).

Letters to the Editor

PROMPT publication of brief reports of important discoveries in physics may be secured by addressing them to this department. The closing date for this department is the third of the month. Because of the late closing date for the section no proof can be shown to authors. The Board of Editors does not hold itself responsible for the opinions expressed by the correspondents. Communications should not in general exceed 600 words in length.

On the Scattering of Neutrons by Protons

LAMEK HULTHÉN
Institute for Mechanics and Mathematical Physics, University of Lund, Lund, Sweden
February 11, 1943

RECENT experiments by Amaldi, Bocciarelli, Ferretti, and Trabacchi[1] give valuable information on the angular distribution of fast neutrons scattered by protons. Measuring the scattered intensity $I(\theta)$ in two directions, $\theta=\pi/2$ and π(θ=scattering angle of the neutron in the center of gravity system), they found values of $I(\pi)/I(\pi/2)$ between 0.71 and 0.52 for average energies of the incident neutrons varying from 12.5 to 14 Mev.

We know, that "symmetrical" and "neutral" theories must give rather different predictions on this angular distribution.[2] From the symmetrical theory expounded by Møller and Rosenfeld[3] we obtain for 14 Mev neutrons, considering the effect of S, P, and D states, a total scattering cross section $\sigma=0.66\times10^{-24}$ cm^2 and

$$I(\theta)\sim1-0.18\cos\theta+0.45\cos^2\theta;^4 \qquad (1)$$

thus $I(\pi)/I(\pi/2)=1.63$. This result can hardly be reconciled with the experience of Amaldi and his collaborators.

Because the convergence of the power series in $\cos\theta$ is somewhat slow, it seems necessary to estimate the influence of the neutron-proton states with greater angular momenta. Using a Born approximation, we get, assuming again the static interaction V_n of Møller and Rosenfeld:[5]

$$I(\theta)=\frac{1}{4}\left(\frac{M}{\hbar^2}\right)^2\left\{3\left(\frac{g_1^2+g_2^2}{4\pi}\right)^2\left(\frac{1}{\kappa^2+4k^2\sin^2\frac{1}{2}\theta}+\frac{2}{\kappa^2+4k^2\cos^2\frac{1}{2}\theta}\right)^2+\left(\frac{3g_2^2-g_1^2}{4\pi}\right)^2\left(\frac{1}{\kappa^2+4k^2\sin^2\frac{1}{2}\theta}-\frac{2}{\kappa^2+4k^2\cos^2\frac{1}{2}\theta}\right)^2\right\} \qquad (2)$$

where $k=(ME_i/2\hbar^2)^{\frac{1}{2}}$, and E_i is the energy of the incident neutron. For $E_i=14$ Mev and a meson mass $=200\,m_e$, we have $k=0.8\kappa$. Equation (2) then gives $\sigma=0.53\times10^{-24}$ cm^2 and $I(\pi)/I(\pi/2)=4.8$. The discrepancy mentioned above thus becomes still more striking. Besides, the comparison between (1) and (2) indicates that the usually accepted approximation, if we take only S and P states into consideration,[6] may be too rough for these high energies (k nearly equal to κ).

The effect of the non-static potential W_n[7] has also been taken into account. It does change the angular distribution in the "right" direction, but the correction is too small to be significant.

Comparing with theory, Amaldi, Bocciarelli, Ferretti, and Trabacchi find that their results agree with the angular distribution deduced by Ferretti[8] from the neutral theory of Bethe,[9] but are inconsistent with the outcome of the symmetrical theory according to Rarita, Schwinger, and Nye.[2] Still it should be noted that the distribution calculated by the latter authors from another special form of the neutral theory[2] gives practically the same value of $I(\pi)/I(\pi/2)$ as that of Ferretti (because $1+b\cos\theta=1+(b+c)\cos\theta+c\cos^2\theta$ for $\theta=\pi/2$ and π, irrespective of c).

It should also be observed that noncentral forces are not necessary to explain the effect considered here. In fact, the simple potential

$$V(r)=-[G_1+G_2(\sigma^{(1)}\sigma^{(2)})]e^{-\kappa r}/r \qquad (3)$$

ensuing from a "mixed" neutral theory,[10] gives, to the same approximation as (2):

$$I(\theta)=(M/\hbar^2)^2(3G_2^2+G_1^2)/[\kappa^2+4k^2\sin^2(\theta/2)]^2. \qquad (4)$$

For $k=0.8\kappa$ this gives $I(\pi)/I(\pi/2)=0.41$.

Thus the experiment of Amaldi and his collaborators seems to speak in favor of a neutral meson theory of nuclear forces and against the symmetrical possibility. This appears to be the first really serious difficulty which the theory of Møller and Rosenfeld has met.

It is, of course, not possible to draw more extensive conclusions until more detailed evidence of the angular distribution is obtained. In this connection the importance of analogous experiments on the photo-disintegration of the deuteron[3] should again be stressed.

[1] E. Amaldi, D. Bocciarelli, B. Ferretti, and G. C. Trabacchi, Naturwiss. **30**, 582 (1942).
[2] Cf. W. Rarita, J. Schwinger, and H. A. Nye, Phys. Rev. **59**, 209 (1941). Professor L. Rosenfeld kindly called my attention to an earlier discussion of the subject by E. Philipp, Zeits. f. Physik **107**, 683 (1937).
[3] C. Møller and L. Rosenfeld, Danske Vidensk. Selsk. math.-fys. Medd. **17**, No. 8 (1940).
[4] Dr. C. Møller kindly informed me that a similar calculation has been made by B. Ferretti. Particulars are not known here yet.
[5] Reference 3, p. 38.
[6] C. Kittel and G. Breit, Phys. Rev. **56**, 744 (1939); Rarita, Schwinger, and Nye, reference 2.
[7] Reference 3, p. 42.
[8] B. Ferretti, Ricerca Scient. **12**, 843, 993 (1941).
[9] H. A. Bethe, Phys. Rev. **57**, 261, 390 (1940).
[10] Reference 3, p. 34.

Energies for Self-Diffusion in Zinc

H. B. HUNTINGTON
Washington University, Saint Louis, Missouri
April 17, 1943

EXPERIMENTS by Miller and Banks[1] on self-diffusion in zinc have shown that the diffusion constants for flow in the basal plane and along the hexagonal axis have widely different temperature dependence. If one expresses the diffusion constant in the form $Ae^{-Q/RT}$, then in the basal plane $A=8\times10^6$ cm^2/day and $Q=3.1\times10^4$ cal./mole, and along the hexagonal axis $A=4\times10^3$ cm^2/day and $Q=2.04\times10^4$ cal./mole. Accordingly diffusion is always more rapid along the axis because of the smaller activation energy involved. The anisotropy of the temperature-independent factor has relatively less effect. Some geometrical considerations have already been put forward to explain the difference between the A values on the basis of diffusion by vacancies.[2]

The fact that Q_{basal} is larger than Q_{axial} might be ex-

pected since the Debye temperature for lattice vibrations in the basal plane is higher than for the vibrations transverse to these planes. If the hypothesis of vacancy diffusion is correct, then it would appear that the diffusing atom halfway between two vacancies in the same basal plane is in a position of higher energy than a similar atom halfway between vacancies in adjoining planes. A comparison of the electrostatic energy of the two situations has been made on the assumption that the two valence electrons per atom are uniformly distributed in space. For a close-packed hexagonal lattice the migrating atom would have in each case four nearest neighbors at a distance $\sqrt{\frac{3}{2}}$ times the lattice constant and the difference in energy would be small. The zinc lattice, however, departs considerably from close-packing (c/a is 1.86). The calculations for this case were carried out by the Ewald method[3] and showed that the configuration corresponding to basal diffusion lies higher by $0.055(2e)^2/a$ or 2.7×10^4 cal./mole. This is about two and a half times the difference between the Q values. It might be expected that such simplified considerations would give too large a result, first because the two conduction electrons in metallic zinc probably behave quite differently from free electrons, and secondly because polarization effects will tend to reduce all electrostatic terms and differences between such terms.

[1] P. H. Miller, Jr., and Floyd R. Banks, Phys. Rev. **61**, 648 (1942).
[2] H. B. Huntington, Phys. Rev. **61**, 325 (1942).
[3] P. P. Ewald, Ann. d. Physik **64**, 253 (1921).

Erratum: Simple Method for the Investigation of Secondary Electrons Excited by γ-Rays and the Interference of These Electrons with Measurements of Primary β-Ray Spectra

LISE MEITNER
Forskningsinstitutet för Fysik, Stockholm, Sweden
(Phys. Rev. **63**, 73 (1943))

ON page 76, first column, the lines which read "for the primary β-particles a range of 0.36-mm Al corresponding to 0.098 g/cm^2," should be changed to read "for the primary β-particles a range of 0.36 mm corresponding to 0.13 g/cm^2."

Mesotron Mass and Heavy Tracks on Mt. Evans

CARL E. NIELSEN AND WILSON M. POWELL*
Department of Physics, University of California, Berkeley, California
April 30, 1943

ABOUT ten fairly reliable observations of the mesotron mass have been published.[1] Most of these are consistent with a mass approximately 180 times the electron mass, but they do not constitute conclusive evidence for uniqueness of the mass. It is thus clearly desirable that more observations of the mass be obtained, both to determine whether it is unique and to fix its value more precisely.

An expedition to Mt. Evans was made for the primary purpose of obtaining such observations. The ionization and momentum of cosmic rays were observed simultaneously in a Wilson cloud chamber by photographing tracks curved by a magnetic field of 2500 oersted, and diffused sufficiently to permit photographic resolution of single droplets. A delay of ~0.15 second between reduction of the clearing field from ~20 v/cm to ~2 v/cm and expansion of the chamber was provided. Most of the photographs were of random expansions, and this time of reduced clearing field corresponds to the interval before expansion during which a track remains to be observed. It has been shown[2,3] that condensation upon even a small fraction of the negative ions indicates a supersaturation sufficient to give condensation upon substantially all positive ions; and this result is valid for any water-ethyl alcohol mixture in a broad range around the 70 percent alcohol mixture requiring minimum expansion. The number of droplets formed in a positive track with an associated negative is therefore equal to the number of ion pairs. An enlarged section of a typical mesotron track pair is reproduced in Fig. 1.

Mass determination from ionization and curvature depends upon a knowledge of the relation between ionization and speed. The generally accepted form of this relation is expressed in the theoretical equation

$$I=\frac{A}{\beta^2}\left(\log\frac{\beta^2}{1-\beta^2}+K-\beta^2\right).$$

This is the function used by Corson and Brode[4] to obtain mass from ionization and curvature. The experiments of C. T. R. Wilson and E. J. Williams[5] have yielded an experimental relation based upon counts of primary ionization of slow electrons. Their work is summarized by the equation $I=I_0\beta^{-1.4}$, which has been used by Williams and Pickup to derive mass values. For comparison it is interesting to note that the theoretical equation is well represented in the interval $0.20<\beta<0.90$ by $I=I_0\beta^{-1.8}$. Mass values derived from the experimental curve are larger than values from the theoretical curve. This uncertainty in interpretation would be removed and at the same time the possibility of error from inaccurate ionization measurement would be eliminated if one were to observe under identical conditions the curvature and ionization of slow electrons of the same speed as the mesotrons. This procedure would permit an unambiguous mass assignment: Two particles with equal charge ionize equally when moving at the same speed, and their masses are then proportional to their momenta or $H\rho$ values. Experiments to determine the ionization of slow electrons are in progress, but until their completion the mass values are subject to a possible error. For the present, computations from the Corson and Brode nomograph and the Williams curve are both given.

Approximately 7000 photographs were taken on Mt. Evans, 14,100 ft. and 1800 were taken at Summit Lake, 12,700 ft. The photographs show numerous heavily ionizing tracks with negligible curvature produced by particles —presumably protons—much heavier than mesotrons. These heavy tracks were present in about eight percent of the pictures at 14,100 ft. and in about four percent of the pictures at 12,700 ft. Each picture records events in an interval ~0.3 sec., and in a volume ~1500 cm^3. Only six heavily ionizing mesotrons have yet been identified. Since

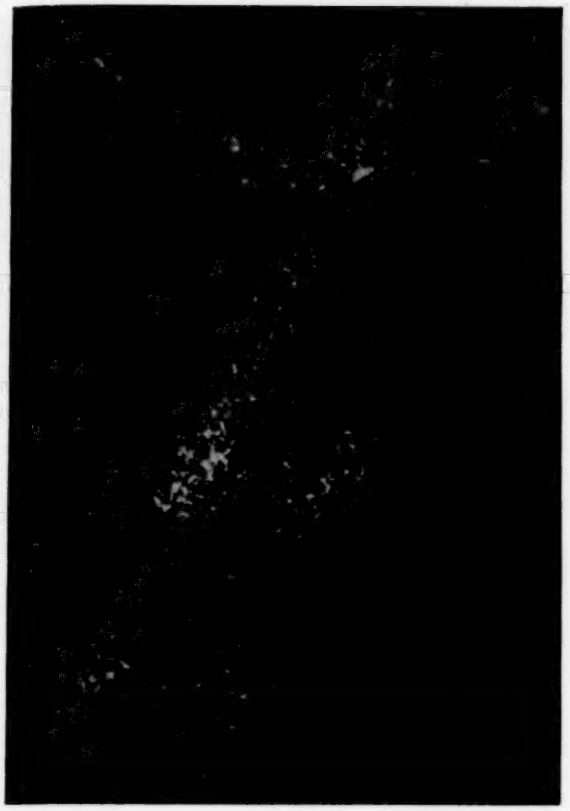

FIG. 1. Section of mesotron track 6949, enlarged to about three times its size in the cloud chamber. Ion pairs are separated into positive and negative columns, with the positive on the left side. At the top a sharp electron track crosses the picture.

they are quite conspicuous it is probable that not many more will be found by additional study of the pictures. Most of the heavy tracks thus do not represent slow mesotrons;[6] in fact, the fraction of slow mesotrons may not greatly exceed the figure of 0.001 found by E. J. Williams at sea level.

Four of these slow mesotrons yield mass values as follows:

Track	Ionization	$H\rho$	Mass: C. & B.	Mass: William[8]
8–21, 2	$2.5\times I_0$	2.26×10^5	210 ± 20	230 ± 20
1621	6.0	1.08	180 ± 20	225 ± 20
6941	6.2	1.11	190 ± 15	240 ± 15
6949	2.4	1.6	145 ± 30	155 ± 30

The probable errors are estimated to include chamber distortion of curvature and statistical uncertainty deriving from the finite number of droplets counted. Curvature was measured by plotting micrometer readings of coordinates along the track and fitting a curve to the points by the method of least squares. The curvature of the first track, for example, was determined from 13 points, with a probable error in fitting of 3.5 percent. The ionization of this track was determined by a count of 335 droplets, hence the statistical error is ~5 percent (or more, since each ion is not the result of a single independent event).

We are grateful to all who have assisted with this experiment, and to the Carnegie Institution of Washington, the Fund for Astrophysical Research, and the Rumford Fund of the American Academy of Arts and Sciences for generous financial support.

* Guggenheim Fellow at the time of preparing and assembling the apparatus.

[1] J. A. Wheeler and R. Ladenburg, Phys. Rev. **60**, 754 (1941).
[2] R. B. Brode and G. D. Bagley, Phys. Rev. **56**, 209A (1939).
[3] C. E. Nielsen, Phys. Rev. **61**, 202A (1942).
[4] D. R. Corson and R. B. Brode, Phys. Rev. **53**, 773 (1938).
[5] E. J. Williams, Proc. Roy. Soc. **A172**, 194 (1939).
[6] Compare results of W. M. Powell, Phys. Rev. **61**, 670 (1942).

X-Ray Line Broadening by Cold-Working Alpha-Brass

MAX PETERSEN AND C. W. TUCKER
Lehigh University, Bethlehem, Pennsylvania
May 3, 1943

NIEMANN and Stephenson have reported[1] that the x-ray diffraction line broadening produced by small amounts of cold-working of alpha-brass is enhanced by speed of working, while the internal friction thus introduced is not. The first of these facts, which might be of great importance to practical metal forming, is not confirmed by our observations.

Three like-tensile specimens of cartridge brass having sections 6.3 by 0.53 mm, sealed in nitrogen, were annealed for ninety minutes at 400°C, and showed fine-grained strain-free diffraction by back-reflection. Each was then cold-stretched about 7.5 percent, one by a falling weight at a speed exceeding 30 ft./sec., one by a hammer-blow of somewhat less speed, and one slowly in a small tensile stressing frame. The back-reflection patterns from these three strained specimens show no significant difference of line broadening. In each the Ni $K\alpha$ doublet has become nearly irresolvable visually. If any difference can be found it is that both fast-worked specimens gave traces of coarse-grain irregularity in the photographs, as the other did not.

These observations seem to remove the disparity between line broadening and internal friction effects of cold work. The earlier observations may have been effected by initial differences between the specimens.

[1] F. Niemann and S. T. Stephenson, Phys. Rev. **62**, 330 (1942).

The Forces Between Hydrogen Molecules

HENRY MARGENAU
Sloane Physics Laboratory, Yale University, New Haven, Connecticut
May 1, 1943

THE difficult part in an *a priori* calculation of intermolecular forces is the determination of the repulsive exchange forces. For this reason, complete interaction curves have hitherto been obtained for a few simple spherical atoms only. Yet to understand even the most elementary properties of molecules, such as their size and shape, and also to locate the position of the minimum of their van der Waals forces, a knowledge of the exchange forces is required. Attracted by the fundamental nature of the problem, I have undertaken to calculate them for the simplest molecule and herewith report the results.

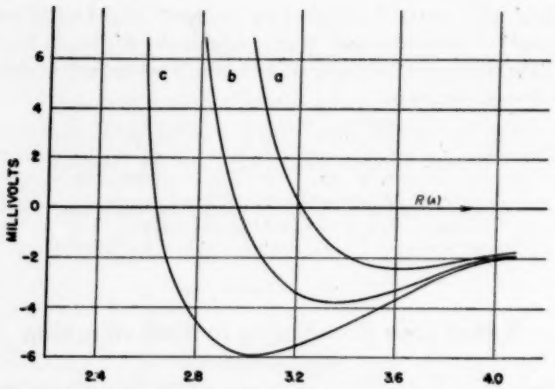

FIG. 1. Interaction energies of two hydrogen molecules, in millivolts, plotted against distance between their centers (in A). Relative orientation of molecules is as follows: (a) — —, (b) — |, (c) | |.

A function of the Heitler-London-Wang type was chosen to represent the electronic charge distribution of a single molecule. As is well known, this function yields the best molecular energy when the effective nuclear charge, Ze, is taken to be 1.166 electronic units.[1] In the present calculation, Z was at first left undetermined.

The interaction was investigated for three relative positions of the molecules: (a) both molecular axes are parallel to the line connecting the centers; (b) one molecule is parallel, one perpendicular; (c) both molecules are perpendicular to the center line. The customary approximation of neglecting double exchange integrals leads to results which are entirely erroneous in this problem, and it is necessary to retain all terms. Unwieldy four-particle integrals, however, can be reduced with good validity to known three- and even two-particle integrals.

One feature emerging from the calculation is the following. When Z is taken to be 1.166 (Wang's value), the exchange forces are *attractive*. This emphasizes the fact that the effective nuclear charge does not have a unique physical significance and that its constancy may not be assumed in molecular problems where the charge symmetry is far from spherical. On further consideration it turned out that in the other two-electron problem, the interaction of He atoms, there is a limiting value of Z, namely $(11/8)e$, below which the exchange forces are also attractive in the interesting range of atomic separations. But in this case the normal value of Z is great enough to cause no difficulty. The physical reason for the inadequacy of the customary value of Z in the intermolecular problem is to be found in the circumstance that the electronic charge is strongly concentrated between the two nuclei of a molecule, leaving the nuclei bare to an abnormal degree.

The calculations were therefore carried out for several different values of Z. Various considerations lead to $Z \approx 1.4$ as the most reasonable choice. Hence the results will here be given for that case only.

An H_2-molecule represents a static quadrupole. The part of the interaction arising from this fact is almost negligibly small throughout. It can be expressed in the simple form

$$\Delta E_Q = \frac{3}{25}\left(\frac{\Delta^2}{1+\Delta^2}\right)^2 \frac{e^2 d^4}{R^5} \cdot f$$

where Δ is the usual overlap integral between the atoms of a single molecule and d the distance between these atoms. The function f expresses the characteristic angular variation for forces between linear quadrupoles.

Finally the attractive van der Waals energy must be included. This may be taken from the work of Massey and Buckingham,[2] whose result, however, is larger than can be obtained from dispersion data on H_2 vapor. When the dipole-quadrupole forces are added, the result is in fair agreement with that derived by the latter authors.

Composition of all these effects yields the interaction curves (drawn for cases (a), (b), and (c) as defined above) which are given in Fig. 1. As would be expected, collinear molecules repel at larger distances and produce a shallower minimum than parallel ones. When the distances at which the minima occur, and also their depths, are compared with the empirical curves derived by Lennard-Jones and others[3] from gas kinetic effects, satisfactory agreement is found.

[1] S. C. Wang, Phys. Rev. 31, 579 (1928).
[2] H. S. W. Massey and R. A. Buckingham, Proc. Roy. Ir. Acad. 45, 31 (1938).
[3] R. H. Fowler and E. A. Guggenheim, *Statistical Thermodynamics* (Cambridge University Press).

The Disintegration Scheme of Na^{24}

L. G. ELLIOTT, M. DEUTSCH, AND A. ROBERTS*
Massachusetts Institute of Technology, Cambridge, Massachusetts
April 30, 1943

THE gamma-rays of Na^{24} have been studied by several authors. Various energies between 0.8 and 3 Mev were announced at different times. In 1941 Itoh[1] reported finding only two gamma-rays of 1.38- and 2.8-Mev energy respectively and equal intensity. Our experiments, completed before we received Itoh's paper, confirmed his results and therefore were reported only briefly at a section meeting of the Physical Society.[2] Since then these results were again questioned by C. E. Mandeville.[3] We have since repeated the measurements with improved accuracy.

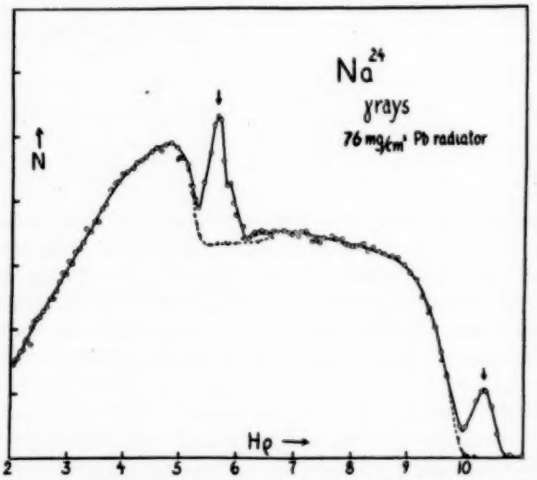

FIG. 1. Secondary electron spectrum showing photoelectron (arrows) and Compton electron (dotted line) groups due to the 1.38 and 2.76 Mev gamma-rays of Na^{24}.

Figure 1 shows the momentum distribution of secondary electrons ejected from a thin lead radiator (and its brass backing) observed in the magnetic lens spectrometer. The observed counting rates were not divided by $H\rho$ as is customary. This procedure was adopted to keep the ordinates of the curve more nearly equal throughout the entire range. Besides, we wish to emphasize the two photoelectron lines (marked by arrows) whose heights should *not* be divided by the transmitted momentum interval since they represent nearly monokinetic electron groups.

The half-width of the transmitted momentum band is about 3.5 percent, but the observed width of the photoelectron lines is slightly greater because of the thickness of the radiator and the presence of the unresolved L photoelectron groups. The statistical counting errors are negligible for most of the points. However the probable error, as indicated by the scatter of the points is about two percent, due partly to small errors in correcting for decay of the sources and in normalizing the several runs of which the curve is a composite.

All regions where photoelectron lines were suspected were studied in separate runs, and it seems quite certain that the intensity of any other gamma-ray above 0.34 Mev (if present at all) does not exceed ten percent of the intensity of the two observed lines.

The distribution of Compton recoil electrons from a copper radiator was also studied. Its absolute intensity and shape deviate by several percent from the Compton groups from lead, probably because of the difference in scattering of the secondary electrons in the two radiators. Therefore only the regions near the end points are indicated in Fig. 1 (crosses and dotted line).

The energies of the gamma-rays, obtained both from the photoelectron lines and the Compton end points are 1.38 ± 0.03 and 2.76 ± 0.06 Mev. The ratio of the intensities may be obtained by correcting the heights of the lines for the variation in photoelectric cross sections and retardation in the radiator. Details of this correction will be published soon in a paper dealing with spectrometer technique. The ratio thus obtained is $I_{1.4} : I_{2.8} = 0.9 : 1$, uncertain to about fifteen percent.

While some of the divergent results previously obtained by other authors were probably due to misinterpretation of data, others may have been due to impurities. The remote possibility cannot be excluded entirely that there may be *several* gamma-rays of very low intensity in the energy range between the two intense lines.

Coincidence measurements of beta- and gamma-rays and of gamma-rays with each other were also performed, and the results agreed with those of other workers,[1-4] showing that each beta-ray is followed by a 1.38- and a 2.76-Mev gamma-ray in cascade. Mr. W. C. Peacock of this laboratory has recently repeated these experiments with carefully calibrated gamma-ray counters, and it appears quite certain that the great majority (at least 90 percent) of the disintegrations proceeds by this scheme. As in the case of Y^{86} the fact that the gamma-ray energies are in the ratio 1 : 2 has therefore no evident significance in terms of the disintegration scheme.

Our thanks are due to Professors Evans and Livingston and the cyclotron crew.

* Now at the M. I. T. Radiation Laboratory.
[1] J. Itoh, Proc. Phys. Math. Soc. Japan **23**, 605 (1941).
[2] L. G. Elliott *et al.*, Phys. Rev. **61**, 99A (1942).
[3] C. E. Mandeville, Phys. Rev. **62**, 309 (1942).
[4] Feather and Dunworth, Proc. Camb. Phil. Soc. **34**, 442 (1938).

Gamma-Rays from Na^{24} and La^{140}

C. E. MANDEVILLE
The Rice Institute, Houston, Texas
April 30, 1943

MEASUREMENTS on the energies and relative intensities of the γ-rays from Na^{24} have been repeated with a magnetic spectrograph which has been previously described.[1] Recent measurements[1] seemed to indicate the

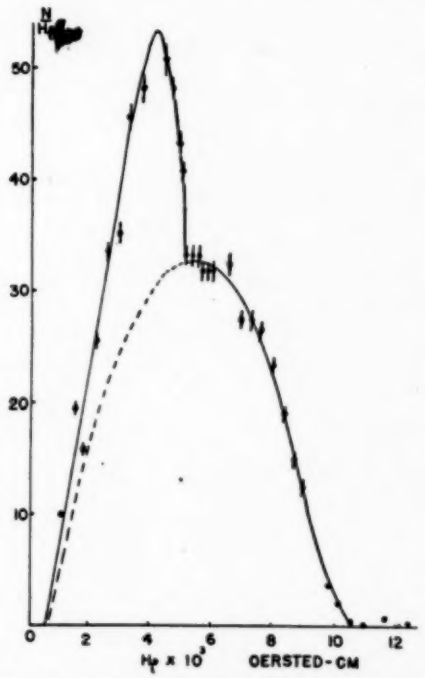

FIG. 1. Momentum distribution of the Compton recoils of the γ-rays from Na^{24}.

presence of quanta at 0.84, 1.31, 1.66, and 2.90 Mev. Subsequent improvements and modifications in the operation of the spectrograph and experiments[2,3] on the γ-rays from Sc^{48} and As^{76} have disclosed that the spectrograph was not satisfactorily designed for the measurement of γ-rays of energy less than 1.0 Mev and with an intensity less than fifty percent of that of any high energy γ-rays present when the first experiments[1] on the gamma-radiation from Na^{24} were performed. In addition to measurements of the energies of the γ-rays from Sc^{48} and As^{76}, observations as yet unpublished, extending over a wide range of energy, have been made upon a considerable number of the radioactive isotopes of other elements. On plotting the distributions in momentum of the Compton recoils of the γ-rays from these various radioactive isotopes, it became apparent

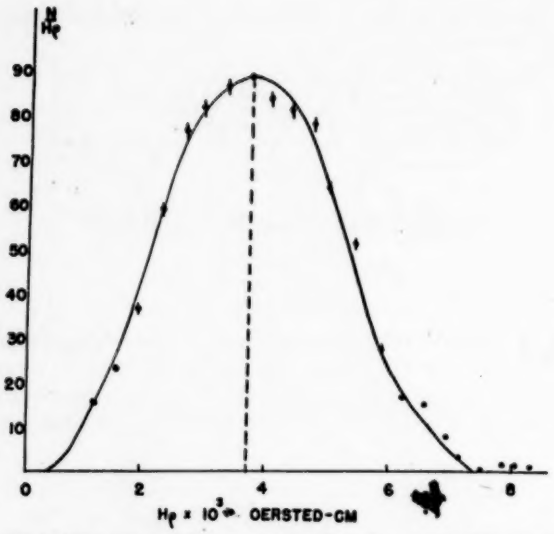

FIG. 2. Momentum distribution of the Compton recoils of the γ-rays from La^{140}. The symmetry of the distribution about the broken line is to be noted.

that for a single γ-ray, and for the geometry of this spectrograph, the momentum distribution of the Compton recoils is symmetrical about a line through the midpoint of the peak of the distribution and parallel to the $N/H\rho$-axis. With this fact in mind, it soon became clear that the momentum distribution of the Compton recoils of the 2.9-Mev γ-ray from Na^{24} lacked the above-mentioned symmetry; that is, the $H\rho$ coordinate of the peak of the distribution appeared to be too large.

NaF has been irradiated by slow neutrons from the cyclotron at Washington University, St. Louis, Missouri. The momentum distribution of the Compton recoils of the γ-rays from Na^{24} is given in Fig. 1. It is to be noted that the spectrum is composed of two electron groups corresponding to quantum energies of 1.38 ± 0.03 Mev and 2.94 ± 0.06 Mev, respectively. The intensity ratio is 0.84 and therefore not inconsistent with the view that the quanta are in cascade. Measurements with this spectrograph are now in agreement with those of J. Itoh[4] and Elliott, Deutsch, and Roberts.[5] The distortion of the peak of the 2.9-Mev γ-ray and the presence of what appeared to be the peak of a γ-ray at 1.66 Mev reported in the first experiments on Na^{24} may be attributed to the presence of an impurity unknown in character, perhaps related to deuteron bombardments. A similar explanation might apply to the strong 2.04-Mev line reported by Richardson.[6]

The symmetry of the Compton distribution of a single γ-ray is illustrated in Fig. 2 where is presented the distribution in $H\rho$ of the Compton recoils of the γ-rays from La^{140}. The γ-rays appear to be monochromatic, and their energy computed from the end point of the momentum distribution is 2.04 ± 0.04 Mev, in surprisingly good agreement with the value 2.00 ± 0.05 Mev obtained by Weimer, Pool, and Kurbatov,[7] using lead absorption.

It was not at first realized that the peak of the electrons from the 2.9-Mev γ-ray of Na^{24} had been misplaced, since its position seemed to agree very well with the position suggested by what appeared to be the peak of the 2.62-Mev γ-ray from Th(C+C″). However, several γ-rays of lower energy accompany the 2.62-Mev γ-ray so that the exact position of its peak may be obscured somewhat by their presence. An examination of the curves for Th(C+C″) and Na^{24} given by Curran, Dee, and Strothers[8] will reveal that the 2.00-Mev radiation from Na^{24} reported by them may actually be part of the peak of a symmetrical momentum distribution of Compton recoils from their 3.03-Mev radiation. The spectrograph of the writer is very similar in geometry and design to the one employed by them.

One conclusion of this research is therefore that the end point of the momentum distribution of the recoils of the 2.62 Mev γ-ray from Th(C+C″) may be used for calibrating spectrographs of this type, but no particular significance should be attached to the shape of the curve.

Shortly after completion of this repetition of the measurements on Na^{24}, the writer was informed of the results of a further study of the γ-rays from Na^{24} which has been conducted by Elliott, Deutsch, and Roberts.[9] Their newly performed spectrometer and coincidence experiments indicate that the two quanta are in cascade and that the β-ray spectrum of Na^{24} is simple.

The theoretical status of Na^{24} appears to be very unsatisfactory. Objections to the cascade arrangement of the two γ-rays have been discussed by Guthrie and Sachs,[10] and possible complexity of the Na^{24} β-ray spectrum has been suggested by the recent results of Konopinski and Uhlenbeck.[11]

The writer wishes to acknowledge the energetic cooperation of the members of the cyclotron group at Washington University, St. Louis, Missouri. They prepared and sent to him the radioactive materials used in the course of these experiments.

[1] C. E. Mandeville, Phys. Rev. **62**, 309 (1942).
[2] C. E. Mandeville, Phys. Rev. **62**, 555 (1942).
[3] C. E. Mandeville, Phys. Rev. **63**, 91 (1943).
[4] J. Itoh, Proc. Phys. Math. Soc. Japan **23**, 605 (1941).
[5] L. G. Elliott, M. Deutsch, and A. Roberts, Phys. Rev. **61**, 99 (1942).
[6] J. Reginald Richardson, Phys. Rev. **53**, 124 (1938).
[7] K. E. Weimer, M. L. Pool, and J. D. Kurbatov, Phys. Rev. **63**, 67 (1943).
[8] S. C. Curran, P. I. Dee, and J. E. Strothers, Proc. Roy. Soc. **A175**, 546 (1940).
[9] L. G. Elliott, M. Deutsch, and A. Roberts, Phys. Rev. **63**, 386 (1943).
[10] A. Guthrie and R. G. Sachs, Phys. Rev. **62**, 8 (1942).
[11] E. J. Konopinski and G. E. Uhlenbeck, Phys. Rev. **60**, 308 (1941).